The Role of CHD1 during Mesenchymal Stem Cell Differentiation

Dissertation

for the award of the degree
“Doctor rerum naturalium (Dr. rer. nat.)”
Division of Mathematics and Natural Sciences
of the Georg-August-Universität Göttingen

submitted by
Simon Baumgart
born in Gießen

Göttingen, 2015

Members of the Thesis Committee:

Prof. Dr. Steven A. Johnsen (Reviewer)
Department of General, Visceral and Pediatric Surgery
University of Göttingen Medical School, Göttingen

Prof. Dr. Heidi Hahn (Reviewer)
Department of Human Genetics
University of Göttingen Medical School, Göttingen

Prof. Dr. Jürgen Wienands
Department of Cellular and Molecular Immunology
University of Göttingen Medical School, Göttingen

Date of oral examination: 22nd of February, 2016

Affidavit

I hereby declare that the PhD thesis entitled “The Role of CHD1 during Mesenchymal Stem Cell Differentiation” has been written independently and with no other sources and aids than quoted.

_____

Simon Baumgart

December, 2015

Göttingen

Table of Contents

Abbreviations

°C	degree Celsius / centrigrade
A	ampere
Adi	adipocyte
ALPL	alkaline phosphatase, liver/bone/kidney
AR	androgen receptor
ATP	adenosine triphosphate
BA	bone area
BA/ TA	bone area/ total area
BAM	binary alignment/map
Bejamini	Bejamini-Hochberg procedure
BGLAP	bone gamma-carboxyglutamate (gla) protein
BGP	β-glycerophosphate
BMP4	bone morphogenetic protein 4
bp	base pair
BSA	bovine serum albumin
CBP	CREB-binding protein
cDNA	completentary DNA
CEAS	cis-regulatory element annotation system
CHD1	chromodomain helicase DNA binding protein 1
ChIP	chromatin immunoprecipitation
ChIP-seq	ChIP with subsequent high-throughput sequencing
cm	centimetre
CO_2	carbon dioxide
COL11A1	collagen, type XI, alpha 1
CRC	chromatin remodeling complex
CTCF	CCCTC-binding factor
CTD	carboxy-terminal domain
CTGF	connective tissue growth factor
Da	Dalton
DBD	DNA-binding domain
ddH_2O	double destilled water
DKK1	dickkopf Wnt signaling pathway inhibitor 1

DMEM	Dulbecco´s modified eagle´s medium
DMSO	dimethyl sulfoxide
DNA	deoxyribonucleid acid
dNTP	deoxyribonucleotide
DTT	dithiothreitol
DUSP1	dual specificity phosphatase 1
DUSP5	dual specificity phosphatase 5
e.g.	exempli gratia = for example
ECM	extra cellular matrix
EDN1	endothelin 1
EDTA	ethylenediaminetetraacetic acid
ELN	elastin
EMP3	epithelial membrane protein 3
ENCODE	encyclopedia of DNA elements
ESC	embryonic stem cell
et al.	*et alii* = and others
EtOH	ethanol
expr.	expression
F	forward
FACT	facilitates chromatin transcription
FBS	fetal bovine serum
FC	fold change
FDR	false discovery rate
Fig	figure
FOB	fetal osteoblast
g	gravity (9.81 m/s^2)
GAPDH	glyceraldehyde-3-phosphate dehydrogenase
GB	gene body
h	hour
H&E	hematoxylin and eosin
H1	histone 1
H2A	histone 2A
H2A.Z	H2A histone family, member Z
H2B	histone 2B

H2Bub1	histone H2B monoubiquitination at lysine 120
H3	histone 3
H3.3	H3 histone, family 3
H3K27ac	histone H3 acetylated at lysine 27
H3K27me3	histone H3 trimethylation at lysine 27
H3K36me3	histone H3 trimethylation at lysine 36
H3K4me1	histone H3 monomethylation at lysine 4
H3K4me2	histone H3 dimethylation at lysine 4
H3K4me3	histone H3 trimethylation at lysine 4
H4	histone 4
HA	hydroxyapatite
HAT	histone acetyltransferase
HDAC	histone deacetylase
hg19	human genome project version 19
HMT	histone methyltransferase
HRP	horseradish peroxidase
hs	homo sapiens
HSC70	heat shock 70kDa protein 8
IBSP	integrin-binding sialoprotein
IGF	insulin-like growth factor 1
IgG	immunoglobulin G
IGV	integrative genomics viewer
INO80	INO80 complex subunit
iPSC	induced pluripotent stem cells
ISWI	imitation SWI
K	lysine residue
kb	kilo base pairs
kDa	kilo Dalton
kg	kilogram
LiCl	lithium chloride
log	logarithm
LPL	lipoprotein lipase
m	milli (10^{-3})
M	methionine residue or molar, mol/L

MACS	model-based analysis of ChIP-seq
MED1	mediator complex protein-1
min	minute
mRNA	messenger RNA
MSC	mesenchymal stem cell
n	number of indivual values
n	nano (10-9)
n.s.	non-significant
NDR	nucleosome depleted region
NEM	N-ethylmaleinmide
NF-κB	nuclear factor of kappa B cells
NP-40	nonidet P-40
NuRD	nucleosome remodeling deacetylase
Ost	osteoblast
p	probability
P/S	penicillin/streptomycin
p300	E1A binding protein p300
PBS	phosphate buffered saline
PC	principle component
PCA	principle component analysis
PCIA	phenol:chloroform:isoamyl alcohol
PCR	polymerase chain reaction
pH	*potentia hydrogenii* = potential of hydrogen
PLIN1	perilipin 1
POSTN	periostin
PPARG	peroxisome proliferator-activated receptor gamma
PRC	polycomb repressive complex
ptm	post translational modification
qPCR	quantitative real-time PCR
R	arginine residue or reverse or Pearson correlation coefficient
RAR	retinoic acid receptor
RIN	RNA integrity number
RING	reallyinteresting new gene

RNA	ribonucleic acid
RNA-Pol II	RNA polymerase II
RNA-seq	sequencing of rt-transcribed RNA
RPKM	reads per kilo base per million mapped reads
RPLP0	ribosomal protein, large, P0
RSC	chromatin structure remodeling complex
RT	room temperature
RT-PCR	reverse transcription PCR
RUNX2	runt-related transcription factor 2
s	second
s.d.	standard deviation
SAGA	spt-ada-gcn5 acetyltransferase
SAM	sequence alignment/map
SCID	severe combined immunodeficiency
SDS	sodium dodecylsulfate
SDS-PAGE	SDS polyacrylamide gel electrophoresis
shCHD1	shRNA directed against CHD1
shCon	shRNA non-targeting
shRNA	short hairpin RNA
siCHD1	siRNA directed against CHD1
siCon	siRNA control
siRNA	short interfering RNA
SIX1	SIX homeobox 1
SP7	sp7 transcription factor
SPP1	osteopontin
SSRP1	structure specific recognition protein 1
SUMO	small ubiquitin-like modifier
SWI/SNF	SWItch/sucrose nonfermentable
TA	tissue area
Taq	*Thermus aquaticus*
TBP	TATA-binding protein
TCP	tri-calcium phosphate
TEMED	N,N,N´,N´-tetramethylethylenediamine
TFF1	trefoilfactor 1

TFIIA/B	transcription factor A/B
TGFβ	transforming growth factor, beta
Tris	Tris(hydroxymethyl)aminomethane
TSS	transcriptional start site
TTS	transcriptional termination site
U	unit (enzyme activity)
ub	ubiquitin
un	unregulated
Und	undifferentiated
up	up regulated
UTR	untranslated region
V	voltage
v/v	volume per volume
VDR	vitamin D (1,25- dihydroxyvitamin D3) receptor
VIM	vimentin
vs.	versus
w/v	weight per volume
wt	wild type
α	alpha
β	beta
γ	gamma
µ	micro (10^{-6})

List of Figures

Summary

Nucleosome remodeling, histone modifications and exchange of histone variants are interconnected mechanisms involved in regulation of gene transcription. Nucleosomes can act as strong barriers and are remodeled during RNA-Pol II-mediated transcription elongation. Remodeling of nucleosomes is tightly regulated in particular during activation and inhibition of cellular differentiation. The nucleosome remodeler CHD1 is a transcriptional co-activator involved in RNA-Pol II *processivity* downstream of the transcriptional start site (TSS). In this study we hypothesized that CHD1 not only acts as a general co-activator of transcription but can also regulate gene specific expression. Therefore, we investigated the role of CHD1 on gene regulation after induction of adipocyte and osteoblast differentiation.

Genome-wide binding analysis of CHD1 during differentiation revealed high occupancy at TSS-regions of adipocyte and osteoblast activated genes. Further we observed direct regulation of these activated genes by enriched CHD1 binding around TSS. Concordantly, CHD1 was required for ectopic bone formation in mice. Besides these biological aspects it could here be shown that global RNA-Pol II stalling downstream of TSS was caused by CHD1 depletion. This highlights its genomic role for efficient early RNA-Pol II-mediated transcription elongation. A group of highly activated genes during osteoblast differentiation was found to be repressed by significantly increased RNA-Pol II stalling ratios in parallel with decreased CHD1 protein levels. Interestingly, high steady-state levels of the histone variant H2A.Z at the TSS-region were revealed to be dependent on CHD1. This presumably increases the nucleosome stability and thus cause the observed global RNA-Pol II stalling. Summarized, CHD1 was shown to be necessary for a genome-wide, efficient RNA-Pol II-mediated early transcription elongation, probably achieved by decreasing the nucleosome barrier at the TSS-region. In particular, CHD1 was required for the activation of a group of genes involved in osteoblast differentiation. This implies a function for CHD1 as a regulatory protein in cell differentiation. Further we propose that CHD1 should be considered in quality control of MSC in skeletal stem cell therapies.

1 Introduction

1.1 DNA organization

The approximately 2 m long human DNA is highly compacted and organized in an approximately 10 µm diameter sized nucleus within a dynamic structure called chromatin (Alberts B, Johnson A, Lewis J, et al., 2002). The chromatin consists of DNA, protein and RNA. Besides packaging and protecting the DNA, it also regulates the DNA accessibility required for cellular processes such as transcription and replication. The basic structural unit of chromatin is the nucleosome which is defined as 146 bp of DNA wrapped around an octamer of 4 core histone proteins consisting of H2A, H2B, H3 and H4 (Luger et al., 1997). Two H2A/H2B heterodimers connect with two H3/H4 heterodimers to form a stable histone octamer (Kornberg, 1974). These interact via a “hand-shake motif” and connect in the presence of DNA. In addition to the core particles, the histone H1 binds to linker DNA between two nucleosomes. This further stabilizes the DNA wrapped around the nucleosome and helps to fold the higher compacted chromatin (Allan et al., 1986; Hansen, 2002).

The differences in the compaction of chromatin can be differentiated within a cell and associates with different functions (Figure 1). After the nucleosome, the next level of compaction is the 10 nm fiber or “beads on a string” structure, which defines open accessible chromatin for example at transcriptional start sites or regulatory sequences (Cooper, 2000). Further packaging includes the 30 nm and 300 nm fibers, which both represent highly compacted chromatin (Tremethick, 2007). Though, the 30 nm fiber can be actively remodeled to the open 10 nm fiber and is associated with actively transcribed genes (Li et al., 2010), the 300 or 700 nm structure characterizes condensed chromatin which is present in the interphase of mitosis.

In general, two states of chromatin are distinguished, the eu- and heterochromatin. Euchromatin represents 10 to 30 nm thick fibers which characterize open and accessible chromatin. Cellular processes which involve the direct contact with DNA such as transcription, DNA-repair and -replication require euchromatin (Cooper, 2000). Heterochromatin in contrast defines closed and condensed chromatin, located most often at the centromere or telomere with repetitive elements (Grewal and Jia, 2007).

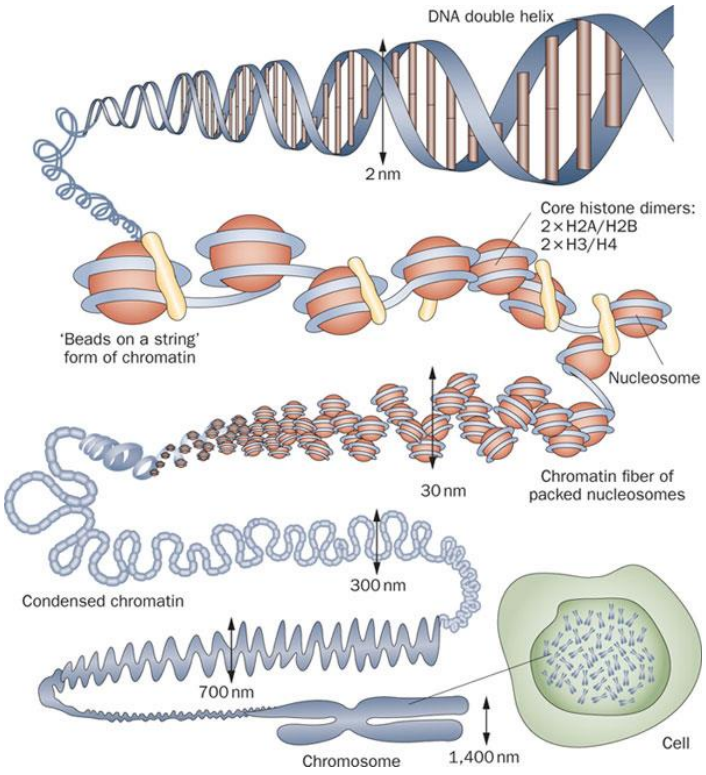

Figure 1: Organization of DNA from decondensed (top) to higher condensed (bottom) chromatin structures. In the lowest condensed chromatin state, the "beads on a string" structure is the DNA wrapped around a histone octamer associated with histone H1 (yellow). Further compression includes 30 nm, 300 nm and 700 nm chromatin structures which leads to the organization of interphase chromosome within a cell nucleus (Figure taken from Tonna et al., 2010)*.*

1.2 Histone modifications

Negatively charged DNA and positive charged histones are tightly bound when forming the nucleosome, however N- and C-terminal tails of histones protrude from nucleosomes and are often targets of different post-translational modifications (PTM) (Luger et al., 1997; Van Holde et al., 1980). However, some histone amino acids lying within the core of nucleosomes between the tails and get modified, too (Tropberger et al., 2013). The most common PTMs include acetylation, methylation, phosphorylation, ubiquitination and SUMOylation (Figure 2) (Bannister and Kouzarides, 2011). The modifications consist of relatively small, covalently bound acetyl-, phospho- or methyl-groups up to relatively large protein moieties like ubiquitin or Small Ubiquitin-like Modifier (SUMO) attached to specific amino acids of histones. Interestingly, the high variability in PTMs leads to extensive changes in the chromatin, mainly either loosening DNA-histone interactions and/or changing the binding properties with other proteins or complexes (Bannister and Kouzarides,

2011). These changes have a broad impact on nearly all cellular processes, although cause and effect of histone modifications have to be considered carefully.

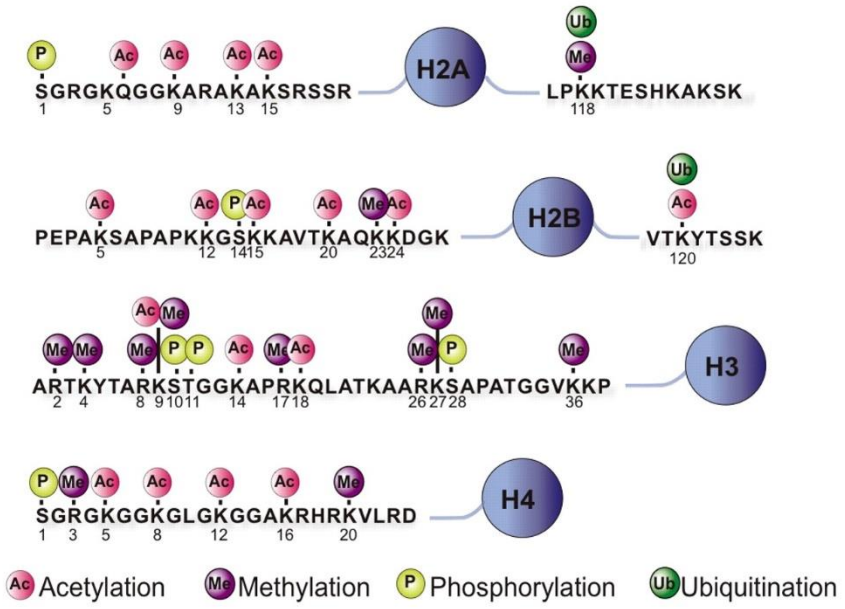

Figure 2: Post-translational histone modifications in humans. Schematic view of N- and C-terminal tails of Histone 2A, 2B, 3 and 4 (H2A, H2B, H3, H4) shows post-translational histone modification (explained at bottom) at respective amino acid residues of each histone (Figure taken from Kato et al., 2010).

1.3 Deciphering the "histone code"

Extensive modifications on one nucleosome raised the hypothesis for a "histone code" stating the association of various epigenetic changes defining a single functional and regulatory event (Strahl and Allis, 2000). Since then, thousands of genome-wide chromatin immunoprecipitation with subsequent deep sequencing (ChIP-seq) studies were performed analyzing different histone modifications in different cell lines and organisms (Bernstein et al., 2010; ENCODE Project Consortium, 2012). Indeed, these great amount of data confirmed the early hypothesis and revealed that histone marks could characterize the active and repressed regions of genomic elements in a cell type-specific manner (Álvarez-Errico et al., 2015; Li et al., 2007). These data also revealed that active transcriptional start sites (TSS) in eukaryotes are frequently marked by histone H3 tri-methylated at lysine 4 (H3K4me3) and histone H3 acetylated at lysine 27 (H3K27ac). Actively transcribed gene bodies show marks like monoubiquitinated H2B (H2Bub1) and H3K36me3. In contrast, inactive and repressed gene regions are frequently characterized by H3K27me3 marks, whereas condensed chromatin is typically

associated with H3K9me3. Furthermore, co-occupancy of functionally active and repressive histone modifications like H3K4me3 and H3K27me3 describe a specific subset of genes, called bivalent genes. Bivalent genes are in a transcriptionally inactive state, but often occupied already with RNA-Polymerase II (RNA-Pol II), and ready to be transcribed very fast after a certain stimulus (Bernstein et al., 2006; Min et al., 2011). These genes are often involved in regulation of differentiation of developmental processes which can induce further cell fate committing genes. It has been shown that especially undifferentiated cells such as embryonic stem cells tend to have genes in a bivalent state (Grandy et al., 2015; Ravens et al., 2015). In addition to its role in transcription regulation the histone code is associated with processes such as DNA-repair, histone exchange and dosage compensation (Heard and Disteche, 2006; Venkatesh and Workman, 2015; Zhu and Wani, 2010).

This altogether indicates that the “histone code” can be used to describe not only the genomic regions, but also regulatory processes and characteristic cellular functions. Moreover, since cells have characteristic histone modification “landscapes” this can be further used for cell type specification or even for predictions of gene expression (Heintzman et al., 2009; Heinz et al., 2015; Karlić et al., 2010; Koch et al., 2007).

1.4 Histone variants

Nucleosomes can be changed in their canonical histone composition by histone variants. Several conserved histone variants were described for each histone except H4 (Kamakaka and Biggins, 2005). H2A and H3 show the highest diversity in variants like H2A.X, H2A.Z, macro H2A, H2A.Bdb and for H3 like H3.1, H3.2, H3.3. These variants can change the interaction of DNA and proteins when replacing canonical histones within the nucleosomes (Bönisch and Hake, 2012). Furthermore, they also regulate nucleosome stability or occupancy of modifications (Kamakaka and Biggins, 2005). The functionality and homology of histone variants compared to their canonical counterparts vary greatly. For example, the histone variant H3.3 is almost identical to the H3 and differs only in 4 or 5 amino acids, whereas H2A.Z has only a 60% homology to H2A (Zlatanova and Thakar, 2008). Additionally, histone variants can be associated with a common regulatory feature of cellular processes as known for H2A.Z or H3.3 in transcription (Jin et al., 2009). Interestingly, some of them are also associated with cell type-specific functions like the histone variant H3.5 in sperm and testis (Schenk et al., 2011). Moreover, they can also differ in their occupancy

within genome. H2A.Bdb is restricted to autosomes and the active X-chromosome, whereas macro H2A is mainly found in the inactive X-chromosome (Chadwick and Willard, 2001; Costanzi and Pehrson, 1998).

1.4.1 Histone variant H3.3

H3.3 can be incorporated into nucleosomes in a replication-independent manner and is mainly associated with active promoters, gene bodies or enhancer regions (Ahmad and Henikoff, 2002; Jin et al., 2009; Sarai et al., 2013). A study showed that H3.3 containing nucleosomes are more sensitive to low salt concentrations and are less stable than those with the canonical histone H3 (Jin and Felsenfeld, 2007). Concordant with these earlier studies it was also shown that H3.3 causes higher nucleosome turnover, a characteristic believed to keep the DNA in a transiently accessible state for regulation (Mito et al., 2005; Wirbelauer et al., 2005). Interestingly, H3.3 appears also to be required for instance for the maintenance of a specific chromatin landscape in embryonic stem cells by associating with the polycomb repressive complex 2 (PRC2) complex mediated by H3K27me3, despite high nucleosome turnover still being present (Banaszynski et al., 2013). Furthermore, in 31% of pediatric glioblastoma samples H3.3 was shown to be mutated at sites corresponding to H3K27, the modification which is well known to play an important role in gene regulation (Schwartzentruber et al., 2012).

1.4.2 Histone variant H2A.Z

H2A.Z is a highly conserved protein present in the protozoan *Plasmodium falciparum*, *Saccharomyces cerevisiae* and human with approximately 90% sequence conservation (Iouzalen et al., 1996; Zlatanova and Thakar, 2008). In the nucleosome H2A.Z can form a heterodimer with H2B in either a homotypic (H2A.Z/ H2A.Z) or heterotypic (H2A/ H2A.Z) fashion and thus alter the interaction with the H3/ H4 heterotetramer (Suto et al., 2000). Though the overall nucleosome structure is less changed to its canonical counterpart, the homotypic H2A.Z-containing nucleosomes are more sensitive to low salt concentrations and less stable (Weber et al., 2010). Interestingly, H2A.Z was found to be enriched in mammals and *S. cerevisiae* at the +1 nucleosome, the first nucleosome downstream of the TSS, which is thought to have regulatory roles in transcription by forming a barrier for RNA-Pol II (Bönisch and Hake, 2012; Zhang et al., 2005). However, besides its broadly described association

with gene activation H2A.Z has been correlated also with gene repression (Marques et al., 2010). Therefore, H2A.Z is rather thought to affect nucleosome positioning by sliding (nucleosome sliding described below) than solely reducing nucleosome stability and decreasing the hurdle for RNA-Pol II (Albert et al., 2007; Bönisch and Hake, 2012; Guillemette et al., 2005). These features link them to a broad range of cellular processes such as DNA-repair, transcription regulation and segmentation of euchromatin and heterochromatin (Bönisch and Hake, 2012; Meneghini et al., 2003).

Interestingly, H3.3 and H2A.Z histone variants often co-occupy positions at the +1 nucleosome and may promote a decreased nucleosomal barrier for RNA-Pol II around the TSS (Jin et al., 2009). Concordant with that, a previous study showed that nucleosomes with H2A.Z and H3.3 were even more sensitive to low salt concentrations, however another group found only subtle differences in their stability, but increased variability in the nucleosome positioning (Jin and Felsenfeld, 2007; Thakar et al., 2009). With the exception of TSS, additional regulatory regions are co-occupied with the two histones variants such as enhancer and insulator regions supporting their role in the maintenance of DNA accessibility (Chen et al., 2014b; Jin et al., 2009).

1.5 Nucleosome remodeling

Another mechanism of chromatin rearrangement is the remodeling and movement of nucleosomes. Nucleosome remodeling and positioning were shown to be important in transcription, DNA-repair or DNA-recombination (Green and Almouzni, 2002; Kamakaka and Thomas, 1990; Roth and Roth, 2000). Although the DNA sequence is a strong indicator for nucleosome positioning, half of the human genome is covered by regularly spaced nucleosomes and around 10% of them show highly consistent positioning, which indicates a genome-wide role of nucleosome remodeling (Gaffney et al., 2012). In general, four nucleosome remodeling mechanisms are described: i) sliding of nucleosomes by an ATP-dependent remodeler, ii) ejection of a complete histone octamer, iii) replacement or iv) removal of the H2A/ H2B histones from a nucleosome (Cairns, 2007).

1.5.1 Nucleosome sliding

Nucleosome sliding is performed by enzymes which are closely related to helicases and characterized by a highly conserved ATPase domain. The exact molecular

mechanism how nucleosome sliding is performed is still a matter of debate (Mueller-Planitz et al., 2013). However, one model predicts that the ATPase remodeler bind at two distal sites on the nucleosome and loosen the interaction between the DNA and histones. The free DNA is then directionally pulled from the nucleosome and is thought to form a loop. By this ATP-dependent process linker DNA is dragged behind which transfers around the nucleosome and finally results in a shift. The majority of ATP-dependent chromatin remodelers act in modular multi-protein complexes and are broadly expressed (Mueller-Planitz et al., 2013; de la Serna et al., 2006). These are classified into several families such as SWItch/Sucrose Non-Fermentable (SWI/SNF), imitation SWI (ISWI), chromodomain helicase DNA-binding (CHD), INO80 complex (INO80), etc. (Clapier and Cairns, 2009). Further, the modularity of the associated complexes connects them to a variety of cellular processes with spatial and temporal regulation like differentiation and development (Chi et al., 2003; Das et al., 2007; Reynolds et al., 2012).

In general, these chromatin remodeling complexes (CRC) can be divided into repressing or activating ones. For instance, the nucleosome remodeling deacetylase (NuRD) complex is a repressive CRC with multiple components like histone deacetylases-1 or 2 (HDAC1/2) and SNF2-ATPase domain containing chromodomain helicase DNA-binding protein-3/4 (CHD3/4) (Xue et al., 1998). In contrast, the SWI/SNF complex is an activating CRC with histone acetyl transferase activity (HAT) and AT-rich interactive domain 1A/B (ARID1A/B) (Kwon et al., 1994). Interestingly, active and repressive CRC often can have competitive roles in regulation of cell fates (Gao et al., 2009). However, CRC are difficult to analyze because of their modularity and often cell type specific functions (Voss and Hager, 2014).

Nucleosome sliding in general can cause three different outcomes: Nucleosome spacing, phasing or positioning (Figure 3) (Mueller-Planitz et al., 2013). Nucleosome spacing creates a regular array of nucleosomes which is often associated with dynamic and active chromatin (Gaffney et al., 2012). Approximately half of the human genome is covered by these arrays. It was shown in yeast that defects in nucleosome spacing due to depletion of a nucleosome remodeler led to cryptic transcription in the gene bodies (Hennig et al., 2012; Shim et al., 2012). Furthermore, regularly spaced

arrays might be important for the integrity of chromatin fibers during DNA replication (Fletcher and Hansen, 1996).

Nucleosome phasing describes a patterning of nucleosomes relative to a nucleosome depleted region (NDR). NDRs are long-term open DNA regions caused by i) DNA sequences rich in AT which repels the association with histones, ii) due to the occupancy of DNA-bound proteins e.g. at the TSS or iii) ATP-dependent remodeling (Struhl and Segal, 2013). These regions are important regulatory sites which are required for the recruitment and binding of proteins like transcription factors or RNA-Pol II associated proteins (Venkatesh and Workman, 2015). The +1 nucleosome is a strong determinant for nucleosome phasing (Mavrich et al., 2008). Depletion of the Snf2-related nucleosome-spacing enzymes showed strong alterations in histone phasing after the +1 nucleosome reaching into the gene body(Gkikopoulos et al., 2011; Pointner et al., 2012). Surprisingly this had however weak influence on global transcription, but increased cryptic transcription. Interestingly, the +1 nucleosome is *the* well positioned nucleosome and belongs to the 10% of the most consistently positioned nucleosome in the human genome (Gaffney et al., 2012). Furthermore, neither loss of histone chaperones (described below) nor the loss of ATP-dependent remodeler appears to regulate this solidly positioned nucleosome.

During nucleosome positioning, DNA sequences can be disclosed or exposed by interaction with histones within the nucleosomes and thus for example regulate an active or inactive state. In yeast, the chromatin structure remodeling complex (RSC), which is related the human SWI/SNF complex, maintains NDR, whereas the ATP-dependent nucleosome remodeler Imitation Switch subfamily 2 (Isw2) was reported to shift nucleosomes at the TSS and thus inhibit transcriptional initiation (Badis et al., 2008; Whitehouse and Tsukiyama, 2006).

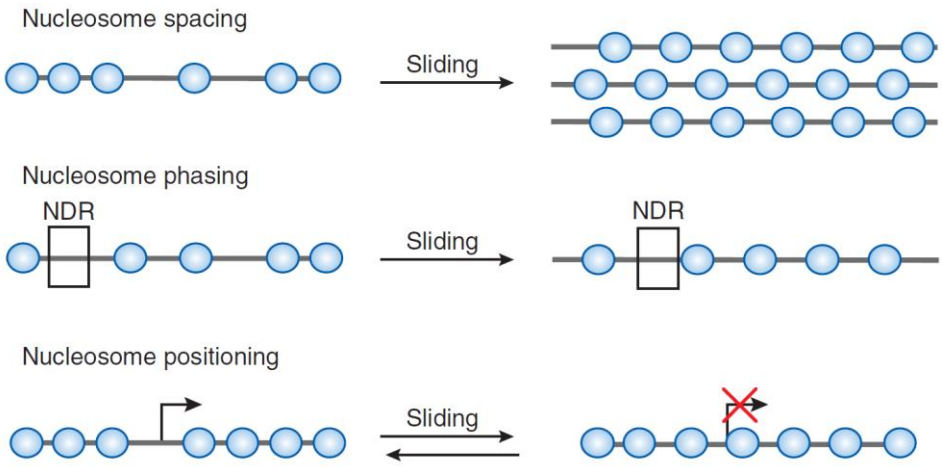

Figure 3: Different outcomes of nucleosome sliding. The model depicts nucleosomes (blue) on a DNA (grey line) in a decondensed status which are remodeled from left by respective mechanisms, as named top left, respectively. Black arrow on the nucleosome and DNA indicates transcriptional start site and its directionality, NDR – Nucleosome depleted region (Figure modified after Mueller-Planitz et al., 2013).

1.5.2 Ejection and histone replacement/removal

The canonical nucleosome is a stable structure, however, a dynamic exchange of histones occurs over various regions e.g. gene bodies (Das and Tyler, 2013). The main challenge during remodeling is to disturb the histone-histone or DNA-histone interactions within one nucleosome to remove or replace it. DNA-histone interactions are modified by ATP-dependent chromatin remodeler whereas histone-histone interactions are changed by histone chaperones (Gurard-Levin et al., 2014). These proteins often act together in complexes to unfold nucleosomes, as shown in yeast and humans (Cho et al., 2013; Okada et al., 2009; Simic et al., 2003).

1.5.3.1 Histone dynamics in transcription

Early studies on RNA-Pol II elongation has shown that nucleosomes can block transcription *in vitro*, whereas *in vivo* the nucleosomes are remodeled so that Polymerase can passage (Chang and Luse, 1997; Kireeva et al., 2002). During the process of remodeling the histone chaperones facilitates chromatin transcription (FACT) complex and Nef-associated protein 1 (Nap1) destabilize the interaction between the H2A/H2B dimer and the H3/H4 tetramer which causes the ejection of H2A/H2B (Petesch and Lis, 2012). This is often sufficient for the RNA-Pol II to overcome the nucleosome barrier. Interestingly, H2Bub1 is stimulating the FACT dependent nucleosome remodeling and enhances the RNA-Pol II passage frequency

(Pavri et al., 2006). This highlights the interplay on chromatin remodeling between histone modifications and CRC. Further, it also shows possible regulatory mechanisms of transcription by modulating histone dynamics over the gene body. Concordant with that, the chaperone specific recruitment to genes might play a role in fine tuning gene expression (Jimeno-González et al., 2006).

After RNA-Pol II passage, histones are reassembled to the DNA by FACT and ordered into a spaced array by ATP-dependent chromatin remodeler (Hsieh et al., 2013; Smolle et al., 2012). This might be a coordinated process between CHD1 and FACT as studies pointed out in yeast, *Drosophila melanogaster* and human by the interaction of both proteins (Krogan et al., 2002; Simic et al., 2003; Sims et al., 2007). Defects in either of both proteins were shown to increase cryptic transcription by RNA-Pol II (Carvalho et al., 2013; Smolle et al., 2012).

1.5.3.2 Histone dynamics at the TSS

Similar to gene bodies, nucleosomes at the transcriptional start sites are strong barriers for initiating RNA-Pol II *in vitro* (Lorch et al., 1987). After RNA-Pol II recruitment to the TSS and accomplished transcription of 20 – 50 bp into the gene, often a pause follows (Sainsbury et al., 2015). This pausing RNA-Pol II requires further signaling to continue transcription into the gene body. Additionally, the +1 nucleosome needs to be overcome. Interestingly, this nucleosome position is slightly shifted downstream relative to the TSS when the RNA-Pol II is paused (Jonkers and Lis, 2015; Li and Gilmour, 2013; Weber et al., 2014). This “pushed” nucleosome by pausing RNA-Pol II indicates a transcriptional block. Further evidence for a +1 nucleosome dependent barrier *in vivo* was provided by decreased RNA-Pol II pausing at H2A.Z enriched genes, which destabilizes nucleosomes (described above). Concordantly, knockdown of H2A.Z caused higher stalling of RNA-Pol II around the TSS by decreasing the +1 nucleosome turnover (Weber et al., 2014). Thus, regulation of the +1 nucleosome barrier directly affects the gene transcription by RNA-Pol II.

Factors which are involved in the turnover of the nucleosome barrier at the TSS have been described previously. In particular, ATP-dependent chromatin remodeler, histone modifications or histone variants play a pivotal role (Skene et al., 2014; Svensson et al., 2015; Venkatesh and Workman, 2015). Hereby, the incorporation of

H2A.Z or H3.3 could affect the gene regulation by modulating the nucleosomal barrier. H2A.Z is incorporated into human nucleosomes either by the p400/TIP60 complex or the Snf2-related CREBBP activator protein (SCRAP), which are both ATP-dependent remodelers (Billon and Côté, 2013). In contrast, H3.3 is incorporated into nucleosomes by the histone cell cycle regulation defective homolog A (HIRA) chaperone (Ray-Gallet et al., 2002). Interestingly, impairment in H3.3 gene specific incorporation showed defects during development and differentiation rather than global transcription effects (Dutta et al., 2010; Szenker et al., 2012).

1.6 CHD1

The highly conserved chromodomain helicase DNA binding protein-1 (CHD1) is a ATP-dependent chromatin remodeler and belongs to the CHD family with 9 members (CHD1 – 9) (Marfella and Imbalzano, 2007). CHD1 has a tandem chromodomain at the N-terminal site, a central SNF2-like ATPase domain and a DNA binding domain (DBD) at the C-terminal site (Figure 4A). The tandem chromodomain was dispensable for chromatin binding but especially important for its substrate recognition (Hauk et al., 2010; Morettini et al., 2011). However, indispensable was the DBD domain for fast and directional nucleosome sliding by interaction with the linker DNA of nucleosomes (McKnight et al., 2011; Ryan et al., 2011). Moreover, also mutations in the DBD domain did not prevent CHD1 from chromatin association (McKnight et al., 2011). Surprisingly, substitution of the DBD domain and changed tethering of CHD1 directly onto the nucleosome substrate changed its sliding properties and even caused disruption of the nucleosome (Patel et al., 2013).

1.6.1 The role of CHD1 in yeast and drosophila

In *S. cerevisiae* and *D. melanogaster* CHD1 is not necessary for their viability, but latter showed impaired development and fertility (McDaniel et al., 2008; Tsukiyama et al., 1999). However, CHD1 deletion in *S. cerevisiae* or its orthologue histidine-rich protein (hrp3) in *Saccharomyces pombe* showed changes in nucleosome positioning over the gene body relative to the stable positioned +1 nucleosome (Gkikopoulos et al., 2011; Hennig et al., 2012; Shim et al., 2012). Furthermore, H3K36me3 was reduced and gene bodies were more acetylated after passage of RNA-Pol II. The resulting changes in nucleosome array and open acetylated chromatin structure at the gene body caused cryptic transcription, but did not alter global transcription.

Consistently, another study showed that H2Bub1, a mark for transcriptional elongation at gene bodies, was reduced after loss of CHD1 and gene bodies had less nucleosome occupancy (Lee et al., 2012a). Moreover, CHD1 mutant strains showed an increased accumulation of RNA-Pol II Serine 5 phosphorylated form at TSS, which characterizes early elongating defects of the RNA-Pol II, probably by an altered nucleosome array (Park et al., 2014). Besides transcription regulation CHD1 was also required for deposition and regular spacing of H3.3 in the male pronucleus of *D. melanogaster* (Konev et al., 2007).

1.6.2 Role of CHD1 in higher eukaryotes

In contrast to *S. cerevisiae* and *D. melanogaster* CHD1 is required for the embryonic development in mice (Guzman-Ayala et al., 2015). CHD1 deletion caused prenatally lethality between day five and six which indicates its importance in developmental processes. Similar to *S. cerevisiae*, CHD1 is mainly linked to transcriptional processes in higher eukaryotes. It was described to bind to H3K4me3 with its tandem chromodomain and interact with the transcription machinery (Figure 4B) (Lin et al., 2011; Sims et al., 2007). In particular, CHD1 is recruited by the mediator complex and probably further stabilized or positioned to its nucleosome substrate by its binding to H3K4me3. However, it had been shown that CHD1 is not associated with H3K27me3 which indicates its association with active, but not bivalent, genes (Gaspar-Maia et al., 2009). Global binding patterns of CHD1 in human and mice revealed high similarities to yeast. Further, genome-wide occupancy analyses uncovered CHD1 binding also at gene bodies, which is supported by previous interaction studies between CHD1 and structure specific recognition protein 1 (SSRP1), a histone chaperone (Kelley et al., 1999; Skene et al., 2014). If CHD1 is also necessary for the maintenance of H3K36me3 and H2Bub1 at the gene body like it was observed in yeast was not investigated yet (Gkikopoulos et al., 2011; Hennig et al., 2012; Shim et al., 2012).

However, a recent study in mouse embryonic fibroblasts showed that overexpression of a CHD1 mutant protein increased the nucleosome turnover at the gene body which indicates its role in ordering the chromatin after RNA-Pol II passage (Skene et al., 2014). Furthermore, it reduced the nucleosome turnover at the TSS of all expressed genes and caused decreased RNA-Pol II Serine 2 phosphorylation levels, a mark for elongating polymerase. This indicates that functional CHD1 was required for the

RNA-Pol II to overcome the +1 nucleosome barrier and order the nucleosomes at the gene body after passage of RNA-Pol II.

Next to its transcriptional effects, studies also highlighted a role for CHD1 in the segmentation of hetero- and euchromatin. In *D. melanogaster* and mice, reduced CHD1 levels caused increased marks of heterochromatin, like HP1alpha and H3K9me2 (Bugga et al., 2013; Gaspar-Maia et al., 2009). CHD1, however, is restricted to open chromatin states, as it was mutually exclusive with the H1 histone (Lusser et al., 2005).

The role of CHD1 in transcription was also shown to regulate developmental processes and tumorigenesis. A recent study highlighted that CHD1 is required for the maintenance of mouse embryonic stem cells (mESC) and self-renewal capacity (Gaspar-Maia et al., 2009). The same group also observed that endothelial-specific deletion of CHD1 caused a loss of hematopoietic progenitor cells, however, interestingly, after hematopoietic differentiation CHD1 deletion had no obvious effects on subsequent blood cell development (Koh et al., 2015). This indicates a specificity in certain differentiation processes and demonstrates that CHD1 played a role in stem cell differentiation and maintenance.

Besides developmental processes, CHD1 is frequently mutated or deleted in human prostate cancer (Grasso et al., 2012), although mutations in transcriptional co-activators are less frequently reported in high proliferative cancer cells. Interestingly, recent studies highlighted the interaction of CHD1 with the androgen receptor (AR) and its role in regulating AR-dependent gene transcription (Burkhardt et al., 2013). However, other studies claim that a subtype of androgen-independent aggressive prostate cancer cells carry CHD1 mutations (Huang et al., 2012; Rodrigues et al., 2015). Although, molecular studies particular in cancer models are missing which address the question how CHD1 affects RNA-Pol II transcription and pausing, the studies so far showed that loss of CHD1 might act gene specific and not on global gene expression.

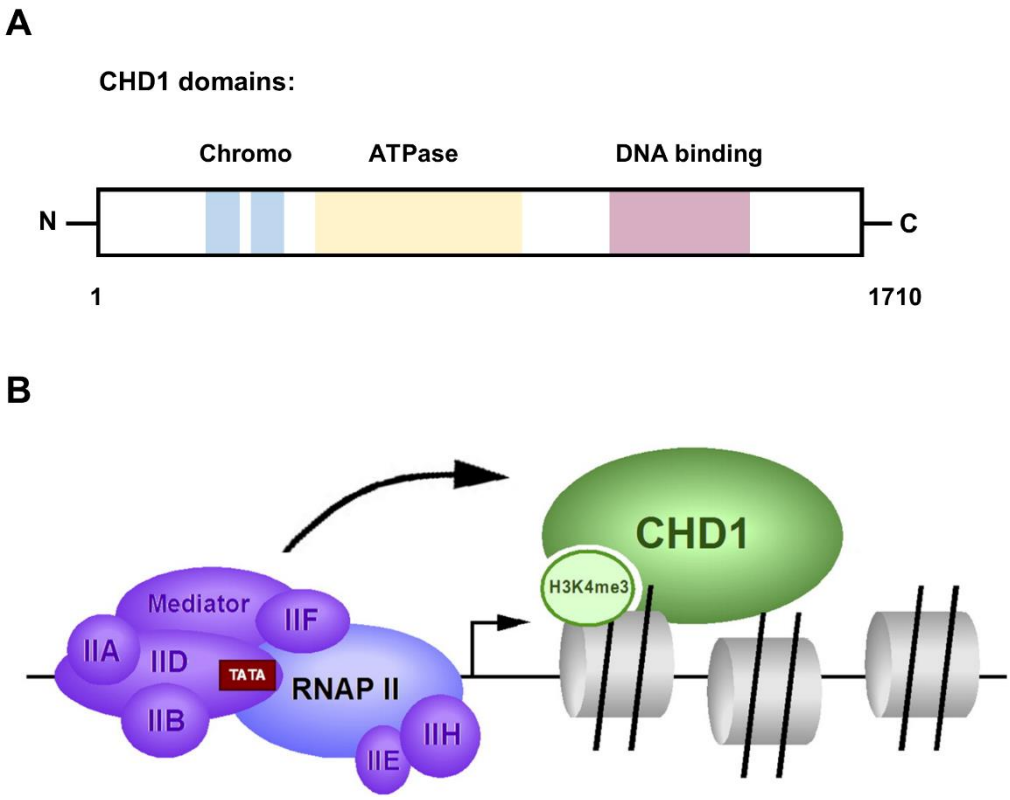

Figure 4:CHD1 domains and its interactions near the transcriptional start site in mammals. A The schematic view of chromodomain helicase DNA-binding protein 1 (CHD1) domains showing the N-terminal tandem chromodomain, SNF2-like ATPase domain and the C-terminal DNA binding domain within the 1710 amino acids long protein. **B** The model represents CHD1 binding to Histone 3 lysine 4 trimethylation at the transcriptional start site (small arrowhead). The transcription machinery (purple) of the RNA-Polymerase II (RNAP II) is recruited at the nucleosome free region with the TATA-box motif site on the DNA (brown box). CHD1 interacts with the mediator complex (Figure modified after Sims et al., 2007).

1.7 Stem cells and differentiation

Stem cells are undifferentiated and unspecialized cell types which have the ability to self-renew throughout their life-span. In general, different classes of stem cells exist which can be distinguished by their differentiation potential (Eckfeldt et al., 2005). Totipotent zygotes have the highest potential and give rise to a complete organism. Moreover, they can differentiate into pluripotent embryonic stem cells (ESC). ESC are characterized by their ability to generate derivatives of the three main germ layers: endoderm, ectoderm and mesoderm. Gradually, each of these three classes can further differentiate and form more committed somatic/adult stem cells (SSC) with the capacity of producing restricted numbers of distinct cells types.

Besides the natural occurring stem cells there exist also induced pluripotent stem cells (iPSC) which were introduced in 2006 and are considered to be a breakthrough

in the stem cell field (Takahashi and Yamanaka, 2006). It had been shown that mouse somatic cells can be transformed into ESC by only four transcription factors, namely POU class 5 homeobox 1 (POU5F1 or Oct3/4), SRY-box 2 (Sox2), v-myc avian myelocytomatosis viral oncogene homolog (c-Myc), and kruppel-like factor 4 (KLF4). However, the induced pluripotent stem cells (iPSC) partially retained the specific epigenetic memory of the parental somatic cell after reprogramming (Polo et al., 2010).

Although all cells within the hierarchical differentiation program carry the same genotype they vary greatly in function and morphology. To accomplish this the accessibility of the DNA in different cell types is altered by chromatin packaging, DNA methylation or regulatory RNAs which together is termed as epigenetic regulation (Jaenisch and Bird, 2003; Li and Reinberg, 2011). Already in 1957 Conrad Waddington introduced a model which describes the role of the epigenetic landscape underlying the stem cell differentiation and cell fate determination (Figure 5A) (Waddington, 1957). As depicted by Waddington, the epigenetic regulation with its various possible modifications in the genome has a great influence on the cell fate determination and regulation.

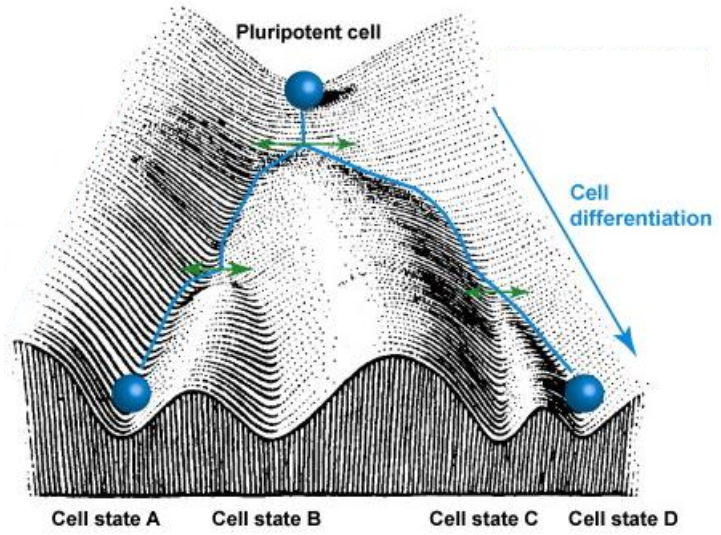

Figure 5: Epigenetic landscape model by Waddington. An undifferentiated pluripotent stem cell (blue ball) on the top of the landscape with a high differentiation potential can differentiate into more committed cell states “downhill”. Each event of cellular commitment will be accompanied by epigenetic changes that are depicted here as valleys which greatly influences the final outcome of the differentiated cell state (Figure modified after Barth and Imhof, 2010).

1.8 MSC and their differentiation potential

MSC are somatic multipotent stem cells which reside in pre- and postnatal tissues like muscle, fat, bone or cartilage (Owen and Friedenstein, 1988). Recent critical rethinking however questioned that there is only one general MSC cell type (Méndez-Ferrer et al., 2010; Zhou et al., 2014). Briefly, it is hypothesized that different types of MSC exist which vary in their internally determined cell fates, defined by their progenitors and tissue they are residing in (Kassem and Bianco, 2015). For example, adipose tissue derived MSCs are reprogrammable to osteoblasts but show neither spontaneous nor *in vivo* capacity to form bone, whereas bone marrow derived MSC do. Furthermore, different MSC can vary in their responses to differentiation stimuli in their outcome of cell states (Al-Nbaheen et al., 2012).

Bone marrow derived MSC (or skeletal stem cells) give rise to different tissues that are present in the skeleton such as bone, cartilage and fat. MSC reside perivascular within a stem cell niche inside the bone marrow together with hematopoietic stem cells (HSC) where they can mutually regulate each other's differentiation (Méndez-Ferrer et al., 2010). In addition, the strong vascular and microvascular environment of the bones influence the interplay between the hematopoietic and mesenchymal cell systems (Bianco and Robey, 2015). This shows that both systems are closely coupled and interact with each other in a paracrine manner. MSC express several receptor types such as insulin growth factor 1 receptor (IGF1R), transforming growth factor receptors (TGFR) or bone morphogenic protein receptors (BMPR) by which different signaling pathways can be triggered and thereby induce cell fate shifts with transcriptional and epigenetic changes.

1.8.1 Adipocyte differentiation

MSC differentiation to adipocytes is a postnatal event usually occurring with aging, however, it is also enhanced in diseased bone with low bone mass or in osteoporosis (Abdallah and Kassem, 2012; Rosen and Bouxsein, 2006). Different studies showed that a more adipocyte or osteoblast precursor cell type can favor the cell lineage differentiation which might be shifted with age or disease (Post et al., 2008; Russell et al., 2010). Adipocyte differentiation is mainly driven by the nuclear hormone receptor peroxisome proliferator-activated receptor gamma (PPARG), which is required for early adipocyte differentiation and maintenance of the adipocyte cell type (Rosen and MacDougald, 2006). Ligands which bind PPARG are still elusive, but

fatty acids and their metabolites or synthetically derivatives of glitazones such as troglitazone were shown to activate PPARG (Ahmadian et al., 2013; Mukherjee et al., 1997). Upon activation, PPARG forms a heterodimer with the retinoid X receptor (RXR) and regulates gene expression by interaction with CRC and co-activators like p300 (Gelman et al., 1999; Salma et al., 2004). Moreover, the transcription factors transcriptional CCAAT/enhancer-binding protein α (C/EBPα) and different KLFs play an important role in early and late stages of adipocyte differentiation (Mori et al., 2005; Oishi et al., 2005; Tang et al., 2003).

1.8.2 Osteoblast differentiation

The bone is a dynamic organ and undergoes life-long remodeling by continuous deposition and absorption of mineralized tissue (Clarke, 2008). In this process the role of osteoblast differentiation is indispensable to maintain the balance between bone formation and resorption. In general, osteoblast differentiation can be divided into early and late stages that involve progenitor cells, pre-osteoblasts and mature osteoblast formation (Long, 2012). During these stages the cells first undergo a high proliferation with subsequent deposition of an organic extracellular-scaffold which is finally mineralized in mature osteoblasts (Lian and Stein, 1992). The early cell lineage commitment happens under the influence of TGF-beta or BMP signaling (Chen et al., 2012).

The osteoblast progenitor cells and early differentiating osteoblasts are mainly determined by the transcription factor runt-related transcription factor 2 (RUNX2) which is activated by different signaling molecules such as TGF-beta and BMP-2 (Lee et al., 2000, 2003). However, unlike PPARG RUNX2 is not required for the maintenance of osteoblastic cell fate and even needs to be inactivated in mature osteoblasts (Komori, 2009).

Another important regulator of osteoblast differentiation is the canonical and non-canonical Wnt signaling pathway (Rodda and McMahon, 2006; Taipaleenmäki et al., 2011). Striking evidence for the role of the canonical pathway for osteogenesis was discovered by studies which showed that removal of β-catenin in MSC progenitor cells reduced osteoblast differentiation (Day et al., 2005; Hu et al., 2005). Interestingly, the repression of osteoblast differentiation was induced by the loss of the β-catenin and favored instead chondrogenic differentiation of the MSCs (Hill et

al., 2005; Rodda and McMahon, 2006). Although, the early osteoblast differentiation marker RUNX2 was still expressed in the surrounding tissue, Sp7 transcription factor (SP7), a marker for later osteoblast differentiation stages, was not.

The multifactorial Wnt signaling plays, however, a more complicated role in osteoblast differentiation by acting either as an activator or suppressor of differentiation which depends on the cell lineage commitment (Regard et al., 2012). Canonical Wnt activation in MSC causes increased proliferation but decreased differentiation (de Boer et al., 2004; Boland et al., 2004; Regard et al., 2012), whereas in pre-osteoblasts or early committed cells Wnt signaling enhances differentiation and growth (Eijken et al., 2008; Rodda and McMahon, 2006). Furthermore, the terminal differentiation can be blocked by active Wnt signaling (Kahler et al., 2006, 2008). This indicates a dynamic pattern of gene expression and complex regulation during osteoblast differentiation.

Concordant with these findings showed recent genome-wide transcriptome studies that the factors involved in osteogenesis can fluctuate in their expression levels during differentiation (Kulterer et al., 2007; Twine et al., 2014). One conclusion of the authors was that the temporal fine tuning in gene expression of osteoblast-associated factors could play pivotal roles for an ordered osteoblast differentiation. This is in line with the different impact of Wnt factors or RUNX2 which are pivotal at certain stages of differentiation but can be repressive at other stages during osteogenesis (Kahler and Westendorf, 2003; Kahler et al., 2006; Kanatani et al., 2006)

1.8.3 MSC in clinical studies

MSCs are one of the most often used cell types for stem cell therapy in clinical approaches (Wei et al., 2013). When comparing the registered clinical trials for MSC in the United States between December 2012 and December 2015 the number doubled from 281 to 565 (ClinicalTrials.gov). For stem cell therapy living cells are either systemically or locally applied so that they home to degenerated or injured tissue to restore its function or to support its regeneration. MSCs have the advantages that they are easy to isolate from different tissues within the body and can be expanded *ex vivo* (Zaher et al., 2014). Moreover, they have immunomodulatory properties which lower the danger of immune-rejection by the

host system (Atoui and Chiu, 2012). Although their division number *ex vivo* is limited, as they undergo replicative senescence, ways of immortalization by telomerase reverse transcriptase (TERT) were described without impairment of their differentiation potential (Simonsen et al., 2002). Nonetheless providing efficient *ex vivo* expansion without changing the cellular properties remain a concern in stem cell therapies (Hoch and Leach, 2014)

Preclinical studies of stem cell therapies showed that MSCs were already successfully used for tissue regeneration processes in liver, lung or bone (Amado et al., 2005; Kim et al., 2007; Lee et al., 2009; Parekkadan et al., 2007; Tzaribachev et al., 2008). In particular for the bone tissue repair of defective cartilage, treatment of patients with *osteogenesis imperfect* or bone fracture healing were reported (Gómez-Barrena et al., 2015; Le Blanc et al., 2005; Wakitani et al., 2007). Regenerative properties of MSC are either provided by direct differentiation into bone tissue within an organic scaffold implanted during surgery or by their paracrine signaling of cytokines inhibiting apoptosis and support angiogenesis (Rosset et al., 2014; Wei et al., 2013). Interestingly, co-transplantation of MSC and HSC increased tissue repair effects in a primate animal models which indicates a potential synergism between the two stem cell systems (Chapel et al., 2003).

Moreover MSC might be also suitable for treatment of osteoporosis (Antebi et al., 2014). Osteoporosis is a disease defined by porous and fragile bone caused mainly by an imbalanced system between bone formation and bone resorption (Rachner et al., 2011). Most of the actual approved therapies are antiresorptive approaches, however, enhancing the bone formation shows alternative ways of therapy which are likely to reduce negative side effects (Chen et al., 2014a). MSC cell therapy could support the bone building process by osteoblast differentiation at the porous sites in vivo (Antebi et al., 2014).

1.9 Aim of the study

The chromatin remodeler CHD1 is a well described co-activator of gene transcription and is associated with various transcription associated complexes. However, so far it is less clear if CHD1 can also act as a regulatory protein in gene expression and if it is required for gene induction. Here we hypothesize that CHD1 is necessary for gene specific expression during adipocyte and osteoblast differentiation and is required for the cell type change. To unravel the molecular mechanism of its gene regulation we performed genome-wide ChIP-seq and RNA-seq in control and CHD1 depleted condition. We focused on changes of the transcriptional hallmarks RNA-Pol II, H2A.Z and H2Bub1 of differentiation and CHD1 depletion regulated genes. Besides the mechanistic effect the biological impact on bone formation was investigated. Therefore, transcriptome wide analysis of deregulated osteoblast-specific differentiation genes was performed. Additionally, ectopic bone formation capacity of stable CHD1 depleted MSC was tested to test the role of CHD1 *in vivo*.

2 Material

2.1 Technical equipment

-150 °C Freezer (MDF-C2156VAN)	Panasonic, Kadoma, Japan
-20 °C Freezer	Liebherr GmbH, Biberach
2100 Bioanalyzer	Agilent Technology, Santa Clara, USA
-80 °C Freezer “Hera freeze”	Thermo Fisher Scientific, Waltham, USA
Agarose gel chamber	Harnischmacher Labortechnik, Kassel
Balance	Sartorius AG, Göttingen
Bandelin Sonoplus Sonicator	Bandelin electr. GmbH & Co. KG, Berlin
Biological Safety Cabinet “Safe 2020”	Thermo Fisher Scientific, Waltham, USA
Bioruptor® Plus sonication device	Diagenode SA, Liège, Belgium
Centrifuge (Megafuge 1.OR)	Thermo Fisher Scientific, Waltham, USA
Centrifuge 4 °C (5417R)	Eppendorf AG, Hamburg
Centrifuge 4 °C (Fesco 21)	Thermo Fisher Scientific, Waltham, USA
Counting chamber (Neubauer)	Brand GmbH & Co. KG, Wertheim
DynaMag™ 2	LifeTechnology, Carlsbad, USA
DynaMag™ 96 Side	LifeTechnology, Carlsbad, USA
Eclipse TS100	Nikon, Tokio, Japan
Electrophoresis & Electrotransfer Unit	GE Healthcare Europe GmbH, München
Gel iX Imager	Intas Science Imaging GmbH, Göttingen
HERAcell 150i CO_2 Incubator	Thermo Fisher Scientific, Waltham, USA
Imager Western Blot	Bio-Rad Laboratories, Hercules, USA
Inverse Microscope “Axiovert 40 CFL”	Carl Zeiss MicroImaging GmbH, Göttingen
Isotemp® water bath	Thermo Fisher Scientific, Waltham, USA
Magnet stirrer “MR3001”	Heidolph GmbH & Co. KG, Schwabach
Microcentrifuge C1413-VWR230	VWR, Radnor, USA
Microwave	Clatronic International GmbH, Kempen
Mini Trans-Blot™ Cell	Bio-Rad Laboratories, Hercules, USA
Mini-PROTEAN Tetra Cell	Bio-Rad Laboratories, Hercules, USA
Mr. Frosty® Cryo Freezing Container	Thermo Fisher Scientific, Waltham, USA
Nano Drop® ND-1000	Peqlab Biotechnology GmbH, Erlangen
Optical Reaction Module CFX96™	Bio-Rad Laboratories, Hercules, USA
pH meter inoLab®	WTW GmbH, Weilheim

Pipette Aid® portable XP	Drummond Scientific Co., Broomall, USA
Pipettes “Research” Series	Eppendorf AG, Hamburg
Power supply Power Pack P25T	Biometra GmbH, Göttingen
PowerPac™ Basic Power Supply	Bio-Rad Laboratories, Hercules, USA
PowerPac™ HC Power Supply	Bio-Rad Laboratories, Hercules, USA
Refrigerator	Liebherr GmbH, Biberach
Repeat Pipette	Gilson Inc., Middleton, USA
Scanner Epson V700 Photo	Seiko Epson, Suwa, Japan
Shaker “Rocky”	Schütt Labortechnik GmbH, Göttingen
Test tube rotator	Schütt Labortechnik GmbH, Göttingen
Thermal Cycler T100™	Bio-Rad Laboratories, Hercules, USA
Thermo mixer C	Eppendorf AG, Wessling-Berzdorf
Vortex-Genie 2	Electro Scietific Industr. Inc., Portland, USA
X-Ray Cassettes	Rego X-ray GmbH, Augsburg

2.2 Consumable materials

96-well Multiplate® PCR plate white	Bio-Rad Laboratories, Hercules, USA
Cell scraper (16 cm)	Sarstedt AG & Co., Nümbrecht
Cellstar 6- and 12-well cell culture plate	Greiner Bio-One GmbH, Frickenhausen
Cellstar PP-tube 15 and 50 ml	Greiner Bio-One GmbH, Frickenhausen
Cellstar tissue culture dish 100×20 mm	Greiner Bio-One GmbH, Frickenhausen
Cellstar tissue culture dish 145×20 mm	Greiner Bio-One GmbH, Frickenhausen
Cryo Tube Vial (1.8 ml)	Thermo Fisher Scientific, Waltham, USA
DNA loBinding Tube 1.5 and 0.5 ml	Eppendorf AG, Wessling-Berzdorf
Gel blotting paper (Whatman paper)	Sartorius AG, Göttingen
Hybond™ -PVDF Transfer Membrane	GE Healthcare Europe GmbH, München
Microtube 1.5 ml	Sarstedt AG & Co., Nümbrecht
Microtube 1.5 ml, conical	VWR International GmbH, Darmstadt
Microtube 2 ml	Sarstedt AG & Co., Nümbrecht
Millex-HV Filer (0.45µM) PVDF	Merck Millipore KGaA, Darmstadt
Parafilm® “M”	Pechiney Plastic Packaging, Chicago, USA
Pipette filter tips	Sarstedt AG & Co., Nümbrecht
Pipette tips	Greiner Bio-One GmbH, Frickenhausen
X-ray films “Super RX”	Fujifilm Corp., Tokyo, Japan

2.3 Chemicals

Acetic acid	Carl Roth GmbH & Co. KG, Karlsruhe
Adefodur WB developing concentrate	Adefo-Chemie GmbH, Dietzenbach
Adefodur WB fixing concentrate	Adefo-Chemie GmbH, Dietzenbach
Adenosin triphosphate	Fermentas GmbH, St. Leon-Rot
Agarose	Carl Roth GmbH & Co. KG, Karlsruhe
Agencourt® AMPure® XP Beads	Beckman Coulter Inc. Brea USA
Albumin Fraction V	Carl Roth GmbH & Co. KG, Karlsruhe
Ammonium persulfate	Carl Roth GmbH & Co. KG, Karlsruhe
Ammonium sulfate	Carl Roth GmbH & Co. KG, Karlsruhe
Ampicilin	AppliChem GmbH, Darmstadt
Anti-Anti	LifeTechnology, Carlsbad, USA
Aprotinin	Carl Roth GmbH & Co. KG, Karlsruhe
Bromophenol blue	Sigma-Aldrich Co., St. Louis, USA
Calcitriol	Biomol GmbH, Hamburg
Calcium Chloride	Carl Roth GmbH & Co. KG, Karlsruhe
Chloroform	Carl Roth GmbH & Co. KG, Karlsruhe
Dexamethasone	Sigma-Aldrich Co, St. Louis, USA
Diethylpyrocarbonate	Carl Roth GmbH & Co. KG, Karlsruhe
dihydrate	
Dimethyl sulfoxide	AppliChem GmbH, Darmstadt
di-Sodium hydrogen phosphate -	Carl Roth GmbH & Co. KG, Karlsruhe
Dithiothreitol	Carl Roth GmbH & Co. KG, Karlsruhe
DMEM	LifeTechnology, Carlsbad, USA
DMEM/F12	LifeTechnology, Carlsbad, USA
dNTP	Promega GmbH, Mannheim
Ethanol absolute	Th. Geyer GmbH & Co. KG, Renningen
Ethidium bromide	Carl Roth GmbH & Co. KG, Karlsruhe
Ethylenediaminetetraacetic acid	Carl Roth GmbH & Co. KG, Karlsruhe
Fetal Bovine Serum	Thermo Scientific HyClone, Logan,USA
Formaldehyde	Sigma-Aldrich Co., St. Louis, USA
Glycerol	Carl Roth GmbH & Co. KG, Karlsruhe

Glycine	Carl Roth GmbH & Co. KG, Karlsruhe
Hydrochloric acid	Carl Roth GmbH & Co. KG, Karlsruhe
Immobilon™ Western HRP substrate	Merck Millipore KGaA, Darmstadt
Insulin	Sigma-Aldrich Co, St. Louis, USA
Iodoacetamide	Sigma-Aldrich Co, St. Louis, USA
Isopropanol	Carl Roth GmbH & Co. KG, Karlsruhe
L-Ascorbic acid	Sigma-Aldrich Co, St. Louis, USA
Leupeptin	Carl Roth GmbH & Co. KG, Karlsruhe
Linear Acrylamide	Thermo Fisher Scientific, Waltham, USA
Magnesium chloride	Carl Roth GmbH & Co. KG, Karlsruhe
MEM α powder	LifeTechnologies AG, Carlsbad, US
Methanol	Carl Roth GmbH & Co. KG, Karlsruhe
Monopotassium phosphate	Carl Roth GmbH & Co. KG, Karlsruhe
N,N-Dimethylformamide	Sigma-Aldrich Co., St. Louis, USA
N-ethylmaleimide	Sigma-Aldrich Co., St. Louis, USA
Nonidet™ P40	Sigma-Aldrich Co., St. Louis, USA
Oil Red O	Sigma-Aldrich Co., St. Louis, USA
Opti-MEM	LifeTechnology, Carlsbad, USA
PBS tablets	LifeTechnology, Carlsbad, USA
Pefabloc SC	Carl Roth GmbH & Co. KG, Karlsruhe
Penicillin-Streptomycin solution	Sigma-Aldrich Co., St. Louis, USA
Peptone	Carl Roth GmbH & Co. KG, Karlsruhe
Polybrene	Sigma-Aldrich, St. Louis, USA
Potassium acetate	Carl Roth GmbH & Co. KG, Karlsruhe
Potassium chloride	AppliChem GmbH, Darmstadt
Potassium dihydrogen phosphate	Carl Roth GmbH & Co. KG, Karlsruhe
Propidium iodide solution	Sigma-Aldrich Co., St. Louis, USA
Protein A Sepharose™ CL-4B	GE Healthcare, Uppsala, Sweden
RNAiMAX	LifeTechnology, Carlsbad, USA
Roti®-Phenol	Carl Roth GmbH & Co. KG, Karlsruhe
Rotiphorese® Gel 30	Carl Roth GmbH & Co. KG, Karlsruhe
Rotipuran® Chloroform	Carl Roth GmbH & Co. KG, Karlsruhe
Rotipuran® Isoamylalcohol	Carl Roth GmbH & Co. KG, Karlsruhe
Sepharose™ CL-4B	GE Healthcare, Uppsala, Sweden

Skim milk powder	Carl Roth GmbH & Co. KG, Karlsruhe
Sodium acetate	Carl Roth GmbH & Co. KG, Karlsruhe
Sodium chloride	Carl Roth GmbH & Co. KG, Karlsruhe
Sodium deoxycholate	AppliChem GmbH, Darmstadt
Sodium dodecylsulfate	Carl Roth GmbH & Co. KG, Karlsruhe
Sodium hydroxide	Carl Roth GmbH & Co. KG, Karlsruhe
ß-Glycerolphosphate	Sigma-Aldrich Co., St. Louis, USA
SYBR Green	Roche Diagnostics GmbH, Mannheim
TEMED	Carl Roth GmbH & Co. KG, Karlsruhe
Tris	Carl Roth GmbH & Co. KG, Karlsruhe
Triton X-100	AppliChem GmbH, Darmstadt
Trypsin-EDTA	LifeTechnology, Carlsbad, USA
Tween-20	AppliChem GmbH, Darmstadt
α,α-Trehalose Dihydrate	Panreac AppliChem GmbH, Darmstadt

2.4 Kits and reagents

Agilent High Sensitivity DNA Kit	Agilent Technology, Santa Clara, USA
Agilent RNA 6000 Nano Kit	Agilent Technology, Santa Clara, USA
Lipofectamine™ 2000	LifeTechnology, Carlsbad, USA
Lipofectamine™ RNAiMAX	LifeTechnology, Carlsbad, USA
MicroPlex Library Preparation™	Diagenode SA, Liège, Belgium
NEBNext® Poly(A) mRNA Module	New England Biolabs, Ipswich, USA
NEBNext® Ultra™ Library Prep Kit	New England Biolabs, Ipswich, USA
Qubit dsDNA HS Assay	LifeTechnology, Carlsbad, USA

2.5 Nucleic acids

2.5.1 Vectors for viral particle production

Construct name	shRNA-sequence	Source
GIPZ shRNA-CHD1 #1 Clone V3THS_312675	TTTTTGTAAGAATCTCCCT	Dharmacon Inc (Lafayette, USA)
GIPZ shRNA-CHD1 #2 Clone V2THS_112971	ATAATTCAGAAATGAGATC	Dharmacon Inc (Lafayette, USA)
GIPZ non-targeting-control	TACTCTCGCCCAAGCGAG	Dharmacon Inc (Lafayette, USA)
psPAX2 packaging vector	-	V. Assmann UKE, Hamburg
pMD2.G envelope vector	-	V. Assmann UKE, Hamburg

2.5.2 Oligonucleotides

2.5.2.1 siRNA oligonucleotides

Name	Target Gene	siRNA Target Sequence	Source
siCHD1-1	CHD1	CAUCAAGCCUCAUCUAAUA	Dharmacon Inc (Lafayette, USA)
siCHD1-2	CHD1	GAUAAGAACUCAUGAAUGG	Dharmacon Inc (Lafayette, USA)
siCHD1-3	CHD1	GAAGAGAGCUGAAACUCAU	Dharmacon Inc (Lafayette, USA)
siCHD1-4	CHD1	GAAACAAGCUCUAGAUCAU	Dharmacon Inc (Lafayette, USA)
Luciferase GL2 duplex	-	CGUACGCGGAAUACUUCGA	Dharmacon Inc (Lafayette, USA)

For siCHD1 transfection reactions the individual siRNAs directed against CHD1 were pooled in a 1:1:1:1 ratio.

2.5.2.2 RT-PCR primers

For reverse transcription reaction random 9mer primer were used. The primers were

purchased from Sigma-Aldrich Co., St. Louis, USA

2.5.2.3 qPCR primers

Primers are shown in a 5´ to 3´ orientation. Own primers were designing by the program primer –blast available at NCBI (www.ncbi.nlm.nih.gov/tools/primer-blast/).

Name	Sequence	Source
18S rRNA F	AACTGAGGCCATGATTAA	Nagarajan et al. 2015
18S rRNA R	GGAACTACGACGGTATCTGA	Nagarajan et al. 2015
ALPL F	TGGGCCAAGGACGCTGGGAA	Karpiuk et al. 2012
ALPL R	AAGGCCTCAGGGGGCATCTCG	Karpiuk et al. 2012
AXIN2 F	ATTTCCCGAGAACCCACCGCCT	This study
AXIN2 R	GGCTGTGGCGGCTCTCCAAC	This study
BGLAP F	CACTCCTCGCCCTATTGGC	Karpiuk et al. 2012
BGLAP R	CTTGGACACAAAGGCTGCAC	Karpiuk et al. 2012
BMP4 F	GGAGCTTCCACCACGAAGAA	This study
BMP4 R	GGAAGCCCCTTTCCCAATCA	This study
CHD1 F	GCCAAGGTTTGTAGCCCTGA	This study
CHD1 R	GCACCAAGAATGAGCAAGCC	This study
COL11A1 F	CTCAGGGACCTGCAGGAAAG	This study
COL11A1 R	GGGTCACCTTTGAGACCAGG	This study
CTGF F	CACCCGGGTTACCAATGACA	This study
CTGF R	GGATGCACTTTTTGCCCTTCTTA	This study
DUSP1 F	GAGCTGTGCAGCAAACAGTC	This study
DUSP1 R	GGGCCACCCTGATCGTAGA	This study
EDN1 F	TTGAGATCTGAGGAACCCAC	This study
EDN1 R	CAGCGCCTAAGACTGCTGTT	This study
ELN F	TCCCGGGAGTTGGCATTTC	This study
ELN R	ACTGGGCGGCTTTGGC	This study
LPIN1 F	CCGCTCGGTGCAGACCAT	This study
LPIN1 R	GGACCCCCATCTTCCCAAAG	This study
LPL F	TCAGCCGGCTCATCAGTCGGT	Karpiuk et al. 2012
LPL R	AGAGTCAGCACGAGCAGGGCT	Karpiuk et al. 2012
PDK4 F	AGAGGTGGAGCATTTCTCGC	Karpiuk et al. 2012
PDK4 R	ATGTTGGCGAGTCTCACAGG	Karpiuk et al. 2012
PLIN1 F	ACCTCCTCCCTCCAGACAAG	This study
PLIN1 R	ATGGTCTGCACGGTGTATCG	This study
POSTN F	TTCATTGAAGGTGGTGATGGTCA	This study
POSTN R	CTTGCAACTTCCTCACGGGT	This study
PPARG F	ACCTCCGGGCCCTGGCAAAA	Karpiuk et al. 2012
PPARG R	TGCTCTGCTCCTGCAGGGGG	Karpiuk et al. 2012
RPLP0 F	GATTGGCTACCCAACTGTTG	Fritah et al., 2005
RPLP0 R	CAGGGGCAGCAGCCACAAA	Fritah et al., 2005

SIX1 F	AAGAACCGGAGGCAAAGAGAC	This study
SIX1 R	AAGGACCGAGTTCTGGTCTG	This study

2.5.2.4 ChIP primers

Primers utilized in ChIP qPCR are shown in 5´ to 3´ orientation.

Name	Sequence	Source
DUSP1 TSS F	CTGAAGCGAGGTTGACAGA	This study
DUSP1 TSS R	GGCCATGGTCATGGAAGTGG	This study
GAPDH TSS F	AAGAAGATGCGGCTGACTGT	Nagarajan et al., 2015
GAPDH TSS R	CGGCTACTAGCGGTTTTACG	Nagarajan et al., 2015
RPLP0 TSS F	CAATCAGAAACCGCGGATAG	Nagarajan et al., 2015
RPLP0 TSS R	CTTCGCGACCCTACTTAAAGG	Nagarajan et al., 2015
TFF TSS F	ACACCCACCTTCCACAACAC	Nagarajan et al., 2015
TFF TSS R	CAGGCTTCTCCCTTGATGA	Nagarajan et al., 2015

2.6. Proteins, enzymes, standards

2.6.1 Molecular weight standards

Gene Ruler™ DNA-Ladder	Fermentas GmbH, St. Leon-Rot
PageRuler™ Prestained Protein Ladder	Fermentas GmbH, St. Leon-Rot

2.6.2 Enzymes

Proteinase K	LifeTechnology, Carlsbad, USA
Reverse Transcriptase (M-MuLV)	New England Biolabs, FFM
RNase A	Qiagen GmbH, Hilden
RNase inhibitor	New England Biolabs, FFM
T4 DNA Ligase	New England Biolabs, FFM
Taq DNA Polymerase	Prime Tech, Minsk, Belarus

2.6.3 Antibodies

2.6.3.1 Primary antibodies

Antibodies used for ChIP and Western blot analysis and the respective dilutions

Target Protein	Cat. No°	ChIP	WB	Source
CHD1	A301-218A	1.5 µg	-	Bethyl Laboratories, Inc., Montgomery, USA
CHD1	sc-271636	-	1:10,000	Santa Cruz Biotech., Inc., Texas USA
H2A.Z	-	5 µl	-	AG Gaudreau
H2B	07-371	-	1:10,000	Merck Millipore, KGaA, Darmstadt
H2Bub1	5546	1.5 µg	-	Cell Signaling, Inc., Danvers USA
H2Bub1	-	-	1:50	Prenzel et al., 2011
HSC70	sc-7298	-	1:25,000	Santa Cruz Biotech., Inc., Texas USA
IgG (non-specific)	ab46540	1 µg	-	Abcam, Cambridge, UK
RNA-PolII	sc-899	1.5 µg	1:10,000	Santa Cruz Biotech., Inc., Texas USA
β-Actin	ab6276	-	1:10,000	Abcam, Cambridge, UK

The antibody dilutions for the immuno based analysis were supplemented with 0.01% sodium azide.

2.6.3.2 Secondary antibodies

Name	WB	Source
anti-mouse (IgG)-HRP	1:10,000	Santa Cruz Biotech., Inc., Texas USA
anti-rabbit (IgG)-HRP	1:10,000	Santa Cruz Biotech., Inc., Texas USA

2.7 Cells

Name	Species	Organ	Source
FOB 1.19	human	bone	T. Spelsberg, Mayo Clinic, USA (Harris et al., 1995)
HEK293T	human	kidney	V. Assmann, UKE, Hamburg
MSC	human	bone	M. Kassem, SDU, Denmark (Simonsen et al., 2002)

2.8 ChIP-seq datasets

Cell line	ChIP	Antibody	Source
FOB	H3K27ac	Diagenode, pAB-196	Z. Najafova (AG Johnsen)
MSC	H3K4me3	Diagenode Mab-003	M. Hennion (AG Johnsen)
MSC	H3K27ac	Diagenode, pAB-196	Z. Najafova (AG Johnsen)

2.9 Software

Name	Developer
Bio-Rad CFX Manager 3.1	Bio-Rad Laboratories, Hercules, USA
Bowtie1 Version 1.1.1	Langmead B. et al., 2009
Bowtie2 Version 2.1.0	Langmead B. et al., 2012
CEAS Version 1.0.2	Shin et al., 2009
Cistrome	Liu et al., 2011
Deeptool Galaxy Server 1.5.9.1.0	Ramirez et al., 2014
FastQC Version 0.11.2	S. Andrews (Babraham Institute)
Image Lab Version 5.2 build 14	Bio-Rad Laboratories, Hercules, USA
Integrative Genome Viewer 2	James T. Robinson et al., 2011
MACS2 Version 2.1.0.	Zhang et al., 2008
Primer designing tool NCBI/Primer-BLAST	Ye et al., 2012
SAMtools Version 0.1.19	Li et al., 2009
Statistical software R, Version 3.1.1	R Development Core Team 2008
useGalaxy Version 15.07	Giardine et al., 2005

R-packages	Developer
DESeq1 V1.16.0 – Bioconductor package	Anders and Huber, 2010
DiffBind V1.10.2 – Bioconductor package	Start and Brown, 2012, Ross-Innes et al., 2012

2.10 Buffers and media

Blocking solution: 1 x TBS-T, 5% (w/v) milk

Cell culture freezing medium: 42% (v/v) DMEM, 50% (v/v) FBS, 8% DMSO

ChIP crosslinking buffer: 1% or 1.42% Formaldehyde in PBS

ChIP IP buffer: 150 mM NaCl, 5 mM EDTA, 50 mM Tris (pH 8), 0.5% (v/v) NP-40, 1% (v/v) Triton X-100

ChIP Wash buffer: 500 mM LiCl, 20 mM EDTA, 100 mM Tris (pH 8.5), 1% (v/v) NP40, 20 mM NaF, 1% (w/v) Sodium deoxycholate

Dexamethasone stock solution: 100 µM Dexamethasone in 100% EtOH

Dilution buffer: 0.01% (w/v) SDS, 1.1% (v/v) Triton X-100, 1.2 mM EDTA, 16.7 mM Tris-HCl (pH 8.1), 167 mM NaCl

DMEM cell culture medium: phenol red-free supplemented with 10% FBS, 100 U/ml penicillin, 100 µg/ml streptomycin

DMEM-F12 cell culture medium: phenol red-free, high-glucose, supplemented with 10% FBS, 100 U/ml penicillin, 100 µg/ml streptomycin

Lämmli buffer (6×): 0.35 M Tris (pH 6.8), 30% (v/v) glycerol, 10% (w/v) SDS, 9.3% (w/v) DTT, 0.02% (w/v) bromphenol blue

MEM α cell culture medium: phenol red, L-glutamine, supplemented with 10% FBS, 100 U/ml penicillin, 100 µg/ml streptomycin

Nuclear preparation buffer: 150 mM NaCl, 20 mM EDTA, 50 mM Tris (pH 7.5), 0.5% (v/v) NP-40, 1% (v/v) Triton X-100, 20 mM NaF

PBS for cell culture: 1 PBS tablet per 500 ml ddH_2O

PBS: 137 mM NaCl, 2.68 mM KCl, 4.29 mM $Na_2HPO_4 \times 2H_2O$, 1.47 mM KH_2PO_4, (pH 7.4)

PBS-T: PBS including 0.1% (w/v) Tween-20

PCI: Phenol: Chloroform: Isoamylalcohol (25:24:1)

Proteinase inhibitor cocktail (ChIP): 1 µg/µl Aprotinin/Leupeptin, 10 mM Glycerol 2-phosphate disodium salt hydrate, 1 mM N-Ethylmaleimide, 1 mM Pefabloc, 1 mM $NiCl_2$ and 10 µM indole acetamide

Proteinase inhibitor cocktail (WB): 1 ng/µl Aprotinin/Leupeptin, 10 mM Glycerol 2-phosphate disodium salt hydrate, 1 mM NEM, 1 mM Pefabloc

qPCR buffer: 75 mM Tris-HCl (pH 8.8), 20 mM $(NH_4)_2SO_4$, 0.01% Tween-20, 3 mM $MgCl_2$, 200 µM dNTPs, 0.5 U/reaction Taq DNA Polymerase, 0.25% Triton X-100, 1: 80,000 SYBR Green I, 300 mM Trehalose and 30 nM primer

RIPA buffer: 1× PBS, 1% (v/v) NP-40, 0.5% (v/v) sodium deoxychelate, 0.1% (w/v) SDS

SDS separating gel (15%): 15% (v/v) acrylamide, 375 mM Tris-HCl (pH 8.8), 0.1% (w/v) SDS, 0.1% (w/v) APS, 0.04% (v/v) TEMED

SDS separating gel (6%): 6% (v/v) acrylamide, 375 mM Tris-HCl (pH 8.8), 0.1% (w/v) SDS, 0.1% (w/v) APS, 0.04% (v/v) TEMED

SDS stacking gel (5%): 5% (v/v) acrylamide, 125.5 mM Tris-HCl (pH 6.8), 0.1% (w/v) SDS, 0.1% (w/v) APS, 0.1% (v/v) TEMED

Sodium acetate: 3 M sodium acetate, (pH 5.2)

Sonication buffer 1: 10 mM EDTA, 50 mM Tris (pH 8), 1% (w/v) SDS

Sonication buffer 2: 300 mM NaCl, 40 mM EDTA, 100 mM Tris (pH 7.5), 2% (v/v) NP-40, 40 mM NaF

TAE buffer (50×): 2 M Tris, 1 M Acetic acid, 0.1 M EDTA

TBS: 150 mM NaCl, 2.68 mM KCl, 4.29 mM $Na_2HPO_4 \times 2H_2O$, 1.47 mM KH_2PO_4, (pH 7.4)

TBS-T: TBS including 0.1% (w/v) Tween-20

TE buffer: 10 mM Tris-HCl, 1 mM EDTA, (pH 8.0)

Tris-glycine electrophoresis buffer: 25 mM Tris, 200 mM Glycine, 0.1% (w/v) SDS

Western blot transfer buffer: 10% (v/v) 10× Western salts, 20% (v/v) Methanol

Western salts (10×): 1.92 M Glycine, 250 mM Tris-HCl (pH 8.3), 0.02% (w/v) SDS

3 Methods

3.1 Cell culture

3.1.1 Cell culturing

Bone marrow derived human mesenchymal stem cells (MSC) and human fetal osteoblast cells (FOB) were cultured at 37 °C and 34 °C, respectively, under 5% CO_2 atmosphere and maintained sub-confluent. MSC were grown in alpha modified Eagle's medium (αMEM) supplemented with 10% fetal bovine serum (FBS), 100 units/ml penicillin, 100 µg/ml streptomycin and the antifungal agent Fungizone® Antimyotic (25 µg/ml) (growth medium). Stable pGIPZ transduced MSC were grown in growth medium supplemented with 1 µg/ml puromycine (selection medium). FOB were cultured in Dulbecco's modified Eagle's medium-F12 (DMEM-F12) supplemented like MSC.

3.1.2 Adipocyte and osteoblast differentiation

Osteoblast differentiation of confluent cells was induced by addition of 10 mM β-glycerophosphate, 0.2 mM ascorbate, 10 nM calcitriol and 100 nM dexamethasone into the growth medium (osteoblast differentiation medium). FOB were shifted 4 h prior to the addition of the osteoblast differentiation mix from 34 °C to 39 °C to inactivate the stably integrated Large-T antigen, which drives proliferation. For adipocyte differentiation confluent cells were cultured in normal growth medium supplemented with 15% FBS and 2 µM insulin, 0.45 mM isobutylmethyl-xanthine, 10 µM troglitazone and 100 nM dexamethasone (adipocyte differentiation medium). The differentiation medium was changed every second day.

3.1.3 Reverse transfection

Small interfering RNA (siRNA) was transfected with Lipofectamine® RNAiMAX according to the manufacturers reverse transfection protocol. Briefly, 30 pmol of siRNA were mixed together with 5 µl RNAiMAX reagent in 500 µl of optiMEM and incubated for 20 min at room temperature. In the meantime, cells were trypsinized and suspended in growth medium without antibiotics or antifungal reagents supplemented (transfection medium). Then 250,000 cells, counted in a Neubauer counting chamber, were seeded in 1.5 ml of transfection medium into a well of a 6-well plate. After 20 min of incubation time the transfection mix was added directly to the medium and incubated for 16 h on the cells. Thereafter the medium was changed

to normal growth medium. For transfections in 10 or 15 cm plates each factor in the mix was scaled up by a factor of 4 or 8 respectively.

3.1.4 Forward transfection

During a differentiation experiment for more than 4 days the cells were transfected again 3 days after the last transfection with siRNA by Lipofectamine® RNAiMAX based on the manufacturer forward transfection protocol. Per Well of a 6-well plate 35 pmol of siRNA were mixed with 7.5 µl RNAiMAX in 500 µl optiMEM and incubated for 20 min at room temperature. Meanwhile the growth medium on the cells was removed and replaced with 1 ml of transfection medium. 20 min after incubation the transfection mix was added directly into the medium and replaced by the respective differentiation medium after 6 to 8 h.

3.1.5 Generation of stable cell lines by lentiviral infection

A microRNA-adapted short hairpin RNA (shRNA), coded on the GIPZ plasmid was stable integrated into the genome by lentiviral transformation. Prior to production of the lentiviral particles the shRNA expressing sequence on the GIPZ plasmid was checked by Sanger sequencing. For the viral particle production human embryonic kidney 293 cells (HEK293T) cells were used. In the following the production of stable cell lines is described.

3.1.5.1 Transfection of HEK293T cells

80% confluent HEK293T cells grown in a 10 cm plate were transfected with the GIPZ, lentiviral packaging and envelope plasmid by Polyethylenimine (PEI) transfection with the following mix:

Reagent	Amount
Vector plasmid pGIPZ	15 µg
Packaging plasmid psPAX2	10 µg
Envelope plasmid pMD2.G	5 µg
Transfection reagent PEI	50 µg
Transfection solution optiMEM	1.1 ml

First, the plasmids were added into the optiMEM solution and then mixed with PEI. The mixture was vortexed for approximately 8 secs and incubated then for 10 min at room temperature. Within the incubation time the medium on the cells was replaced with 6 ml of transfection medium. 1 ml of the transfection mix was pipetted dropwise to the medium of the HEK293T cells. The cells were subsequently incubated for 14 – 16 h before the medium was replaced with normal growth medium. Two days after transfection the constitutive expression of GFP, encoded by the transfected GIPZ plasmid, was controlled by fluorescence microscopy.

3.1.5.2 Collection of viral supernatant

With a transfection efficiency greater than 70% the viral particles were harvested by centrifugation of the supernatant at 300 g for 3 min and subsequent filtered through a 0.45 µm, non-pyrogenic filter. The filtered supernatant was aliquot and stored for either up to 24 h at 4 °C or was snap frozen in liquid nitrogen and stored at -80 °C.

3.1.5.3 Lentiviral infection of cells

For the lentiviral infection of cells 50 – 70% confluent MSC or FOB grown in a 10 cm plate were infected by addition of 1 ml virus particle supernatant into antibiotic free growth medium supplemented with 8 µg/ml polybrene. After 24 h were the cells washed two times with PBS and normal growth medium was added. The infection and stable integration of the pGIPZ part were controlled by puromycine selection, which resistance gene is encoded on the integrative part. Cells were thereafter maintained in selection medium.

3.2 Chemical staining

3.2.1 Oil Red O staining

Oil Red O staining was used to stain lipid droplets of adipocyte differentiated cells. Therefore, cells were washed once with PBS and fixed in a 10 % formalin solution in PBS for 30 min at room temperature. Meanwhile the staining solution was prepared by mixing 3 parts of Oil Red O stock solution with 2 parts of deionized water. The mixture was incubated for 10 min at room temperature and filtered through a 0.45 µm pore filter. After fixation the cells were washed twice with deionized water and incubated while covered with 60% isopropanol for 5 min. Thereafter the isopropanol was replaced with the staining solution and incubated for 5 min. Finally, the cells were washed carefully with deionized water until the water rinsed off clear. Pictures

of the stained cells were taken with a microscope operated at 10- or 20-fold magnification.

3.2.2 Alkaline phosphatase staining

Osteoblast differentiated cells were stained for alkaline phosphatase activity. The staining solution was prepared by dissolving 5 mg of Naphtol AS-MX in 200 µl of NN-Dimethyl formamide. The solution was gently mixed and pipetted into 50 ml of 100 mM Tris-HCl pH 8.4 solution. 30 mg of Fast Blue RR salt were added subsequently to the mixture and vortexed until the solution was homogeneous. Finally, the staining solution was filtrated through a 0.45 µm pore filter. The cells were fixed for 15 min with 4.8% formaldehyde in PBS. Subsequently the cells were washed two times with PBS and covered with the staining solution for a minimum of 15 min in the dark. Afterwards the cells were washed carefully with deionized water until the water rinsed off clear. The stained cells were either scanned within the whole well or images were taken at 10- or 20-fold magnification on a microscope.

3.3 Ectopic bone formation experiment

The ectopic bone formation experiment was performed in the group of Prof. Dr. Moustapha Kassem, University of Southern Denmark by Nicholas Ditzel. For the experiment three different stable transformed MSC cell lines with either two individual shRNA directed against CHD1 or one non-targeting control shRNA were sent on dry ice. The experiment was performed as described (Chen, L. and Ditzel, N., 2015).

3.4 Molecular biology

3.4.1 RNA isolation

RNA isolation was performed according to the manufacturers' instructions. For cells grown in a 6-well plates 500 µl of QIAzol reagent was added to the cells and incubated for 3 min at room temperature. Afterwards the cells were scraped and transferred to a reaction tube with 100 µl Chloroform and vortexed for 15 sec. The mix was centrifuged for 15 min at 12,000 g and subsequently the aqueous supernatant was transferred to a fresh tube with 99% Isopropanol in a 1:1 ratio. The solution was incubated overnight at -20 °C. The next day the solution was centrifuged for 30 min at 15,000 g and subsequently washed two times with 70% ethanol at 12,000 g. The RNA pellet was air dried and solved in 30 µl nuclease free water. The

concentration was measured on a Nanodrop and used for complementary DNA synthesis or for RNA-sequencing library preparation.

3.4.2 complementary DNA synthesis

1 µg of RNA was diluted in 10 µl of nuclease free water and supplemented with 2 µl of 15 µM 9mer random primer and 4 µl of 2.5mM dNTP to a volume of 16 µl. The mix was incubated for 5 min at 70 °C and then placed immediately on ice. After the samples cooled down 0.125 µl of 25 U MMLV-reverse transcription enzyme and 0.25 µl of 10 U Murine RNase-Inhibitor were added together with the reverse-transcription buffer to a final volume of 20 µl. The mix was incubated for 1 h at 42 °C and subsequently heat inactivated at 90 °C for 10 min. The complementary DNA (cDNA) was diluted to 50 µl with nuclease free water and used for real-time quantitative PCR (qPCR).

3.4.3 qPCR reaction

Per reaction either 1 µl of cDNA or diluted DNA of a ChIP experiment was mixed with 24 µl of qPCR buffer. Samples were pipetted in technical duplicates per qPCR measurement. For amplification and read out the following qPCR program was used:

Step	Temperature	Time	Number of cycles
Step 1	95 °C	2 min	1
Step 2	95 °C	15 sec	40 - 45
Step 3	60 °C	1 min	

For PCR amplification step two and three were repeated 40 or 45 times for cDNA or ChIP samples respectively. Subsequent to the PCR amplification a melting curve of the PCR products was measured by a read out every 0.5 °C increasing from 60 °C to 90 °C. Signal intensities of the samples were read out by quantification relative to a dilution curve. Gene expression values were divided over unaffected control genes (*RPLP0* and 1*8S rRNA*) and averaged for at least biological triplicates.

3.4.4 Chromatin immunoprecipitation

Chromatin immunoprecipitation (ChIP) was performed according to a modified protocol of (Gomes et al., 2006; Nelson et al., 2006). All ChIP experiments were performed in biological triplicates.

3.4.4.1 Crosslinking

First protein-protein and DNA-protein interactions were cross-linked with 1 or 1.42% formaldehyde in PBS for 10 min at room temperature. 1.42% formaldehyde concentration was used to ChIP CHD1, all other ChIP crosslinking reactions were performed with 1% formaldehyde concentration. The crosslinking reaction was quenched for 5 min by addition of glycine to a final concentration of 125 mM. The cells were washed two times with ice-cold PBS and scraped in nuclear preparation buffer supplemented with the ChIP inhibitors cocktail. The cell nuclei were extracted by careful mixing and subsequent centrifugation at 10,000 g for 5 min. This step was repeated one time. Thereafter the cell nuclei pellet was either snap frozen in liquid nitrogen and stored at -80 °C or further processed.

3.4.4.2 Sonication

The chromatin was sheared to 300 to 600 bp fragments by ultrasound sonication. Therefore, the nuclei were resuspended in 120 µl sonication buffer 1 (+ proteinase inhibitor cocktail) and incubated for 10 min on a rotating wheel at 4 °C. Notably, for CHD1 ChIP the concentration of the sonication buffer 1 was decreased to 0.2%. After incubation 120 µl sonication buffer 2 (+ proteinase inhibitor cocktail) was added and the suspension was mixed well. Subsequently the chromatin was sonicated with the Bioruptor® for 30 cycles, each cycle containing a 30 sec sonication pulse and a 30 sec pause. For the CHD1-ChIP the chromatin was sheared for 60 cycles.

3.4.4.3 Size control of sonicated fragments

The shearing process was controlled by isolation of the DNA and agarose gel electrophoresis. 5% of the sheared chromatin extract was added to 100 µl of sonication buffer 1 plus 1 µl proteinase K (20 µg/µl) and incubated over night at 65 °C, shaking at 800 rpm. The next day 100 µl deionized water, 10 µl LiCl (8 M), 2 µl linear polyacrylamide (5 µg/µl) were mixed to isolate the DNA by a Phenol-/Chloroform-/ Isoamyl (PCI) extraction. PCI was added in a one to one ratio to the solution, vortexed for 30 secs and centrifuged at 16,000 g for 2 min. The aqueous supernatant was transferred into a fresh tube and another extraction from the

remaining PCI solution was performed by adding 200 µl 10 mM Tris-HCl pH 8 and repetition of the first step of the PCI extraction. The supernatant was added to the first one, mixed with 99% EtOH in a 1:2.5 ratio and incubated over night at -20 °C. The DNA was precipitated by centrifugation at 15,000 g at 4 °C for 30 min with one wash step afterwards by addition of 70 % EtOH and subsequent centrifugation. The pellet was air dried and dissolved then in 10 mM Tris pH 8, containing RNaseA (0.1 µg/ µl) and incubated for 1 h at 37 °C. The DNA fragment size was analyzed by a HD-green 1.5 % agarose gel.

3.4.4.4 Chromatin immunoprecipitation

After control of the correct DNA fragment size the specific protein-DNA complexes were immunoprecipitated. First, unspecific binding to sepharose was decreased by addition of 100 µl 50% slurry sepharose in a total volume of 1 ml of dilution buffer (+ proteinase inhibitor cocktail). The extracts were incubated for 1 h at 4 °C on a rotating wheel. After removal of the sepharose by centrifugation at 10,000 for 5 min, the cleared chromatin extracts were split for ChIP, unspecific IgG control and a 10% input sample (for dilutions of antibodies for ChIP see Material – 2.6.3.1). The ChIP and control samples were filled up with immuno-precipitation buffer (IP-buffer) (+ proteinase inhibitor cocktail) to a total volume of 800 µl and incubated overnight on a rotating wheel at 4 °C. After 14 – 18 h incubation 30 µl of 50% slurry protein-A or protein-G sepharose coupled beads, for rabbit or mouse antibody respectively, were added, and incubated for 2 h on a rotating wheel at 4 °C. After incubation the beads were washed three times with IP-buffer, two times with ChIP wash buffer, three times with IP-buffer again and finally two times with TE-buffer. Between each step the coupled beads were mixed carefully and centrifuged for 2 min at 2,000 g at 4 °C.

3.4.4.5 Isolation of precipitated DNA

The precipitated chromatin was treated with RNAseA (0.2 µg/µl) at 37 °C for 30 min and subsequently the proteins were digested by addition of 1 µl Proteinase-K (20 µg/ml) incubating overnight on a shaker at 65 °C at 800 rpm. The next day the DNA was isolated by PCI extraction identical as performed previously (see 3.3.4.3) and transferred afterwards to DNA low-binding tubes to precipitate overnight. The next day the solution was centrifuged at 15,000 g for 30 min at 4 °C, washed two times with 70 % EtOH and the pellet was subsequently air dried. The pellet was solved in 20 µl of nuclease free water and the DNA concentration was measured by Qubit®

assay according to manufacturer´s protocol. For ChIP-qPCR the DNA was diluted in a ratio of 1:5.

3.5 Protein analysis

3.5.1 Sample preparation

For protein extraction the cells were scraped in ice cold RIPA-Buffer supplemented with the proteinase inhibitor cocktail. The cell lysate was sonicated either by Bandelin Sonoplus tip sonicator for 15 pulses, 10% intensity 3 sec on and off, or by the Diagenode Bioruptor for 15 min high intensity with 30 secs on and off. Before size separation of the proteins the sheared whole cell lysates were diluted with Laemmli buffer to 1x and heated for 10 min at 95 °C. The samples were loaded to an appropriately concentrated polyacrylamide gel respective for the protein size to separate (PAA-gel). The samples and a control protein size ladder were separated by applying constant 100 V.

3.5.2 Western blot and immunostaining

Subsequent to gel electrophoresis the PAA-gel was transferred to a polyvinylidene difluoride (PVDF) membrane using the wet electro blot system. The electro blotting was performed in Western blot transfer buffer according to the manufacturer's instructions. After set up, the proteins were blotted to the membrane for 1.5 h with 100 V. After the transfer, the membrane was stained with Ponceau-S and blocked for unspecific antibody binding in 5 % skim-milk in TBS-T for 1 h at room temperature. Next, the membrane was incubated with the primary antibody in a 5 % skim-milk TBS-T solution over night at 4 °C on a rotator within a 50 ml reaction tube. The next day the membrane was washed 3 times for 10 min in TBS-T and incubated subsequently for 1 hour on a shaker with a secondary horseradish peroxidase (HRP) coupled antibody directed against the primary antibody. After incubation the membrane was washed 3 times in TBS-T and the chemiluminescence signal of the HRP was monitored by an X-ray film or a gel imaging system.

3.6 Next generation sequencing

3.6.1 Library preparation

RNA and DNA were processed by library preparation for unstranded sequencing in biological duplicates for RNA-seq and triplicates for ChIP-seq. In the following the different library preparation protocols for RNA and DNA are described.

3.6.2 RNA-library preparation

Previous to the RNA library preparation the sample quality was controlled for its RNA integrity. Therefore, the RNA was separated by size with a RNA Nano chip on a Bioanalyzer. To estimate the integrity of the RNA a program calculated a RNA integrity number (RIN) based on degradation products and the ratio between the *28S rRNA* and *18S rRNA*. If the samples had a RIN greater or equal to 7 they were processed for the RNA library preparation. The preparation was performed as described in the NEBNext® Ultra™Library Prep Kit. Briefly, 1 µg of total RNA was measured by Nanodrop and used as starting material. The mRNA was isolated by pull down via polyadenylated coated magnetic beads. After several washing steps the mRNA was fragmented at 94 °C and applied for the first and subsequently second strand cDNA synthesis. Single base overhangs at the 5´-ends were repaired and sequencing adaptors were ligated to the cDNA strands. To barcode the samples, the processed cDNA was amplified by PCR with one common and one individual primer. This allows later during sequencing to distinguish individual samples in one sequencing lane. Subsequently the DNA concentration was measured by Qubit® Fluorometer and the length of the library fragments were detected on a Bioanalyzer by a High Sensitivity DNA chip.

3.6.3 DNA-library preparation

The library preparation for ChIP DNA was performed with the MicroPlex™ Library Preparation Kit v2 from Diagenode® and used according to the manufacturer's protocol. The CHD1 ChIP DNA library preparation was performed using the NEBNext® Ultra™ DNA Library Prep Kit for Illumina® according to the manufacturer's protocol. As starting material an equal amount of DNA (between 2 – 10 ng) per ChIP condition was used. Prior to library preparation the DNA was sheared on the Bioruptor for 30 cycles, each cycle divided into 30 sec sonication and 30 sec pause. The library preparation was performed similar to the RNA library preparation protocol above, except the polyadenylated bead purification, heat

fragmentation and reverse transcription of RNA to cDNA, which is described in more detail in the manufacturer´s protocol.

3.6.4 Sequencing

For sequencing up to 12 samples were pooled to a final concentration of 10 nm or 2 nm depending on the lowest concentrated sample after the library concentration. The samples were sequenced on Illumina® HiSeq 2000 sequencers at the Heinrich-Pette-Institute, Hamburg or the Transcriptome Analysis Laboratory (TAL), Göttingen.

3.7 Bioinformatic processing of sequencing data

3.7.1 Mapping of ChIP-seq reads to the genome

The ChIP sequencing reads received from the sequencing facilities or reads downloaded from public available datasets (see Material 2.8 ChIP-seq datasets) were controled for their quality by FASTQ quality check (FastQC) (S. Andrews Babraham Institute) and mapped to the human genome (*hg19*, GRCh37) via Bowtie1 (Langmead et al., 2009). Bowtie1 parameters were set to parameters -m 1 -k 1. The output files in sequence alignment format /map (SAM) were then transformed to binary alignment format/ map (BAM) by the software package SAMtools (Li et al., 2009).

3.7.2 Peak calling via MACS2

Mapped and BAM formatted reads were analyzed for significantly, above background enriched genome regions by the peak calling software model-based analysis of ChIP-seq 2 (MACS2) (Zhang et al., 2008). The background was defined by the sequenced input. As parameter the genome (-g) was set to hs (homo sapiens), the q-value (-q) was set to 0.05 and the input format (-f) was specified to BAM. The narrowpeak option was used for all datasets except RNA-Pol II and H2Bub1. For the peak calling the BAM files of the samples were merged for each condition.

3.7.3 RNA-seq analysis

The sequenced RNA in FASTQ format were mapped to the human reference transcriptome (UCSC hg19) by Bowtie2 with default parameters (Langmead and Salzberg, 2012). The reads per gene were counted by a homemade script, kindly provided by Malik Alawi, UKE Hamburg, Bioinformatic service facility. Subsequently the raw reads were normalized by the DESeq package using the default protocol parameters (Anders and Huber, 2010). For further analysis of the DESeq output

matrix R statistical software or Microsoft Office Excel was used (R Development Core Team, 2008).

3.7.4 Normalization and calculation of ChIP-seq binding affinities

BAM formatted files were uploaded to the public available deepTools server to normalize the sequencing reads either by the bamCompare or bamCoverage tools (Ramírez et al., 2014).. The bamCompare tool calculates a ratio between input and ChIP-seq file over all genomic regions subset to defined region sizes (bins). The parameter was set as default with a bin size of 50 bp. Specific genomic loci, described by the ENCODE Project Consortium as artificial, high signal regions, were excluded for calculations for the scaling factor. Reads were normalized by reads per genomic content (RPGC) to a 1x depth of coverage. Therefore, the total number of mapped reads were multiplied with the fragment length and divided by the effective genome size (2.7 billion). Further settings were set as default in the bamCoverage tool. To calculate the ChIP-seq signal strength at defined genomic regions the tool computeMatrix was used with default settings. The visualization of the computed matrix was done either by the profiler (aggregation plot) or heatmapper (heatmaps).

3.7.5 Visualization by IGV

To visualize profiles of normalized sequencing intensities on the genome at individual regions the Integrative Genome Viewer software was used (Robinson et al., 2011). As input bamCoverage files were used. Tracks were if necessarily overlaid.

3.7.6 Analysis in R

For subset and filtering of datasets as well as calculation of Boxplots and scatter plots the R statistical software was used. For statistical test of non-parametric distributions, the Wilcoxon Rank-Sum test was performed with default conditions set in R. For parametric distributions the Welch´s t-test was used. Correlation co-efficiencies were calculated by the Pearson method with default parameter set in R.

3.7.7 Cis-regulatory element annotation system

By cis-regulatory element annotation system (CEAS) software quantitatively representation of protein binding sites within genomic functional regions were represented (Shin et al., 2009). As an input BED and bigwig files received after MACS2 analysis were used in CEAS with default parameters for the human genome (hg19).

3.7.8 DAVID based analysis of RNA-sequencing

The database for annotation, visualization and integrated discovery (DAVID) software was used for functional annotation of gene ontology (GO) terms (Huang et al., 2009). As a background file the default human genome file within the DAVID software was used.

3.7.9 DiffBind and calculation of RNA-Pol II stalling ratios

DiffBind is a program, which was used to calculate ChIP-seq biding intensities at defined genomic regions with statistical differential binding analysis for biological replicates (Ross-Innes et al., 2012). For calculating the stalling ratio of RNA-Pol II in siCon or siCHD1 treated FOBs the occupancy of RNA-Pol II was measured at TSS-regions as well as the gene body similar as previously described in Lin et al., 2012. Briefly, regions 300 bp up- and downstream of the TSS as well as the gene body were used as input files in bed format for the DiffBind software. The gene body was defined as the region between 30% of the gene length downstream of the TSS to 3 kilobase pair (kb) downstream of the TTS (for graphical illustration see Figure 22). Moreover, all genes shorter than 600 bp were excluded from the analysis. As an output of DiffBind a normalized count matrix was saved for all individual TSS and GB regions with the respective binding intensity values. Values equal to background were excluded from the analysis. For calculation of the stalling ratio the value at the TSS was divided with the value calculated at the gene body.

4 Results

4.1 CHD1 depletion impairs MSC and FOB differentiation

Cellular differentiation is orchestrated by repression and activation of genes mediated by transcription factors and specific signaling pathways. Gene expression changes are often accompanied and maintained by rearrangements in chromatin and histone modifications. In this study the role of the chromatin remodeler CHD1 during the adipocyte and osteoblast differentiation processes was studied. For this purpose multipotent human bone marrow derived mesenchymal stem cells (MSC) (Simonsen et al., 2002) and fetal osteoblast 1.19 cells (FOB) (Harris et al., 1995) were used as a model system. FOB can be differentiated to osteoblasts, and MSC to osteoblasts and adipocytes (Bianco and Robey, 2015; Subramaniam et al., 2002). Further, both cell lines have the potential to form ectopic bone *in vivo* (Simonsen et al., 2002). Since they have been used previously already for over a decade in various differentiation studies they are well described human differentiation models.

Here the differentiation potential of MSC and FOB was studied prior to and post CHD1 depletion. RNA, protein and cell staining of undifferentiated and differentiated adipocytes or osteoblasts, transfected either with CHD1 siRNA (siCHD1) or as a control with luciferase siRNA (siCon), were analyzed.

As expected, osteoblast differentiated MSC and FOB showed cell-type-associated staining by alkaline phosphatase liver/ bone/ kidney (ALPL) specific activity (Figure 6A, Figure 7A), whereas in undifferentiated MSC almost no staining was detected (FOB undifferentiated not shown). Interestingly, stronger ALPL staining was observed in CHD1 depleted MSC-derived osteoblasts compared to siCon transfected cells (Figure 6A). While ALPL staining in FOB after five days of differentiation was similar in control transfected compared to CHD1 transfected cells, the ALPL signal intensity was slightly decreased seven days after differentiation in CHD1 reduced conditions (Figure 7A). This indicates a dynamic and cell-type-specific regulation of *ALPL* in the context of reduced CHD1 levels. Adipocyte-differentiated cells showed an accumulation of lipid droplets compared to undifferentiated control (Figure 6A, panels to the right), which was reduced after CHD1 depletion. This suggests a role of CHD1 in adipocyte differentiation.

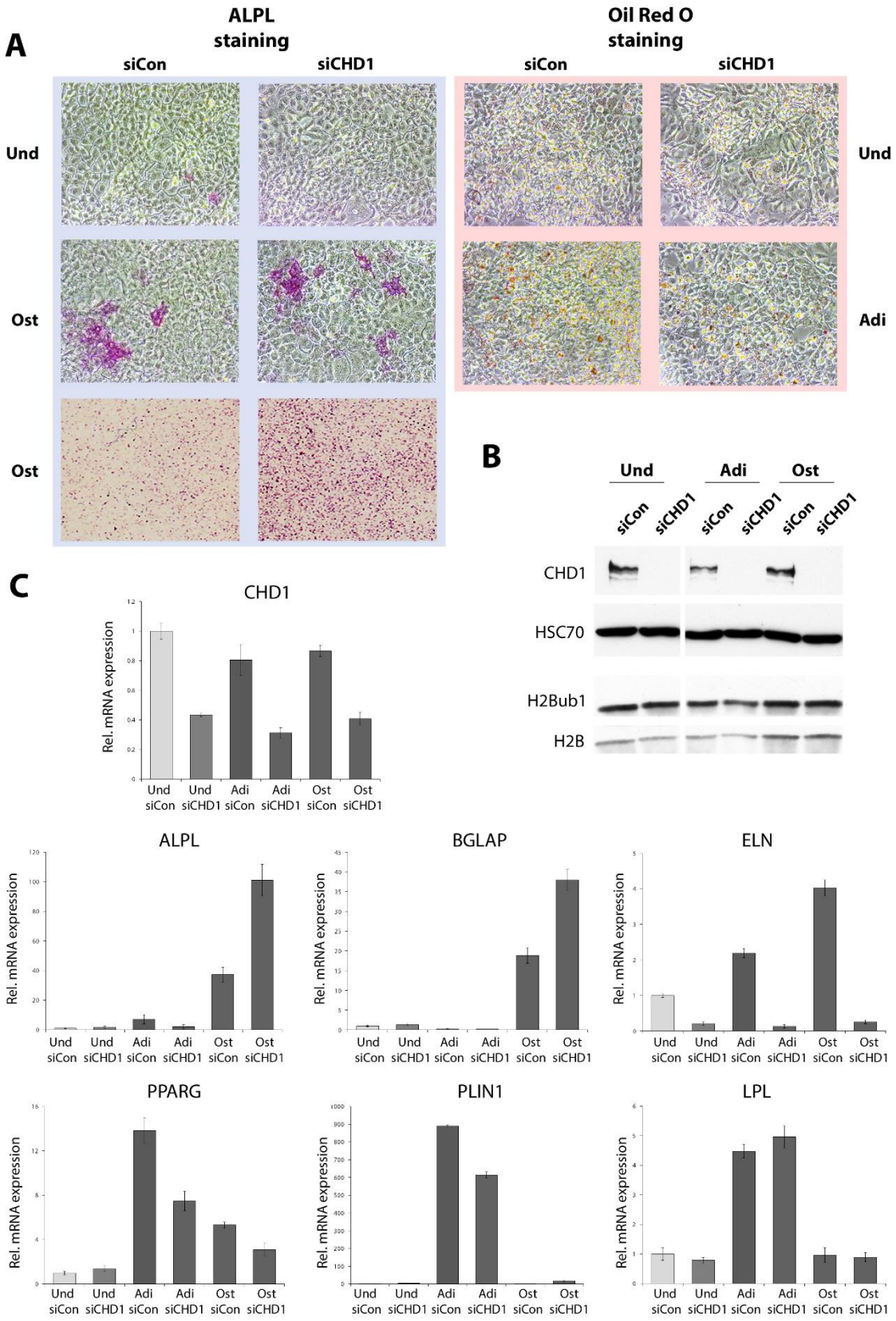

Figure 6: CHD1 depletion alters adipocyte and osteoblast differentiation in MSC. A ALPL activity staining of cells (blue-framed left panels) or of lipid droplets by Oil Red O (red-framed right panels) of osteoblasts (Ost), adipocytes (Adi) or undifferentiated control cells (Und) transfected either with siRNA

directed against CHD1 (siCHD1) or luciferase (siCon). Cells were differentiated for five days and images taken after staining by bright-field microscopy with 10x (second row panels) or 4x (third row panels) magnification. **B** Immunodetection of CHD1, mono-ubiquitinated H2B (H2Bub1), heat shock protein family A member 8 (HSC70) or H2B with antibodies by Western blot analysis of whole cell protein lysates of differentiated MSC, transfected with siRNA as described in A. **C** Relative mRNA levels of specific genes (see below) in MSC transfected and differentiated as described in A. The genes analyzed by real time quantitative PCR (qPCR) with gene specific primers and normalized to the *18S rRNA* gene expression were the osteoblast associated genes osteocalcin (*BGLAP*), alkaline phosphatase (*ALPL*), elastin (*ELN*) and the adipocyte associated genes peroxisome proliferator-activated receptor gamma (*PPARG*), lipoprotein lipase (*LPL*), periliplin 1 (*PLIN1*). Values are shown relative to the expression in undifferentiated cell under siCon-transfected conditions. Error bars represent the standard deviation of at least three biological replicates.

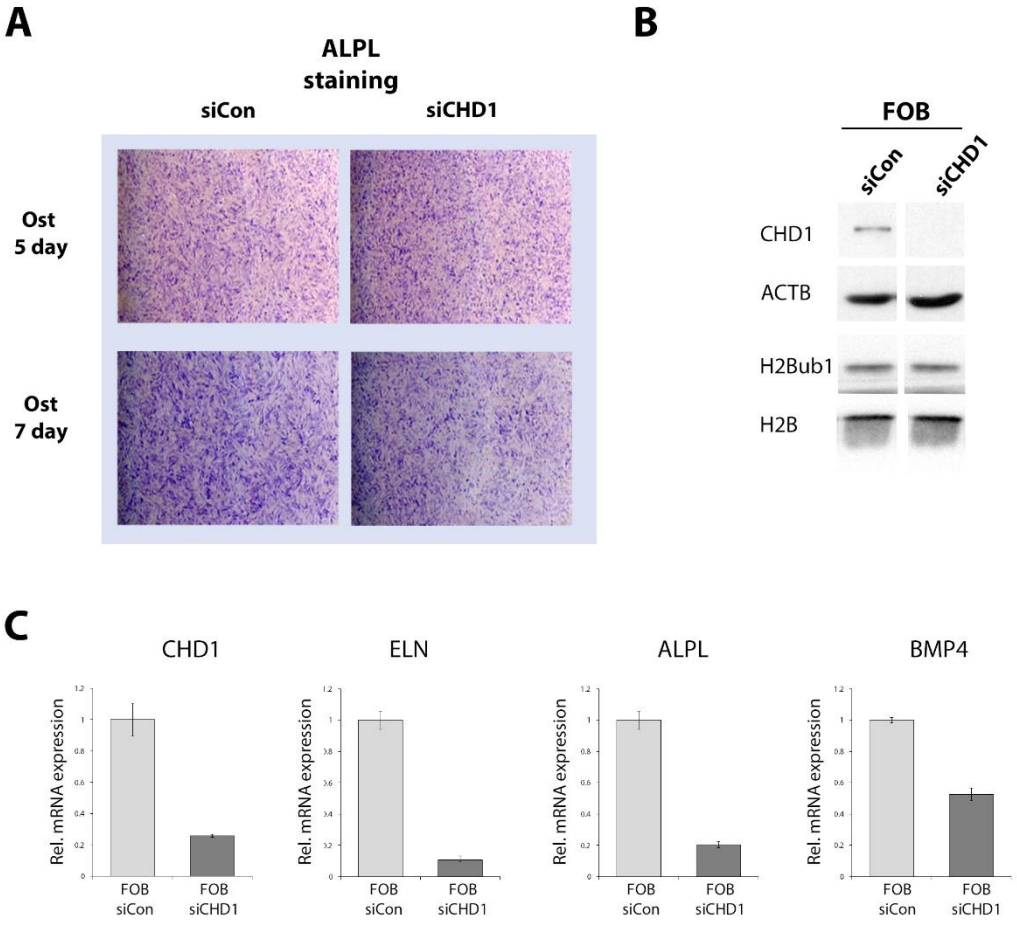

Figure 7: Osteoblast differentiation marker are reduced after CHD1 depletion in FOB.
A Microscopic evaluation of ALPL activity staining of five and seven days' osteoblast differentiated FOB (Ost) transfected with control siRNA against luciferase (siCon) or CHD1 siRNA (siCHD1). Cell culture wells were scanned and representative regions are shown for each condition. **B** Western blot analysis of whole cell lysates of five days' osteoblast differentiated FOB, transfected with siCon or siCHD1. CHD1, Beta-actin (ACTB), H2Bub1 or H2B were immunodetected with corresponding antibodies by immunoperoxidase. **C** Relative mRNA levels of osteoblast associated genes *ELN*, *ALPL* and bone morphogenic protein 4 (*BMP4*) in five days differentiated FOB transfected with siCon or siCHD1 as measured by qPCR with gene specific primer and normalized to the *18S rRNA* levels. Values are shown relative to the expression in undifferentiated cells under siCon-transfected conditions. Error bars represent the standard deviation of at least three biological replicates.

The observed differences in the chemical cell staining shown so far were further analyzed by Western blots to initially validate the CHD1 knockdown efficiency on protein level. Additionally, H2Bub1, a PTM histone mark required for adipocyte and osteoblast differentiation (Karpiuk et al., 2012) and shown to be dependent on CHD1, was measured (Lee et al., 2012b). Surprisingly, H2Bub1 was not reduced with decreased CHD1 protein levels neither in MSC nor in FOB when differentiated or undifferentiated (Figure 6B, Figure 7B). This indicates that global H2Bub1 levels are independent from CHD1 in these cell systems, despite the strongly reduced CHD1 protein levels achieved post siCHD1 transfection. The result of these experiments also indicates that the CHD1-dependent effects on differentiation are probably independent of H2Bub1-mediated events during differentiation.

4.2 Cell lineage specific genes are deregulated with reduced CHD1 levels

To analyze the effect of CHD1 depletion on cell-lineage-specific gene regulation cDNA was analyzed by quantitative real-time PCR (qPCR). Differentiated adipocytes showed a gene induction of lipid storage and glucose-metabolizing proteins perilipin 1 (*PLIN1)* and lipoprotein lipase *(LPL)*, as well as the adipogenic transcription factor peroxisome proliferator-activated receptor gamma *(PPARG)* (Figure 6C). These strong inductions in an adipocyte specific manner support the cell lineage specific differentiation observed previously by Oil Red O staining. Concordant with the reduced Oil Red O staining in CHD1 depleted condition a decreased induction of the adipogenic master regulator *PPARG* and *PLIN1* was observed. *LPL* was however not regulated arguing against a general inhibition of differentiation-induced genes. Consistent with that, osteoblast differentiated cells showed an increased expression of the early induced, cell lineage specific marker genes *BGLAP* and *ALPL* as reported previously (Rickard et al., 1996). In addition, *ELN*, a gene important for ectopic bone formation and expressed during early osteoblast differentiation (Larsen et al., 2010; Twine et al., 2014), was induced, too. Two of the osteoblastic marker genes *ALPL* and *BGLAP* were higher expressed after CHD1 depletion compared to control transfected cells, whereas *ELN* was strongly repressed under all conditions (Figure 6C). This together this strongly argues for a CHD1 specific regulation on cell differentiation. In FOB *ALPL*, *BMP4* and *ELN* were repressed in expression upon reduction of CHD1 levels (Figure 7C). However, *BGLAP*, an early marker for

differentiation, was not expressed, which highlights potential differences in cell lineage commitment between the MSC and FOB.

In sum MSC and FOB were lineage specifically differentiated as evident by the expression of cell type specific marker genes and characteristic phenotypic staining. CHD1 depletion caused an altered differentiation pattern compared to control siRNA transfected cells. The osteoblast specific marker genes *ALPL* and *BGLAP* were higher expressed and showed concordantly increased ALPL staining. This strongly suggests that the cells entered the osteoblast lineage, but possibly in a slightly restricted manner when taking the observed repression of *ELN* as a marker into account. In contrast, in FOB osteoblast associated genes were inhibited by CHD1 depletion and showed minor reduction of ALPL staining at day seven. These observed differences compared to MSC might be caused by different stages of cell lineage commitment, a speculation supported by the observed lack of *BGLAP* expression.

Adipocyte differentiation was inhibited upon CHD1 depletion as deduced from decreased lipid body formation and *PPARG* repression. Although cell type change is often initiated and characterized by single factors, the full differentiation process is multifactorial with timely orchestration of different signaling pathways. To further address the question of global gene regulation during differentiation in CHD1 depleted conditions the transcriptome was analyzed by deep RNA sequencing (RNA-seq).

4.3 Transcriptomic differences in MSC after CHD1 depletion and differentiation

Transcriptome-wide differential expression analysis helps to distinguish and characterize cell states. Here we sought to analyze differences of gene regulatory networks and pathways, which could further elucidate the differentiation effects observed in the previous part. Therefore, poly-adenylated mRNA was isolated from undifferentiated and seven-days-differentiated MSC and FOB, transfected with either siCon or siCHD1.

Genome-wide differences in mRNA expression of the different conditions in MSC were first measured by principal component analysis (PCA). Therefore the variation between all expressed genes were reduced to two dimensions, the principal component 1 and 2 (PC1, PC2). Each condition was plotted in biological duplicates, as used in the RNA-seq study. The PCA plot showed high similarity between the

biological duplicates for each condition (Figure 8). Further we observed that the osteoblast and adipocyte differentiated transcriptomes strongly shifted from the undifferentiated state on PC1, but only the osteoblast condition shifted also on PC2, which indicates differences between all three control transcriptomes. The transcriptome of CHD1 depleted samples shifted mainly on the PC2 axis when compared to their control condition. Interestingly however was that the CHD1 depleted osteoblast condition was shifted apart less from undifferentiated control than the osteoblast control sample was. This implies a decrease in the global change of transcription during osteoblast differentiation when CHD1 protein levels were reduced. However, the smallest change introduced by CHD1 depletion to its relative control was observed in the undifferentiated cells, which suggests a greater influence of CHD1 on gene expression during differentiation than in an undifferentiated condition. Together, this shows that different transcriptome wide changes were introduced with differentiation and CHD1 depletion, however, interestingly, caused reduced levels of CHD1 during osteoblast differentiation decreased changes in the transcription profile.

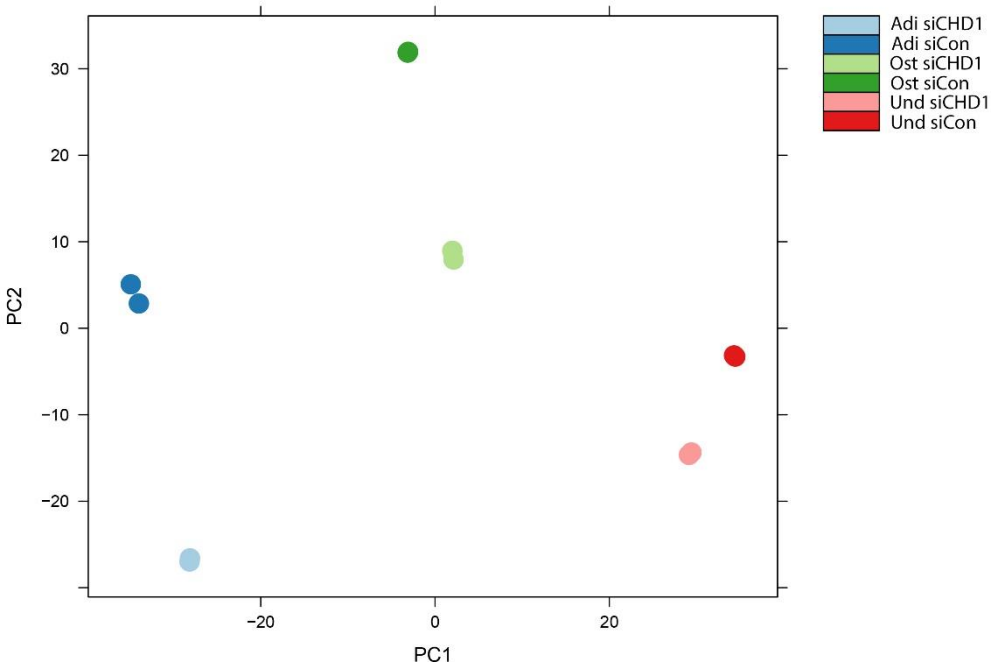

Figure 8: Differentiation and CHD1 depletion causes broad transcriptomic changes. The principal component analysis (PCA) plot represents the transcriptome of all genes in undifferentiated (Und) and 5 days differentiated adipocyte (Adi) or osteoblast (Ost) cells transfected either with siCHD1 or siCon. Each dot shows one of two RNA-seq samples of the respective condition indicated by the color code shown top right. The samples were calculated based on their normalized gene expression counts for all human genes and plotted on the principal component 1 (PC1) and 2 (PC2).

4.4 CHD1 depletion attenuates regulation of differentiation regulated genes

Differentiation specific gene sets in MSC and FOB were grouped by thresholds of plus or minus 0.5 log_2 fold change values (+/- 0.5 log_2FC), with a multiple testing adjusted probability value below 0.05 (p-adj. < 0.05). With these thresholds 2,478 genes were repressed and 1,986 genes were activated during adipocyte differentiation, whereas in osteoblast differentiation a lower number of 1,379 genes showed increased and 1,408 genes showed decreased expression compared to control (Figure 9A, B, left panel). This shows greater gene expression changes in adipocyte differentiated cells than in osteoblasts, which might indicate a closer osteoblast cell fate commitment of the bone marrow derived MSC (Simonsen et al., 2002). During FOB osteoblast differentiation 4,012 genes were increased in their expression and 4,869 were decreased compared to undifferentiated control condition (Figure 9C, left panel).

Next the impact of CHD1 on the genes regulated during differentiation was investigated. Genes induced during adipocyte and osteoblast differentiation were reduced in their activation and repressed genes during differentiation were mitigated in their silencing (Figure 9A, B, C, right panel). Thus CHD1 depletion mainly attenuates the effect on gene regulation taking place during differentiation. To further identify the significant differentially expressed genes after CHD1 depletion the groups selected above were filtered with similar thresholds to the differentiated siCHD1-treated condition (+/- 0.5 log_2FC, p-adj. < 0.05). This showed that the majority of significant CHD1 regulated genes during differentiation were indeed regulated in an opposite manner compared to the control differentiation (Figure 9A, B, C, pie charts). Interestingly, this effect was stronger during osteoblast differentiation than adipocyte differentiation. In particular, out of all 1,379 genes activated by osteogenesis were 550 significantly reduced in their induction, but only 155 were further increased when CHD1 protein levels were reduced (Figure 9B, pie chart). Furthermore, in total 579 genes in FOB were repressed after CHD1 depletion (not shown). Strikingly, 472 of these genes were also regulated during the differentiation process (Figure 9C, blue parts of pie charts). This indicates a major effect of CHD1 especially on the differentiation regulated genes in FOB. In MSC, approximately 40% of all repressed genes with CHD1 knockdown were also regulated during osteoblast differentiation which argues for a broader regulation, not only on differentiation specific genes.

In sum, the transcriptome of MSC and FOB was broadly changed in over thousands of genes within 5 days of differentiation. CHD1 depletion affected the gene expression by weakening the regulatory impact of the differentiation program, most evident in osteoblast differentiation. This attenuation of the differentiation effect was also observed by the decreased shift shown in the PCA plot for CHD1 depleted osteoblasts.

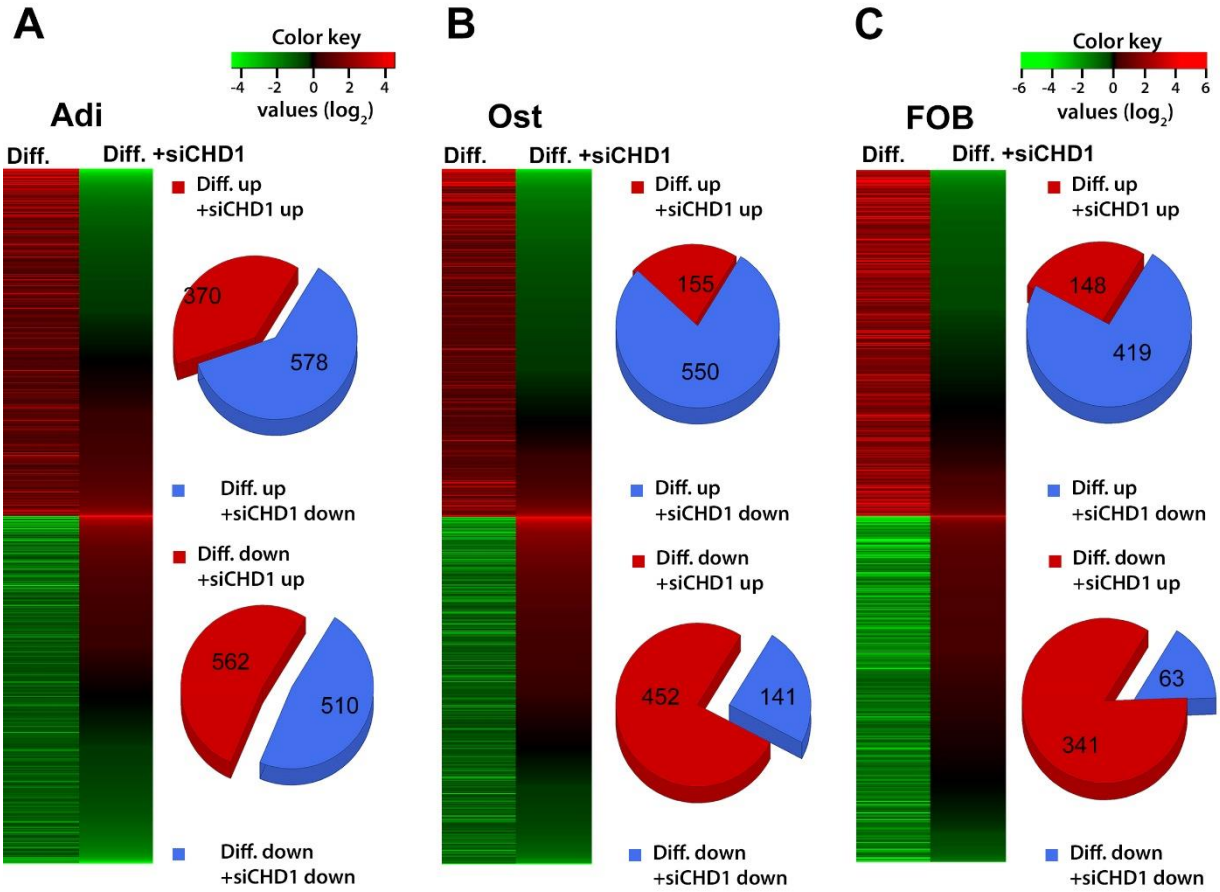

Figure 9: Genes regulated during differentiation are attenuated upon CHD1 depletion. A Heat map represents the log_2fold changes in mRNA expression during adipocyte differentiation (Adi, Diff.) compared to relative changes after CHD1 depletion (Diff. + siCHD1). Genes were defined by differentially expression of undifferentiated siRNA-Control condition compared to adipocyte differentiated siRNA-Control condition (left panel). Further, gene expression changes between adipocyte control (Diff.) and adipocyte CHD1 depletion conditions are shown (right panel). Differentiation genes were filtered by values above or below 0.5 log_2 fold changes (+/- 0.5 log_2FC) and an adjusted probability value below 0.05 (p-adj. < 0.05). In total 1,986 genes higher expressed (upper half) and 2,478 repressed genes (lower half) during adipocyte differentiation are plotted. The log_2FC values of the heat map are shown in the color key. Pie charts depict the numbers of significantly repressed (blue) or activated (red) differentiation genes upon CHD1 depletion with thresholds described above. **B** Heat map and pie charts represent genes regulated during MSC osteoblast differentiation and the relative regulation by siRNA mediated CHD1 depletion. In total 1,379 genes were higher (upper part) and 1,408 were lower (lower part) expressed during osteoblast differentiation. For further description see A. **C** Heat map and pie charts show genes regulated during FOB osteoblast differentiation and the relative regulation by siRNA mediated CHD1 depletion. In total 4,012 genes

were higher (upper part) and 4,869 lower (lower part) expressed during osteoblast differentiation. For further description see A.

4.5 Low transcribed genes require CHD1 for their activation during differentiation

As CHD1 was necessary for the gene regulation during differentiation we sought to further investigate the transcription levels of these CHD1 regulated genes (Figure 9, pie charts). Therefore, the normalized transcription counts were plotted two-dimensionally for differentiated and undifferentiated cells in control and CHD1 depleted condition.

The selected genes showed a broad distribution of expression levels in undifferentiated and differentiated conditions (Figure 10A, B, C). This implies that CHD1 differentiation affected genes were distributed over a wide range of transcription values. To clarify the data, a regression curve was plotted through the gene expression points of undifferentiated and differentiated control conditions. Interestingly, all investigated gene subsets showed particular strong changes during differentiation in the lowly expressed genes (Figure 10, black lines). Particularly, lowly transcribed genes in undifferentiated state were mainly activated during differentiation and not further repressed. Strikingly, these genes were changed less prominent in CHD1 depleted condition and closer resembled the undifferentiated control expression levels (Figure 10, red lines). This suggests that the lowly expressed genes required CHD1 for their full activation.

Next, we sought to quantify the changes in gene expression introduced by CHD1 depletion especially during osteoblast differentiation. The initial data of the PCA plot showed a reduced transcriptomic shift during osteoblast differentiation relative to undifferentiated control when CHD1 was depleted. For further analysis, the Pearson correlation coefficient (R) for the data represented in the scatter plot was calculated. It describes the similarity of data values in a range from -1 (low) to 1 (high). We could observe an increase of the correlation coefficient between undifferentiated and siCHD1 treated osteoblasts compared siCon treated osteoblasts. The increase was similar in FOB and MSC from 0.72 to 0.78 and 0.78 to 0.84, respectively (Figure 10B, C). Interestingly, the regression curve suggests that the most affected genes were low expressed ones. This argues for reduced changes in gene expression during osteoblast differentiation when CHD1 is depleted. Surprisingly, this effect was not observed in adipogenesis. All genes were further changed in their expression relative

to undifferentiated control or the regulation pattern was more heterogeneous which might overlay the effect on induced genes while adipocyte differentiation. This together indicates that the regulatory effects in osteoblast and adipocytes could be different. Further, CHD1 was required to introduce changes in gene expression during osteoblast differentiation and decreased CHD1 protein levels rather maintained the undifferentiated expression profile than further changing it.

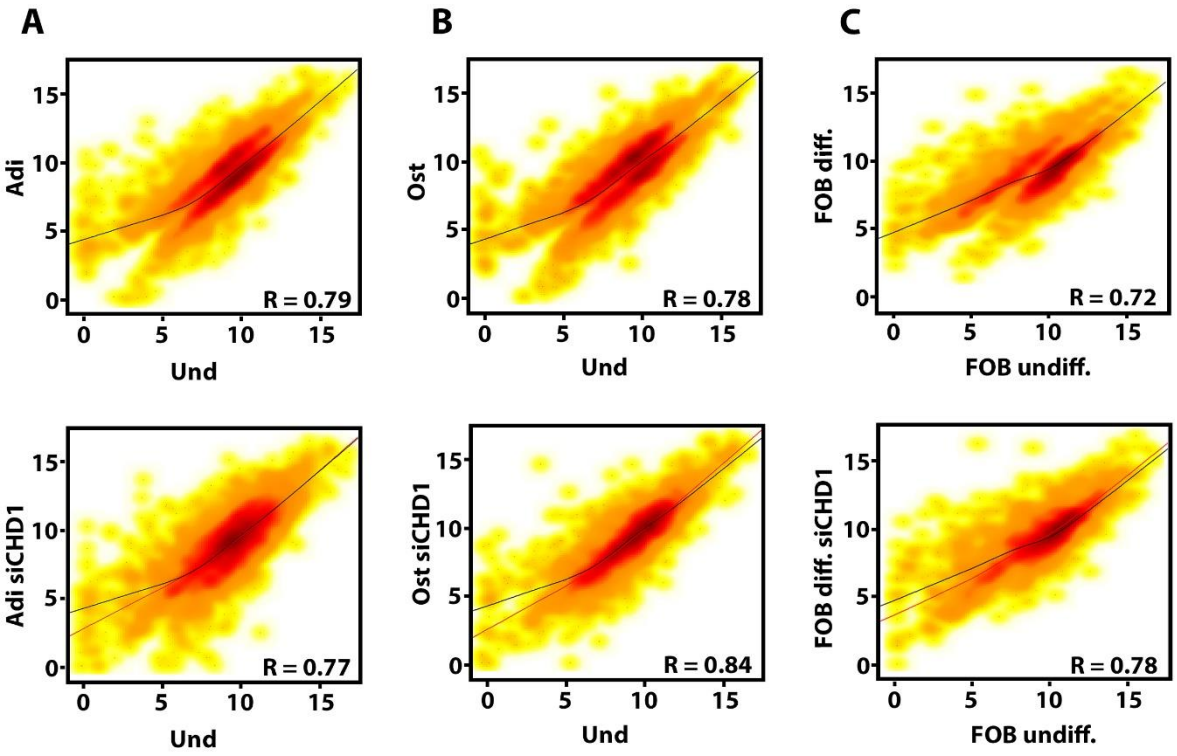

Figure 10: CHD1 is necessary for induced changes in gene expression during osteogenesis. **A** Scatter plots show normalized gene expression values between undifferentiated and adipocyte differentiated condition with siCon (Adi) or siCHD1 treatment (siCHD1) in MSC. Genes were selected by significant changes of expression during differentiation (p-adj. < 0.05, + or - 0.5 log_2FC) and significant regulation by siRNA mediated CHD1 depletion (p-adj. < 0.05, +/- 0.5 log_2FC). A regression curve is shown in black for control and in red for the siCHD1 condition. The Pearson correlation coefficient (R) is shown at the bottom right of each plot. The color of the plot indicates the gene densities from low (yellow) to high (red). In total, 2,020 genes were plotted similar. **B** Scatter plots show normalized gene expression values of undifferentiated and osteoblast differentiated condition with siCon (Ost) or siCHD1 treatment (siCHD1) in MSC. Gene selection, thresholds and figure description were used as described in A. In total 1,298 genes were plotted. **C** Scatter plots show normalized gene expression values between undifferentiated and osteoblast differentiated condition with siCon (Ost) or siCHD1 treatment (siCHD1) in FOB. For further gene selection, thresholds and figure description see A. In total, 971 genes were plotted similar as described in Figure 9C pie charts.

4.6 CHD1 regulated genes are enriched in osteoblastic gene ontology terms

Transcriptome-wide data can be used to analyze regulatory networks or biological functions for a better characterization of cellular states. Therefore, we used all

deregulated genes by CHD1 depletion during the differentiation process in MSC and FOB as described previously (Figure 9A, B, C). These groups were analyzed for their enrichment in Gene Ontology (GO) terms of biological processes and cellular compartments defined by the GO Consortium and built-in the Database for Annotation, Visualization and Integrated Discovery (DAVID) software.

The highest annotation cluster in MSC as well as FOB showed GO terms associated with the extracellular region and extracellular matrix (ECM) (Table 1Table 2Table 3). Both cellular compartments undergo strong changes during differentiation, which are necessary for cell type specific functions like deposition of collagen before matrix mineralization in osteoblasts or structural support of the membrane previous to storage of lipids (Damsky, 1999; Mariman and Wang, 2010). Changes in the ECM during differentiation were also observed in the microscopic images for cell type specific staining (Figure 6A). Besides the ECM organization, the extracellular region term involves secreted protein like BGLAP or ELN. These genes were previously shown to be strongly deregulated by CHD1 depletion (Figure 6C, Figure 7C).

Additionally, the top annotation clusters further selected terms showed impairment of important supportive biological processes for adipocyte and bone formation such as angiogenesis and responses to endogenous stimuli (Eshkar-Oren et al., 2009; Ledoux et al., 2008). This implies that the crosstalk between osteoblast or MSC with vascularizing tissue might be perturbed which could influence proper bone formation. Further, signaling pathways stimulated by differentiation medium or in a paracrine manner required CHD1 for proper regulation. Deregulated signaling pathways maybe involved in indirect gene regulation independent of CHD1.

Strikingly, bone related GO terms were significantly enriched within the deregulated gene groups of osteoblast differentiated MSC and FOB (Table 2, Table 3 bold). We compared the genes of the top term “skeletal system development” with the fold changes in gene expression identified by RNA-seq. Intriguingly, it showed that 44 out of 56 deregulated genes in MSC and 23 out of 30 in FOB were repressed in their activation during osteogenesis when CHD1 protein levels were low. This argues for a role of CHD1 in the activation of skeletal development associated genes. Summarized, biological processes and cellular compartments which are important for bone formation required CHD1 for normal regulation during early osteogenesis. Furthermore, terms related to bone formation also showed perturbed regulation by CHD1 depletion which might affect normal bone development.

Table 1: Gene Ontology terms of CHD1 dependent genes during adipocyte MSC differentiation. The table lists gene ontology (GO) terms of deregulated genes after CHD1 depletion during adipocyte differentiation of MSC. Genes were selected by thresholds described in Figure 9A (pie chart) and analyzed for enriched GO terms with the Database for Annotation, Visualization and Integrated Discovery (DAVID) software. In total 2,020 genes were used as an input with the all human genes set as background. Results were sorted by the enrichment score or their false discovery rate (FDR). The gene number (Count) within the respective GO term (Term) and probability values calculated by the Benjamini-Hochberg procedure (Benjamini) are shown on top of the table.

Annotation Cluster 1	Enrichment Score: 9.90			
Category	**Term**	**Count**	**Benjamini**	**FDR**
Cellular Compartment	Extracellular region part	168	5.37E-11	1.45E-10
Cellular Compartment	Extracellular region	282	3.21E-08	2.60E-07
Cellular Compartment	Extracellular space	112	9.87E-06	1.60E-04

Annotation Cluster 2	Enrichment Score: 8.97			
Category	**Term**	**Count**	**Benjamini**	**FDR**
Cellular Compartment	Extracellular matrix	73	9.35E-08	1.01E-06
Cellular Compartment	Proteinaceous extracellular matrix	68	2.57E-07	3.46E-06
Cellular Compartment	Extracellular matrix part	29	3.39E-04	1.19E-02

Selected terms				
Category	**Term**	**Count**	**Benjamini**	**FDR**
Biological Process	Vasculature development	50	1.17E-03	1.05E-02
Biological Process	Blood vessel morphogenesis	43	1.87E-03	2.94E-02
Biological Process	Angiogenesis	30	2.02E-02	7.59E-01
Biological Process	Response to endogenous stimulus	71	1.13E-03	1.16E-02
Biological Process	Response to hormone stimulus	63	3.97E-03	7.85E-02
Cellular Compartment	Plasma membrane	441	8.78E-04	3.55E-02

Table 2: Gene Ontology terms of CHD1 dependent genes during osteoblast differentiation in MSC.
The table lists gene ontology (GO) terms of deregulated genes after CHD1 depletion during osteoblast differentiation of MSC. Genes were selected by thresholds described in Figure 9B (pie chart) and analyzed for enriched GO terms with the Database for Annotation, Visualization and Integrated Discovery (DAVID) software. In total 1,298 genes were used as an input with the all human genes set as background. For further description of the table see Table 1.

Annotation Cluster 1	Enrichment Score: 11.66			
Category	**Term**	**Count**	**Benjamini**	**FDR**
Cellular Compartment	Extracellular region part	132	4.87E-14	1.55E-13
Cellular Compartment	Extracellular region	205	1.78E-09	1.72E-08
Cellular Compartment	Extracellular space	85	6.04E-07	1.75E-05

Annotation Cluster 2	Enrichment Score: 10.63			
Category	**Term**	**Count**	**Benjamini**	**FDR**
Cellular Compartment	Extracellular matrix	61	4.76E-10	3.06E-09
Cellular Compartment	Proteinaceous extracellular matrix	55	1.03E-08	1.32E-07
Cellular Compartment	Extracellular matrix part	22	6.48E-04	2.92E-02

Annotation Cluster 7	Enrichment Score: 6.02			
Category	**Term**	**Count**	**Benjamini**	**FDR**
Biological Process	**Skeletal system development**	56	4.01E-08	6.31E-08
Biological Process	**Bone development**	24	5.18E-04	8.43E-03
Biological Process	**Ossification**	22	1.40E-03	3.16E-02
Biological Process	**Osteoblast differentiation**	11	1.33E-02	5.67E-01

Selected terms				
Category	**Term**	**Count**	**Benjamini**	**FDR**
Biological Process	Response to endogenous stimulus	59	3.51E-06	2.76E-05
Biological Process	Response to hormone stimulus	53	2.22E-05	2.21E-04
Biological Process	Vasculature development	36	1.51E-03	3.63E-02
Biological Process	Blood vessel development	35	1.86E-03	5.26E-02
Biological Process	Angiogenesis	22	2.43E-02	1.26E+00
Cellular Compartment	Plasma membrane	323	3.69E-07	9.51E-06

Table 3: Gene Ontology terms of CHD1 dependent genes during osteoblast differentiation in FOB. The table lists gene ontology (GO) terms of deregulated genes after CHD1 depletion during osteoblast differentiation of FOB. Genes were selected by thresholds described in Figure 9C (pie chart) and analyzed for enriched GO terms with the Database for Annotation, Visualization and Integrated Discovery (DAVID) software. In total 971 genes were used as an input with the all human genes set as background. For further description of the table see Table 1.

Annotation Cluster 1	Enrichment Score: 8.44			
Category	**Term**	**Count**	**Benjamini**	**FDR**
Cellular Compartment	Extracellular matrix	46	2.25E-07	1.44E-06
Cellular Compartment	Proteinaceous extracellular matrix	43	4.55E-07	4.37E-06
Cellular Compartment	Extracellular matrix part	18	3.26E-03	6.26E-02

Annotation Cluster 2	Enrichment Score: 7.74			
Category	**Term**	**Count**	**Benjamini**	**FDR**
Cellular Compartment	Extracellular region part	98	5.47E-10	1.75E-09
Cellular Compartment	Extracellular region	141	2.37E-04	3.03E-03
Cellular Compartment	Extracellular space	62	2.09E-04	3.34E-03

Selected terms				
Category	**Term**	**Count**	**Benjamini**	**FDR**
Biological Process	**Skeletal system development**	**30**	**4.64E-02**	**8.15E-01**
Biological Process	Blood vessel development	26	2.93E-02	3.53E-01
Biological Process	Vasculature development	26	3.40E-02	5.12E-01
Biological Process	Response to organic substance	62	1.19E-03	7.09E-03
Biological Process	Response to endogenous stimulus	36	3.55E-02	5.77E-01
Biological Process	Response to hormone stimulus	33	4.69E-02	8.80E-01
Cellular Compartment	Intrinsic to plasma membrane	86	1.30E-02	3.76E-01
Cellular Compartment	Integral to plasma membrane	83	2.31E-02	7.45E-01

4.7 Validation of single genes identified by RNA-seq with individual CHD1-siRNAs

To confirm CHD1 specific gene regulation and to exclude off-target effects by the CHD1 siRNA pool, single siRNAs of the pool were used to validate the gene regulation observed in the RNA-seq experiments. MSC and FOB were transfected with CHD1 targeting siRNA #1 and #2 and differentiated for 5 days.

Both single siRNAs #1 and #2 showed strong depletion of CHD1 protein and *CHD1* mRNA in MSC and FOB (Figure 11A, B, C, D). In addition, genes listed in the "skeletal development" GO term in MSC like endothelin 1 (*EDN1)*, SIX homeobox 1 (*SIX1)*, periostin (*POSTN)* or dual specificity phosphatase 1 (*DUSP1)* were confirmed

to be regulated by both single siRNAs in similar efficiency to the siCHD1 pool observed in the RNA-seq. Also genes analyzed in the previous experiments showed similar regulation by single siRNAs in MSC (*ALPL*, *ELN*) and FOB (bone morphogenetic protein 4 (*BMP4)*, *ELN*, *POSTN*) (compare Figure 11B, D to Figure 6C, Figure 7C). Additionally, osteoblastic marker genes were repressed by CHD1 depletion in FOB, like the Wnt-signaling factor *AXIN2* or osteoblast differentiation associated gene connective tissue growth factor (*CTGF*). This together indicates that the genes regulated by the siCHD1 pool are unlikely off-target effects caused by the siRNA pool.

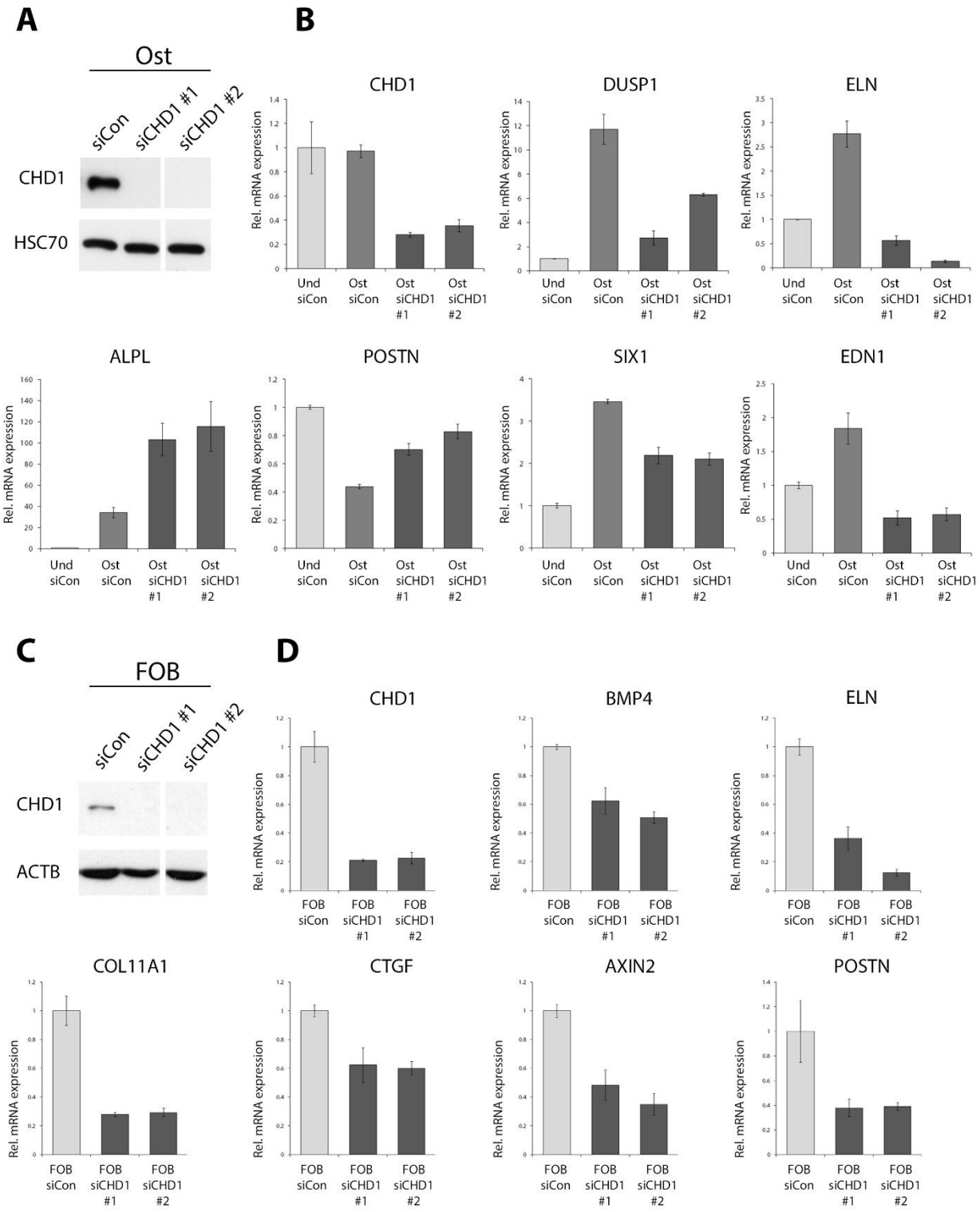

Figure 11: Individual CHD1-siRNAs validate CHD1-specific gene regulation observed by RNA-seq. A Immunodetection of CHD1 and HSC70 by Western blot analysis of whole cell lysates of 5 days' osteoblast differentiated MSC, transfected with siRNA directed against luciferase (siCon) or individual siRNA #1 and #2 against CHD1. **B** qPCR analysis of RNA from cells described in A by using gene specific primer against *CHD1*, alkaline phosphatase, liver/bone/kidney (*ALPL*), elastin (*ELN*), dual specificity phosphatase 1 (*DUSP1*), periostin (*POSTN*), SIX homeobox 1 (*SIX1*) and Endothelin 1 (*EDN1*). Gene expression was normalized to the RNA level of the gene encoding the ribosomal protein, large, P0 (*RPLP0*) and compared relative to that of the osteoblast differentiated siCon condition. Error bars represent the standard deviation of at least 3 biological replicates. **C** Immunodetection of CHD1 and ACTB by Western blots of whole cell lysates of 5 days' osteoblast

differentiated FOB, transfected with siRNA directed against luciferase (siCon) or individual siRNA #1 and #2 against CHD1. **D** qPCR analysis of cDNA from cells described in C by using gene specific primer against *CHD1*, *POSTN*, bone morphogenetic protein 4 (*BMP4)*, *ELN*, connective tissue growth factor (*CTGF*), collagen, type XI, alpha 1 (*COL11A1*) and *AXIN2*. Gene expression was normalized to that of the *RPLP0* gene and compared relative to the osteoblast differentiated siCon condition. Error bars represent the standard deviation of at least 3 biological replicates.

4.8 Heterozygous CHD1 knockout mice show an abnormal bone phenotype

As CHD1 depletion caused deregulated differentiation pattern in MSC and FOB which were connected to GO terms of skeletal development we were curious to see if CHD1 would also impact bone formation *in vivo*. The international mouse phenotyping consortium (IMPC) describes phenotypes for a constitutive homozygous and heterozygous CHD1 knockout mouse model. The homozygous CHD1 knockout mouse is embryonic lethal before day six, but the heterozygous model is viable with a described phenotype. Among other phenotypes the mice showed significant abnormal skull shape and teeth morphology, which is often associated with defects in bone formation by an interplay between osteoblasts and osteoclasts (Gama et al., 2015). Strikingly however was that the mice showed a significant decrease in body length, bone mineral density and bone mineral content (Figure 12A). This clearly indicates defects in the bone in a CHD1 heterozygous genotype. The phenotype on adipocyte-associated tissues were less clear. CHD1 heterozygous mice had a total decrease in fat mass, but in comparison to the total body weight it did not show a significant difference to wild type mice (Figure 12B).

The IMPC data clearly linked CHD1 to the maintenance of normal bones in mice. However, bone formation is a complex process involving different cell types such as MSC, osteoblasts, osteoclasts or osteocytes. Thus we wanted to further specify if MSC differentiation was particularly involved in the defective bone formation with low levels of CHD1.

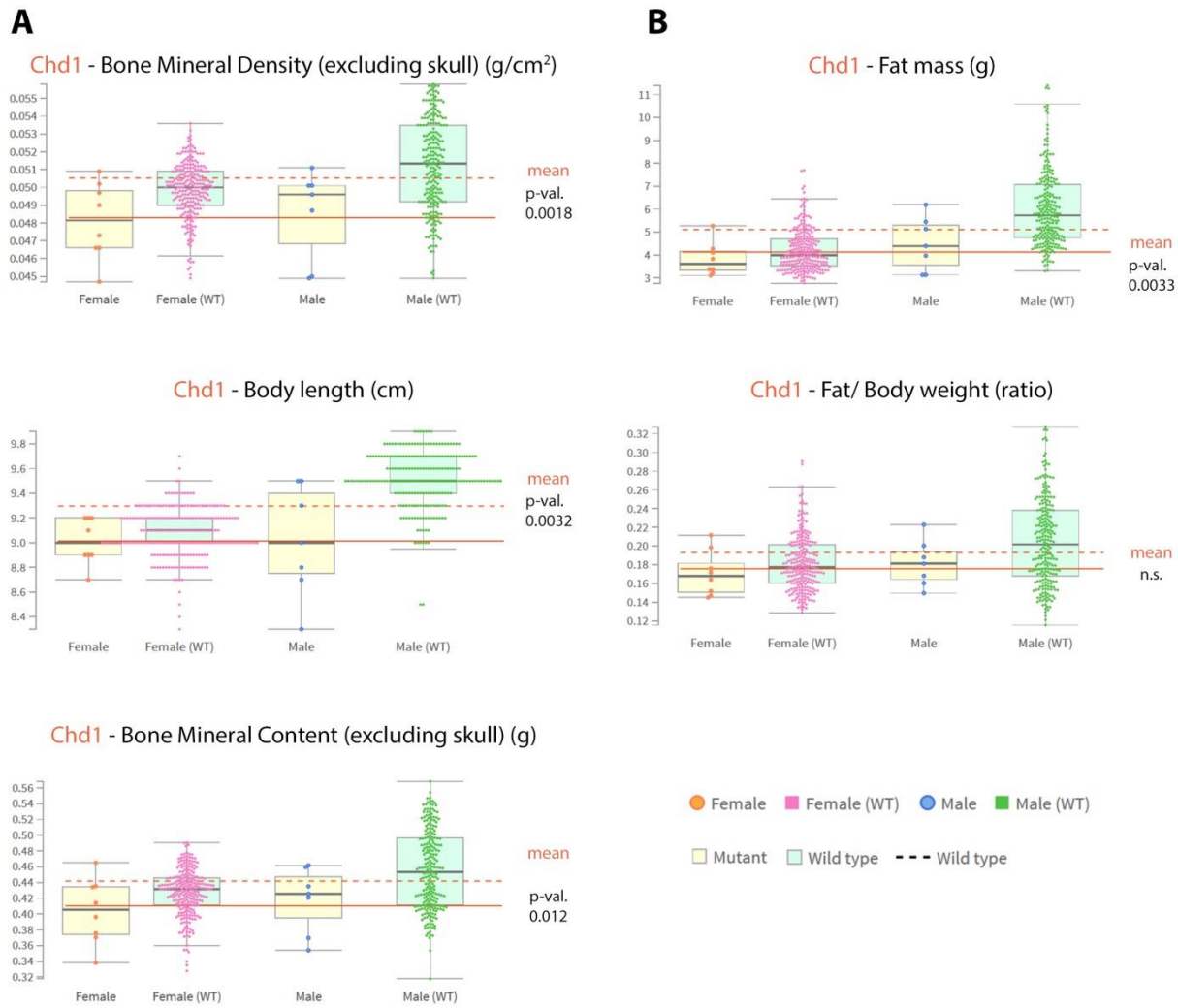

Figure 12: CHD1 heterozygous knockout mice show decreased bone associated parameters. Box plots represent different phenotypical parameters measured in CHD1 heterozygous C57BL/6NCrl CHD1$^{tm1b(KOMB)Wtsi}$ knockout or wildtype mice described by the international mouse phenotype consortium (IMPC). **A** Female or male mice were analyzed for bone mineral density, body length, bone mineral content or **B** fat mass and fat / body weight ratio 14 weeks after birth. Statistic differences between the means of heterozygous CHD1 knockout (female and male; orange line) and wildtype (female and male; dotted orange line) mice for the different parameters were compared by Fisher´s exact test.

4.9 CHD1 depleted MSC form less ectopic bone in mice

As described by others MSC formed ectopic bone *in vivo* after implantation into severe combined immunodeficiency (SCID) mouse (Simonsen et al., 2002). Ectopic bone formation is an easy and meaningful experiment to predict the bone formation capacity of a model system (Abdallah et al., 2008). To test if CHD1 depletion impaired bone formation *in vivo* we created MSC cell lines which stably express a shRNA-targeting CHD1. In total, three cell lines, two with individual shRNA against CHD1 (shCHD1-#1, shCHD1-#2) and one control cell line, expressing a non-targeting control shRNA (shCon), were established and analyzed for CHD1 depletion (Figure 13C). The cells were injected together with a hydroxyapatite/ tri-calcium phosphate (HA/TCP) matrix into SCID mice, which were sacrificed 8 weeks after injection. The ectopically formed tissue sections were stained by hematoxylin and eosin (H&E) and the ratio of formed bone area (BA) relative to the measured tissue area (TA) was calculated. To control whether that the formed bone tissue was of human MSC origin control sections were immunostained for human vimentin (VIM).
Besides the stable shRNA-expressing MSC untransformed MSC were also injected into mice to exclude effects due to the viral integration into the genome. Untransformed MSC and shCon MSC showed no difference in their mean bone formation rate with 3.2% and 3.1% BA/ TA and were combined into one control group (control). Strikingly, both CHD1 depleted MSC cell lines shCHD1 #1 and shCHD1 #2 formed less extracellular collagen matrix compared to control with 0.54% and 1.12% BA/ TA, respectively (Figure 13A, B). Statistical analysis by Tukey multiple comparisons with a p-value threshold of 0.05 showed a significant difference between the control group and shCHD1 #1 and shCHD1 #2, but no difference between shCHD1 #1 and #2 (Figure 13B). These findings support the RNA-seq results, highlighting a defect in MSC early osteoblast differentiation with decreased protein levels of CHD1. Furthermore, the low formation of extracellular collagen matrix implies differentiation defects before day five as others showed that deposition of organic compounds began around the fifth day of osteogenesis (Kulterer et al. 2007).

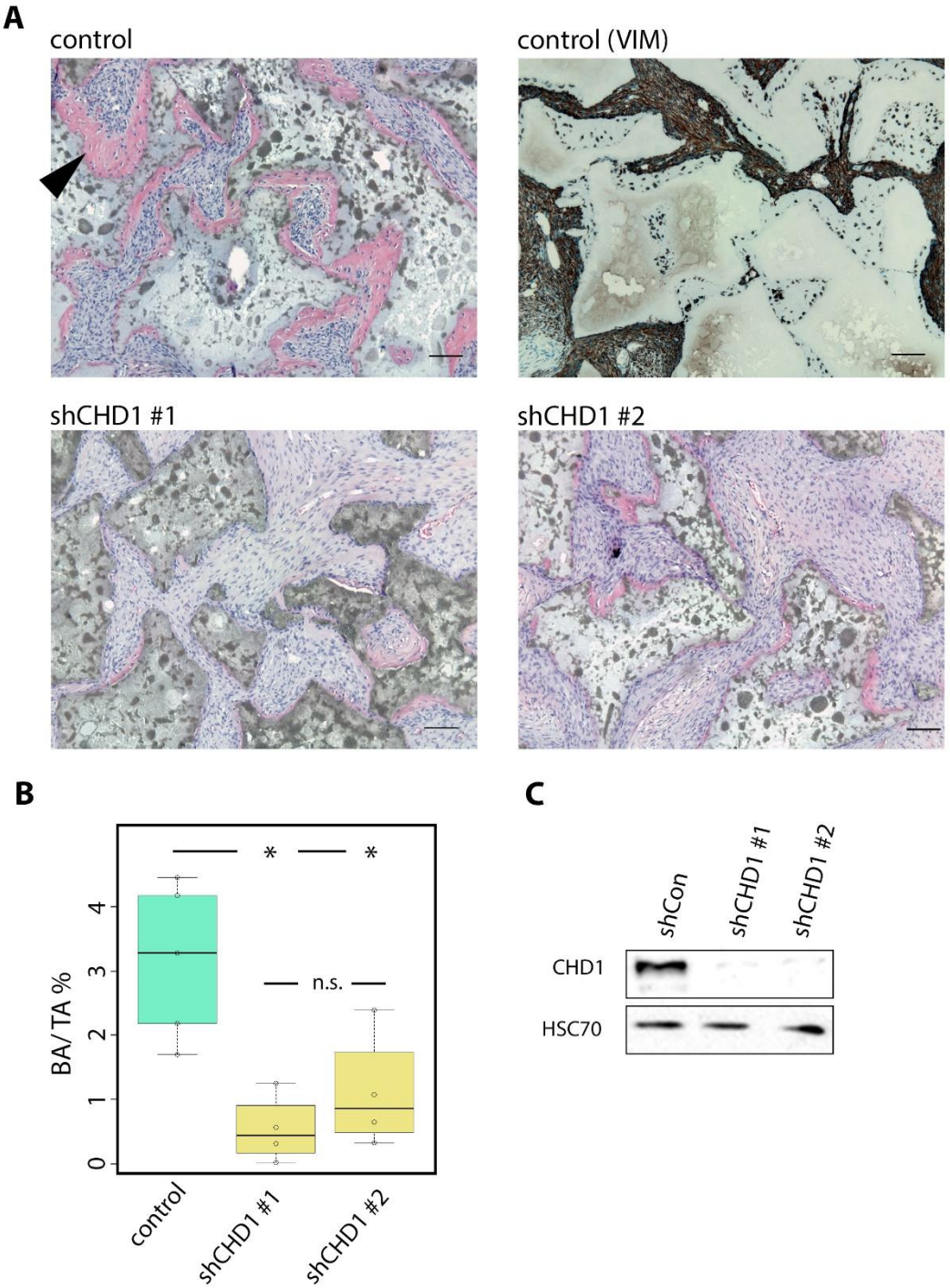

Figure 13: CHD1 depletion reduces ectopic bone formation in mice. A H&E stained tissue slides show ectopic formed bone area (black arrowhead) of control MSC (non-targeting shRNA) or shRNA-CHD1 expressing MSC (shCHD1 #1 or #2) in severe combined immunodeficiency (SCID) mice. MSC cell lines were subcutaneously injected into mice in a hydroxyapatite/ tri-calcium phosphate matrix. Eight weeks after injection mice were sacrificed and tissue sections were analyzed for BA relative to tissue area (TA) measured. Control slides were immunostained for human vimentin as a control for MSC formed tissue (control (VIM)). The scalebar = 100 µm. **B** Boxplot analysis show the ratio of bone area formed relative to tissue area (BA/ TA%) measured in control MSC (*n* = 5) and CHD1 depleted MSC (shCHD1 #1, #2) groups (*n* = 4). Statistical differences between the groups were calculated by Tukey multiple comparison test for a threshold of 0.05 (*). Individually measured values are shown by circles. **C** Immunodetection of CHD1 and HSC70 by Western blot analysis of whole cell protein lysates of stable MSC cell lines used for the ectopic bone formation experiment (see A).

Taken together CHD1 depletion caused deregulated mRNA expression of differentially expressed genes during adipocyte and osteoblast differentiation in MSC and FOB. The deregulation was characterized by repressed gene induction and attenuated gene silencing (Figure 9). Further, osteoblast with reduced CHD1 levels showed a decreased change of global gene transcription and remained closer to an undifferentiated transcriptomic profile (Figure 8). Moreover, CHD1 depletion increased the correlation to undifferentiated transcription levels in a particular group of genes (Figure 10). A closer analysis on this group of genes showed a significant enrichment in skeletal system and bone development related GO terms (Table 2, Table 3) which was concordant with an abnormal bone phenotype observed in heterozygous CHD1 knockout mouse reported by the IMPC (Figure 12). Finally, CHD1 depleted MSC showed decreased ectopic bone formation in mice (Figure 13). This supported the hypothesis that CHD1 is required for functional osteoblast differentiation by normal regulation of gene transcription and activation of skeletal associated genes. Although this combined was likely caused by effects of CHD1 on the transcriptional processes a direct evidence is missing. Therefore, CHD1 ChIP with subsequent deep sequencing (CHIP-seq) was performed to investigate the mechanism how CHD1 is regulating these gene transcription changes.

4.10 CHD1 ChIP-seq reveals high binding near TSS

Initially the CHD1 ChIP was tested by qPCR (ChIP-qPCR) in undifferentiated conditions in MSC to validate its specificity. The histone modification H3K4me3 ChIP was used as a positive control for TSS-regions and to identify potential CHD1 binding sites. To exclude unspecific signals, a non-specific antibody (IgG) was used as a negative control.

CHD1 ChIP-qPCR signals showed an enrichment downstream of the TSS of the genes ribosomal protein, large, P0 (*RPLP0*), glyceraldehyde-3-phosphate dehydrogenase (*GAPDH)* and dual specificity phosphatase 1 (*DUSP1*) (Figure 14A). This specific binding was confirmed by prominent signals of H3K4me3, which indicates TSS of either active or bivalent genes. In contrast, CHD1 and H3K4me3 had comparable low signals like IgG around the TSS of the inactive *TFF1* gene, which was confirmed by RNA-seq. This together shows specificity of the CHD1 ChIP and made the DNA applicable for genome-wide studies by deep sequencing technique.

To elucidate global changes of CHD1 binding during differentiation ChIP-seq was performed in undifferentiated, adipocyte and osteoblast differentiated MSC as well as osteoblast differentiated FOB. Additionally, H3K4me3 and H3K27ac ChIP-seq data from MSC of previous studies were used for further analysis. To validate the ChIP-seq signal specificity, the obtained sequencing reads of undifferentiated MSC were transformed into genome-wide profiles and compared to the previous ChIP-qPCR enriched regions. Concordantly, both techniques showed an overlapping signal in the tested genome coordinates for CHD1 and H3K4me3 ChIP (Figure 14B). Although the CHD1 profile had a high overlap with H3K4me3, further binding was detected in the gene body and the transcriptional termination site, which suggests independent binding of H3K4me3 as well.

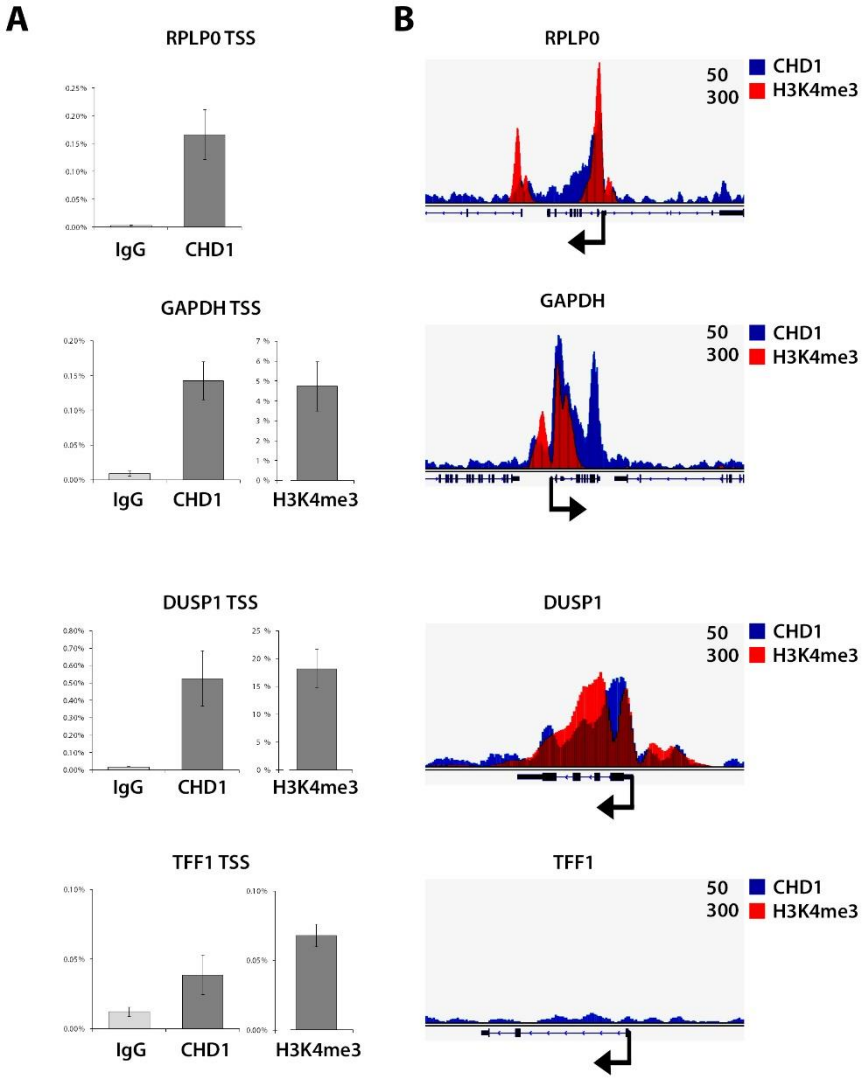

Figure 14: ChIP-qPCR and ChIP-seq profiles of CHD1 and H3K4me3 overlap around TSS. A Bar graphs represent the relative quantification to input of CHD1, H3K4me3 and IgG ChIP signals in MSC at transcriptional start site (TSS) regions measured by qPCR with gene specific primer for ribosomal protein, large, P0 (*RPLP0)*, dual specificity phosphatase 1 (*DUSP1)*, glyceraldehyde-3-

phosphate dehydrogenase (*GAPDH*) and trefoil factor 1 (*TFF1*). Error bars represent standard deviations of biological duplicates. **B** Genomic profiles show ChIP-seq signals of CHD1 (blue) and H3K4me3 (red) at genes described in A. Signals of CHD1 are shown in a range of 0 – 50 of normalized read counts and H3K4me3 in a range of 0 – 300. The signals were overlaid and visualized by the integrative genomics viewer (IGV). Black arrowheads represent the TSS of respective genes and orientation.

4.11 Genome-wide CHD1 binding is broadly associated with gene regions

To elucidate the CHD1 binding pattern and its regulatory role during differentiation, the genome-wide CHD1 binding sites were investigated in undifferentiated, adipogenic and osteogenic conditions in MSC or FOB. All above background and significantly enriched binding sites of CHD1 were overlaid with defined genomic functional segments in the human genome and quantified within them.

The highest proportion of CHD1 binding was observed within the gene regions of introns and exons followed by promoter and 5´- untranslated regions (5´-UTR) (Figure 15A). However, compared to the high distribution of introns within the genome the relative binding was not strikingly enriched of CHD1. Overall, the binding pattern of CHD1 was quite similar between undifferentiated and differentiated conditions, as well as between MSC and FOB. Interestingly, although CHD1 binding was reported at enhancer regions (Siggens et al., 2015), we could detect only low binding within intergenic distal loci. However, this proportion increased slightly during osteoblast differentiation in MSC. Although mapping of CHD1 to the functional regions revealed its distribution over the genome it did not identify the binding intensities at these sites. Therefore, an average binding profile of CHD1 to all gene regions was calculated and plotted on a meta gene (Figure 15B). All gene bodies were scaled into a length of 3 kilo base pairs (kb) with an additional region 1 kb up- and downstream of the TSS or the transcriptional termination site (TTS). The highest CHD1 binding was clearly around the TSS and decreased over the gene body. Interestingly, CHD1 signals also increased again at the TTS. This showed that although the most binding regions were associated within the gene body, the highest binding intensities were around the TSS. These observations indicate that the major role of CHD1 is closely around genes with a likely-highlighted function at the TSS-regions.

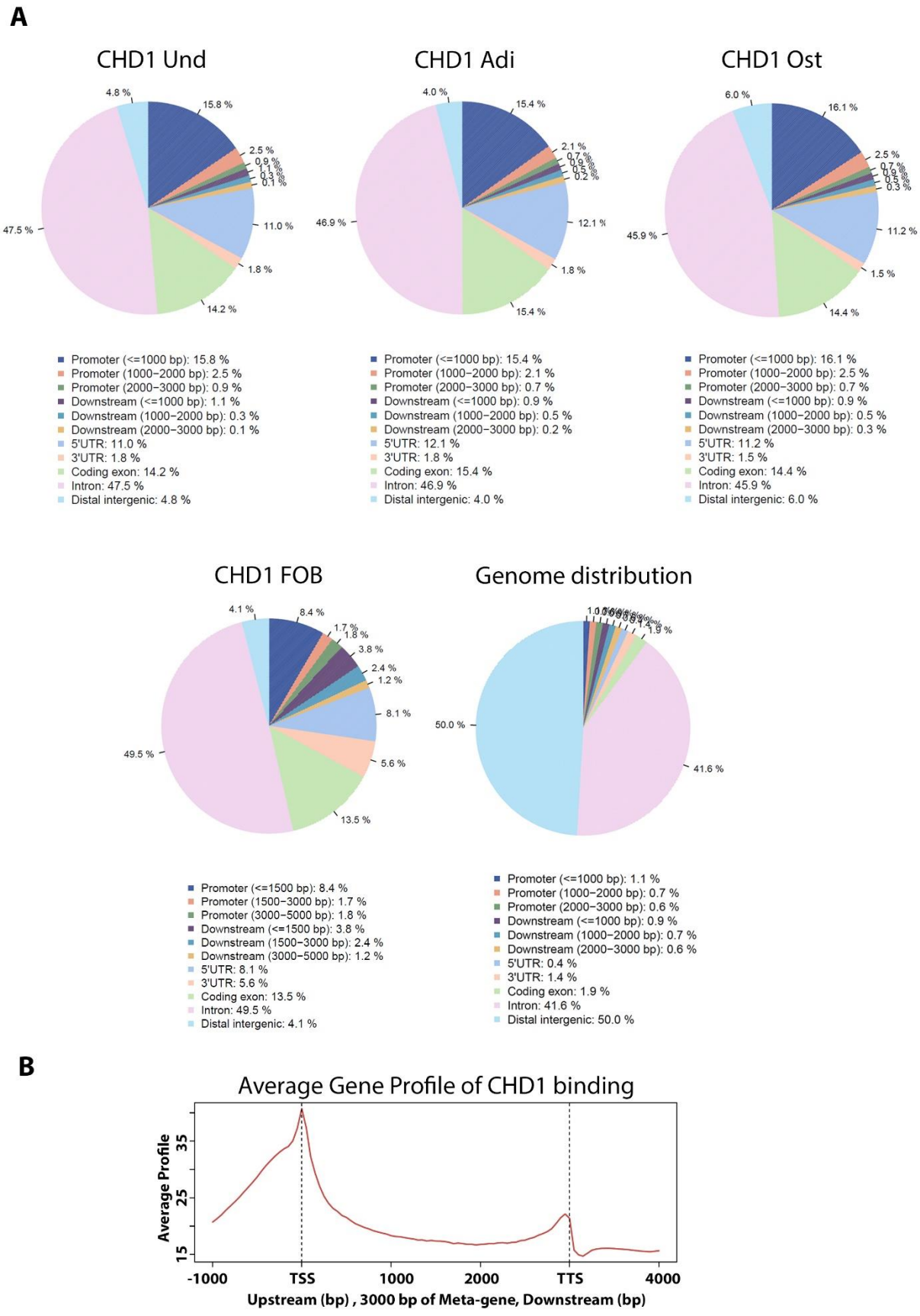

Figure 15: CHD1 distribution on genomic elements. A Pie charts show relative CHD1 binding distribution within functional domains of the human genome in undifferentiated (Und), adipocyte (Adi) and osteoblast (Ost) differentiated MSC or FOB. Significant CHD1 enriched regions were assigned to genomic segments of gene promoter and downstream regions, 3´- and 5´-untranslated regions (UTR),

exons and introns and distal intergenic loci. The color table with the respective functional segments and its relative distribution is depicted under the pie charts. The pie chart on the bottom right shows the normal distribution of the functional segments within the human genome (hg19). Calculations and graphics were produced within CEAS software. **B** Average binding profile represents CHD1 ChIP-seq signals (red line) over all human genes scaled into a meta-gene. The meta-gene includes a region 1,000 base pairs (bp) upstream or downstream of the transcriptional start site (TSS) and transcriptional termination site (TTS) indicated by dotted lines. The averaged CHD1 ChIP-seq signal intensity is represented on the y-axis relative to the meta-gene coordinates, shown on the x-axis. The representative undifferentiated MSC CHD1 ChIP-seq sample was used to plot the profile by the CEAS software.

4.12 CHD1 correlates with active histone modifications and gene expression

As CHD1 is located at and around gene regions and plays a role in gene transcription we sought to further analyze how it was associated with active histone modifications and actively transcribed genes in MSC. H3K4me3 is a hallmark for active and poised TSS whereas H3K27ac mostly decorate actively transcribed TSS. Thus, analysis of binding intensities of both histone marks and CHD1 could clarify which gene states were bound by CHD1 in MSC and in differentiated conditions.

As expected, CHD1 binding correlated well with H3K4me3 binding intensity at TSS-regions between 1 and 1,000 bp downstream into the gene body. A Pearson correlation coefficient score between 0.62 and 0.71 was measured in the different conditions (Figure 16A). No obvious differences between undifferentiated and differentiated cell states in the regression lines were observed. Further TSS-regions highly enriched for CHD1 were also decorated with H3K4me3 marks. But surprisingly, high H3K4me3 levels were not necessarily highly bound by CHD1. Further, the distribution of H3K4me3 intensities was less variable, showing either highly or lowly decorated TSS, but to a lesser extend a fraction in between.

Although H3K4me3 is a descriptive mark for TSS-regions, it does not necessarily indicate active genes. To further investigate the CHD1 binding solely to active transcribed genes the correlation with H3K27ac at TSS-regions was calculated. The observed correlation coefficient in the different conditions was even higher than for H3K4me3 with values between 0.7 and 0.78 (Figure 16A). Additionally, binding levels of CHD1 and H3K27ac showed a tendency for linear correlation, which support the assumption of their co-occupancy at active genes. Moreover, a gradual signal distribution was observed in contrast to H3K4me3 binding patterns around TSS. This could imply a finer readout of gene expression by H3K27ac compared to H3K4me3.

Finally, the correlation of CHD1 binding at TSS-regions in MSC and FOB was compared to the respective normalized gene expression of the occupied sites. In all

conditions the regression line showed a trend between high gene expression and high CHD1 binding intensities (Figure 16B). Notably, also low and medium expressed genes showed medium to high CHD1 binding, especially in MSC osteoblasts. Moreover, the distribution pattern was much broader, supported also by a lower Pearson correlation coefficient between 0.44 in FOB and up to 0.57 in osteoblast differentiated MSC. Summarized, this shows an overall high correlation between CHD1 and active histone marks around TSS. Nevertheless, a lower correlation between CHD1 and gene expression was observed. This was partially caused by low or medium levels of gene expression but relatively high binding of CHD1.

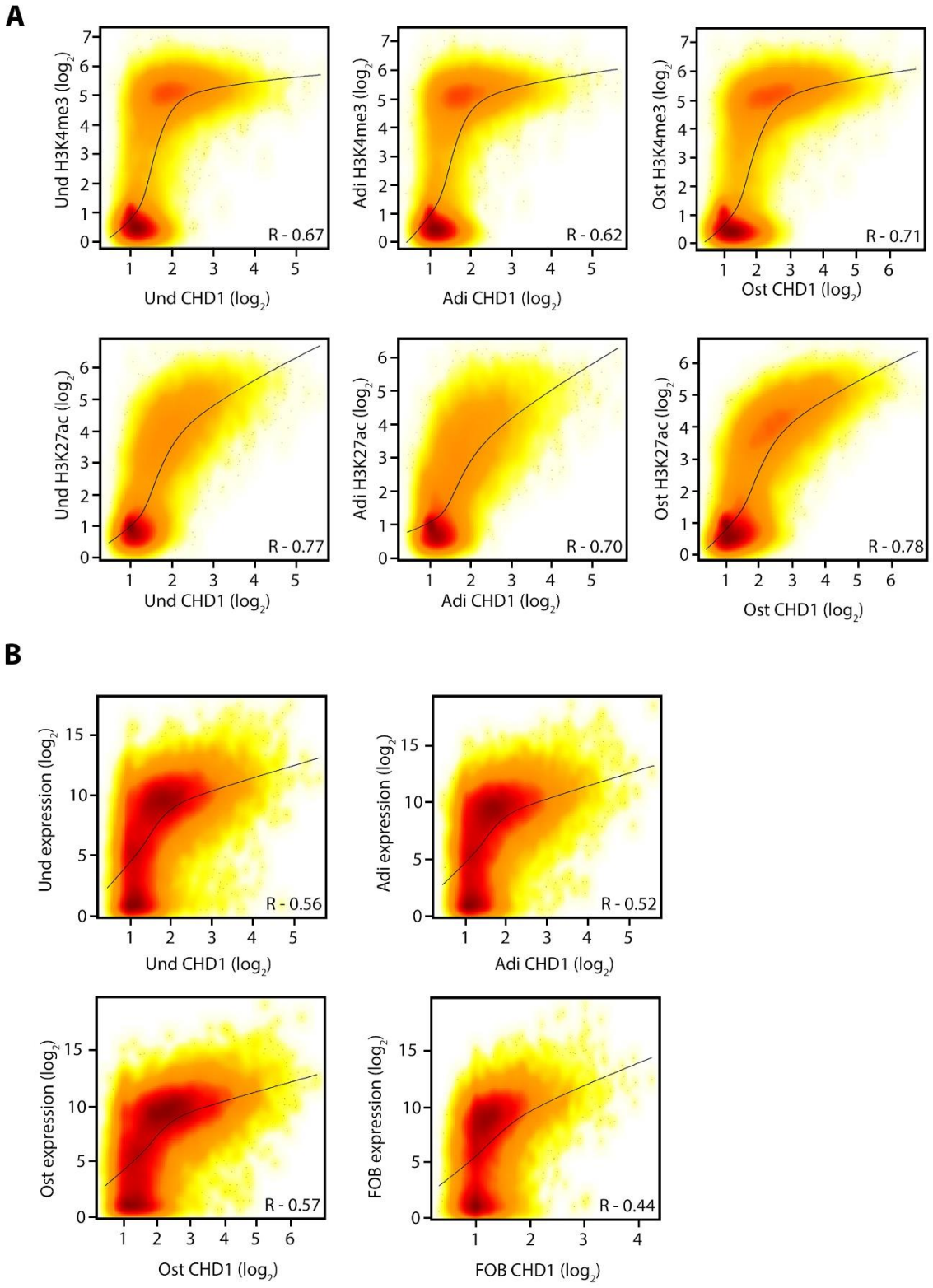

Figure 16: CHD1 positively correlates with active histone marks and gene expression. A Smooth scatter plots show binding intensities of CHD1 (x-axis), H3K4me3 (upper panel) and H3K27ac (lower panel) downstream of the TSS (0 – 1 kb). The Pearson correlation coefficient for each dataset is shown at bottom right of the respective plots (R). Black lines represent the regression curves. ChIP-seq values of the respective samples in undifferentiated (Und), adipocyte (Adi) and osteoblast (Ost) condition were used for the calculation of binding intensities and were log_2 transformed. **B** Smooth scatter plots depict CHD1 binding intensities (x-axis) against gene expression in undifferentiated

(Und), adipocyte (Adi) and osteoblast (Ost) condition in MSC or osteoblast differentiated FOB. All human (hg19) genes were used for analysis. For further description see A.

4.13 Induced genes during differentiation are enriched in CHD1 binding around their TSS

Since the previous sections showed that CHD1 was variably correlated with gene expression, we especially sought to investigate how differentiation-regulated genes were bound by CHD1. Genes which were induced, unchanged, or repressed during differentiation in MSC were grouped and analyzed for their CHD1 binding at their TSS-region. Subsets were formed with thresholds as described before (Figure 9 , +/- 0.5 $\log_2$FC, p-adj. < 0.05).

Adipocyte- and osteoblast-differentiated genes which were induced during differentiation had increased CHD1 binding downstream of their TSS, compared to unregulated or repressed genes (Figure 17A, B). Additionally, when comparing CHD1 binding in the undifferentiated state to these genes no or minor differences in their average profile were observed. These findings strongly suggest that genes which were induced during differentiation required CHD1 for their activation, as many of the activated genes were rather inhibited in their induction after CHD1 depletion (Figure 9A, B).

Next, we investigated if the genes induced during the osteogenesis of MSC had also increased CHD1 binding in FOB. This would imply similarities between the cell lines in osteoblast-specific gene activation and requirement of CHD1 for their induction. Indeed, increased CHD1 binding at TSS-sites of genes activated during MSC osteogenesis were also enriched in FOB differentiated osteoblasts (Figure 17B).

Additionally, it was surprising that CHD1 binding signals were higher in osteoblast-differentiated MSC than in undifferentiated or adipocytes. The reason is unknown, but it can be hypothesized if this was due to higher binding affinity, more recruitment by cofactors or technique procedures. However, binding patterns, gene expression levels and protein levels of CHD1 were not altered in osteoblast or undifferentiated condition (Figure 6B, C, Figure 15A).

A key question was if CHD1 binding around TSS was directly connected to CHD1 mediated gene regulation. To answer this question, all TSS-regions were subset into genes which were higher, lower, or unregulated after CHD1 depletion. Genes were therefore classified by thresholds described before (Figure 9, +/- 0.5 $\log_2$FC, p-adj. < 0.05) and their mean CHD1 binding was calculated in the region between the TSS

and 1 kb downstream. This analysis showed that genes which were less expressed after CHD1 depletion had significant higher CHD1 binding compared to unregulated or higher expressed genes (Figure 17C). Strikingly, this observation was consistent between all differentiation conditions and in MSC as well as FOB. Higher expressed or unregulated genes were not significant differential bound or had low differences in binding. This key finding associated CHD1 protein occupancy around the TSS with direct transcriptional regulation of these respective genes.

Previously, we showed that CHD1 binding was increased at TSS-regions of genes induced during MSC differentiation. Furthermore, these genes were likely to be repressed after CHD1 depletion. Thus, we asked if the genes higher expressed during differentiation, but repressed with CHD1 depletion, were further enhanced in their CHD1 binding around TSS. Indeed, a significant increased CHD1 binding was measured at these TSS-regions (Figure 17D). In FOB however no significant difference was detected (not shown). These findings further support the idea that CHD1 is required for full induction especially of differentiation-activated genes.

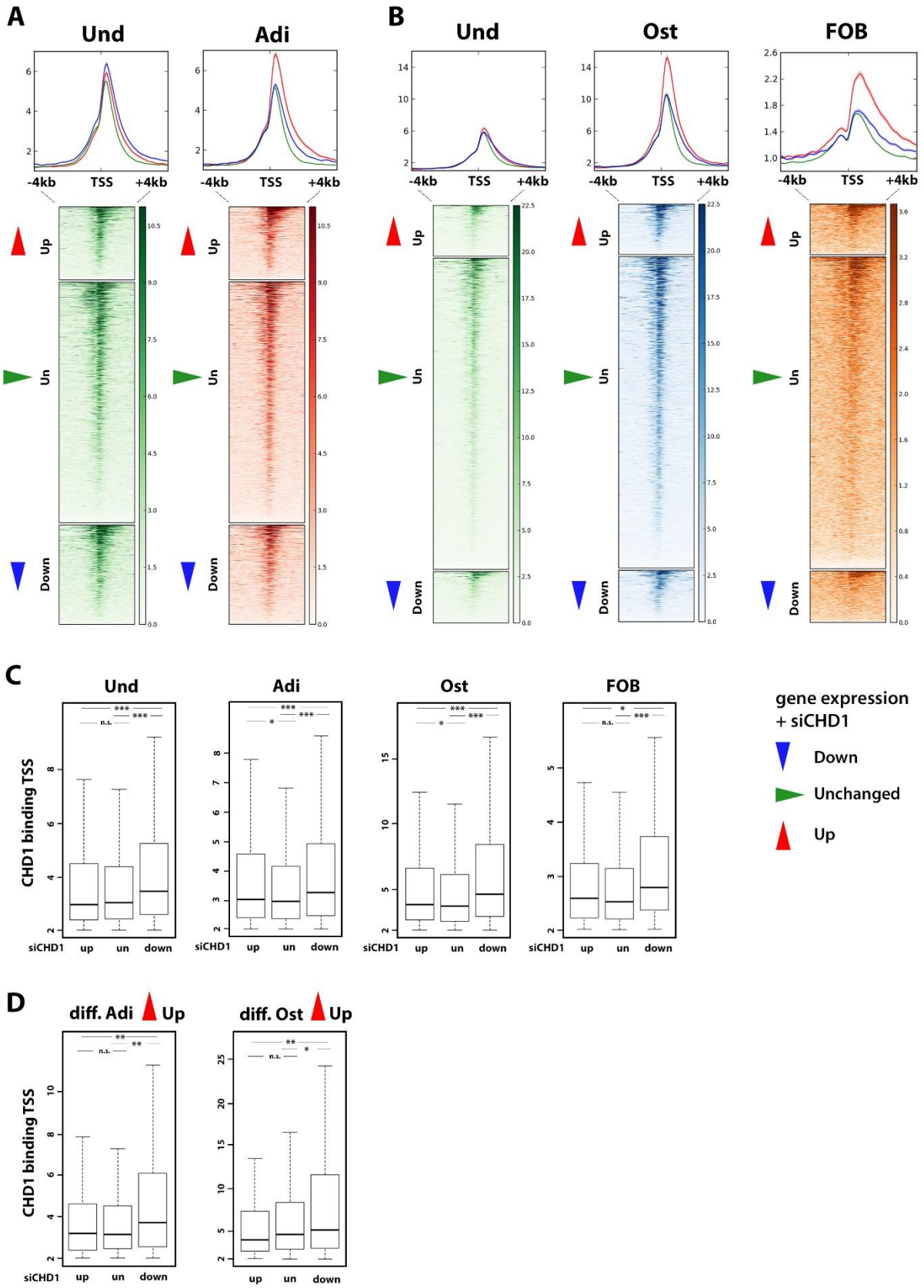

Figure 17: CHD1 binding is enriched near the TSS-regions of induced genes during MSC differentiation. A Heat maps represent CHD1 ChIP-seq binding signals in undifferentiated (Und) or adipocyte differentiated MSC (Adi) relative to a 4 kb region around the centered TSS of genes which were activated (Up, red arrowhead), unchanged (Un, green arrowhead) or repressed (Down, blue

arrowhead) after five days of adipocyte differentiation. Genes were selected based on RNA-seq analysis with previous described thresholds (Figure 9A, +/- 0.5 log_2FC, p-adj. < 0.05). The color keys are shown at the right side of the respective heat map. Aggregate plots above the heat maps represent the mean CHD1 binding values with their standard deviation for the respective regulated gene set indicated by the color code described before. **B** Heat maps show CHD1 ChIP-seq binding in undifferentiated (Und), osteoblast differentiated MSC (Ost) or osteoblast differentiated FOB (FOB) to regions described in A of genes regulated during MSC osteoblast differentiation with thresholds described before (Figure 9B, +/- 0.5 log_2FC, p-adj. < 0.05). For further figure explanation see A. **C** Box plots represent mean CHD1 binding values near TSS of genes regulated by CHD1 depletion in undifferentiated, adipocyte or osteoblast differentiated MSC or osteoblast differentiated FOB. Gene regions between the TSS and 1 kb downstream of higher (up), lower (down) or unregulated (un) expressed genes after siCHD1 transfection were used to calculate normalized CHD1 ChIP-seq values to. Unbound or below background detected TSS were subtracted from calculation. Statistical analysis was performed by Wilcoxon-rank sum test (n.s. – non significant, * p-val. < 0.5, ** p-val. < 0.01, *** p-val. < 0.001). **D** Box plots depict CHD1 binding values to regions as described in C of genes activated during adipocyte or osteoblast differentiation in MSC. Further these genes were grouped by CHD1 regulation. For further description see C.

4.14 Single gene analysis reflects genome-wide observed effects

Next, we sought to test whether the genome-wide findings of CHD1-dependent regulation on genes by binding to their TSS-regions could also be observed on the single gene level. Therefore, ChIP-seq profiles of CHD1, H3K4me3, H3K27ac, H3K27me3 in osteoblast differentiated and undifferentiated conditions together with RNA-seq signals were compared. Genes, which were transcriptionally induced during osteoblast differentiation and either repressed (*SIX1*, *DUSP1*, *DUSP5*) or enhanced (*ALPL*, *BGLAP*) after CHD1 depletion were analyzed. Epithelial membrane protein 3 (EMP3) was selected as an unregulated control gene.

As expected, these selected genes, except for the negative control, showed as expected an increase of the activating marks H3K4me3 and H2K27ac (Figure 18), whereas the repressive mark H3K27me3 was barely detectable except for *ALPL*. This indicates that these genes were probably not primed for transcription-activation before differentiation. Interestingly, *ALPL* showed only minor changes in H3K4me3 and H3K27ac, but H3K27me3, a repressive mark, was high in undifferentiated and still weakly present in differentiated state. Most intriguingly, however, was the strong increase of CHD1 binding at the TSS-regions of the activated genes *SIX1*, *DUSP1* and *DUSP5* after differentiation. Nevertheless, only a minor increase of CHD1 binding was observed around the TSS of *ALPL* and *BGLAP* which were upregulated after CHD1 depletion. In sum, these findings support the role of CHD1 specific regulation at the TSS of differentiation-induced genes in osteoblasts. Additionally, it

suggests that the marker genes *ALPL* and *BGLAP* were probably indirectly regulated after CHD1 depletion.

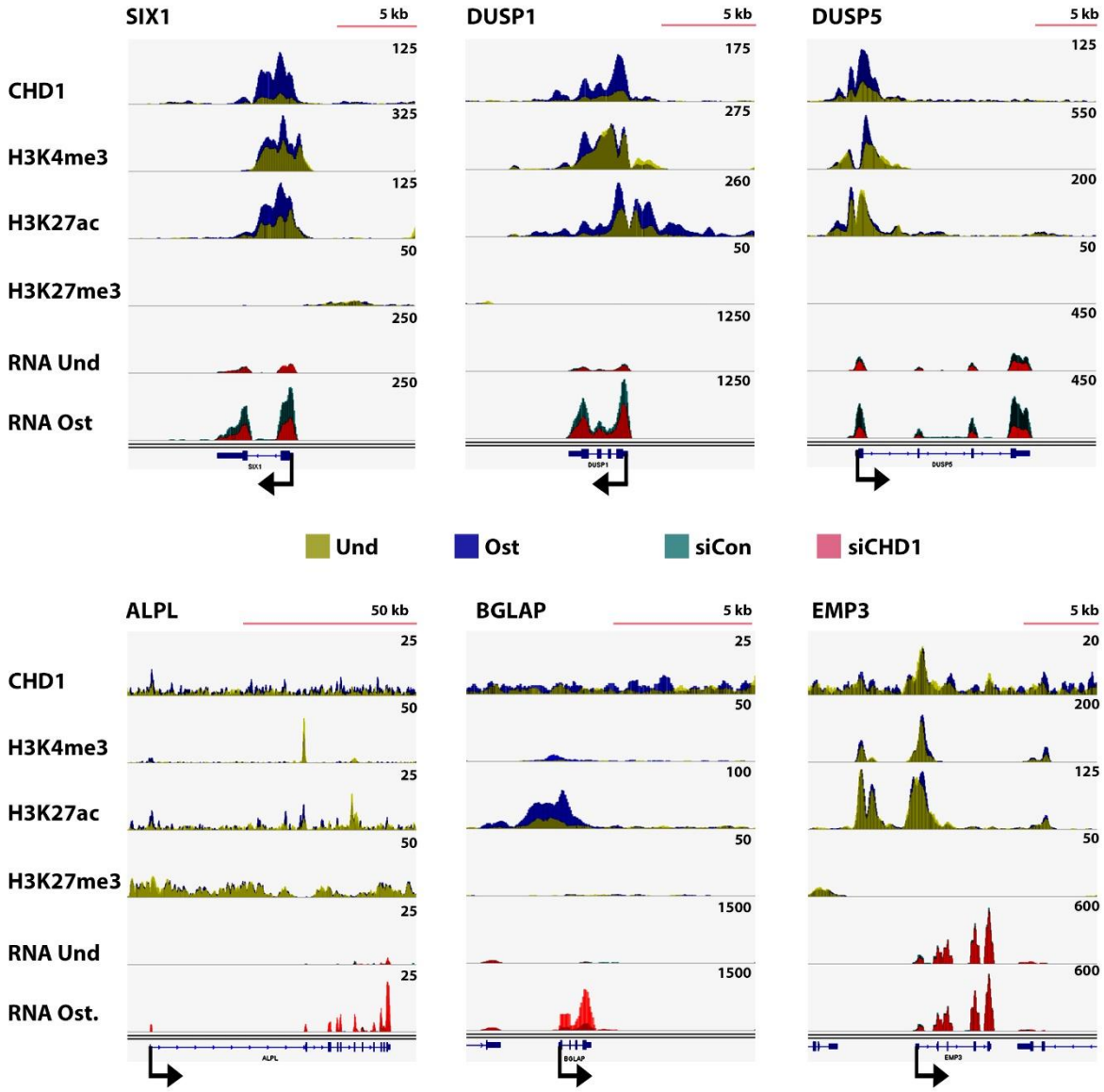

Figure 18: CHD1 binding signals increase around TSS during osteogenesis at CHD1 dependent genes. ChIP-seq profiles of CHD1, H3K4me3, H3K27ac, H3K27me3 in undifferentiated (Und, yellow) and differentiated (Ost, blue) conditions are shown along with RNA-seq signals in siCon (green) or siCHD1 (red) transfected MSC. Genes significantly activated during osteoblast differentiation and repressed by CHD1 depletion (SIX homeobox 1 (*SIX1*), dual specificity phosphatase 1 (*DUSP1*), *DUSP5*, alkaline phosphatase liver/ bone/ kidney (*ALPL*), bone gamma-carboxyglutamate (Gla) protein (*BGLAP*)) or unregulated by differentiation and CHD1 depletion (epithelial membrane protein 3 (*EMP3*)) were selected. Scale bars are shown top right of each panel and represent sizes in kilo base pairs (kb). Normalized read counts are shown top right of each lane and black arrowheads indicate directionality and transcriptional start sites (TSS) of genes.

4.15 Global RNA-Pol II occupancy increases around TSS after CHD1 depletion

In the previous sections we saw that repressed genes after CHD1 depletion had higher binding of CHD1 at the TSS than unregulated or enhanced expressed genes. To address the mechanism of how CHD1 depletion caused less transcription at these genes we decided to analyze the occupancy of RNA-Pol II, H2A.Z and H2Bub1 at these genes in control and CHD1 depleted condition. Previous studies have shown that CHD1 was necessary for RNA-Pol II to overcome the nucleosome barrier downstream of the TSS (Skene et al., 2014). Further, the histone variant H2A.Z, which is also located at the TSS and correlates well with H3K4me3 (Ku et al., 2012) is associated with gene transcription (Zlatanova and Thakar, 2008) and decreased nucleosome stability (Abbott et al., 2001; Henikoff et al., 2009). A connection between CHD1 and H2A.Z had been discussed but was to our knowledge not subjected to an experimental study before (Persson and Ekwall, 2010). As CHD1 is a chromatin remodeler, involved in shifting of nucleosomes and is co-localized with H2A.Z downstream at the TSS we hypothesized that CHD1 depletion could cause alterations in H2A.Z and RNA-Pol II occupancy in FOB. Further, although no global change of H2Bub1 was detected with low CHD1 protein levels gene specific regulation could not be excluded. Therefore, H2Bub1 was analyzed via ChIP-seq to obtain information for specific gene groups and further used as a read-out for gene transcription, as H2Bub1 levels correlate well with transcription elongation levels (Fuchs et al., 2014).

First genome-wide distribution of RNA-Pol II, H2A.Z and H2Bub1 were analyzed in control and CHD1 depleted condition around all TSS. Intriguingly, a genome-wide increase of RNA-Pol II at the TSS was observed when CHD1 was depleted (Figure 19A). Yet, no obvious difference between the total number of bound TSS was observed when comparing the heat maps. As RNA-Pol II binding was recently also described at enhancers we sought to analyze these loci too (Lam et al., 2014). Therefore, FOB specific and active enhancer regions, defined by BRD4, H3K4me1 and H3K27ac occupancy, were analyzed. Interestingly, no difference was observed between the tested conditions (Figure 19B). To exclude that the different binding intensities at TSS were due to higher global RNA-Pol II levels in the CHD1 depleted condition Western blot analysis was performed. We detected no change in the total RNA-Pol II levels by Western blot between control and CHD1-depleted condition (Figure 19C). This in sum supported the idea that higher RNA-Pol II binding at TSS

sites is independent from total RNA-Pol II levels and restricted around TSS, but not at enhancers. Additionally, CHD1 binding mainly occurred around TSS and less at intergenic regions. This indicates that CHD1 is directly involved in the regulation of these binding occupancies.

The H2A.Z signals showed a biphasic peak around the TSS, flanking the RNA-Pol II peak, as described by others as well (Ku et al., 2012) (Figure 19A). Interestingly, reduced H2A.Z levels downstream and upstream of the TSS were observed when CHD1 was depleted (Figure 19A). Moreover, lower differences in the ratio between the peak height downstream and upstream of the TSS were obvious in CHD1-reduced condition. The total number of H2A.Z bound regions however did not change when comparing the signals of the heat maps. Like RNA-Pol II H2A.Z is present at enhancers (Jin et al., 2009). To analyze if the observed effects were also taking place at enhancers, the regions described above were used to map H2A.Z under the different conditions. Surprisingly and contrary to the pattern at the TSS, a slight increase of H2A.Z occupancy at these regions after CHD1 depletion was observed. This suggests that regulation of H2A.Z exchange taking place at the enhancer is different than at the TSS and that latter is likely connected to CHD1. We wondered whether these changed H2A.Z histone distributions at TSS were caused by different H2A.Z protein levels in the cells. Therefore, we performed Western blot to measure the H2A.Z level, but did not detect a change in protein levels of H2A.Z (Figure 19C).

Finally, H2Bub1 occupancy to all gene regions between TSS and 5 kb downstream of TSS were compared in CHD1 depleted and control condition. Concordant with the results of the Western blot (Figure 7A) no global change in H2Bub1 binding was observed at these regions. This also showed that although a global increase of RNA-Pol II at the TSS was measured, no global increase of the transcription elongation marker H2Bub1 was detected. Further, based on the RNA-seq results less than then percent of all genes were significantly regulated with low levels of CHD1. This indicates that no global effect on gene expression regulation occurred, although increased RNA-Pol II was measured around the TSS.

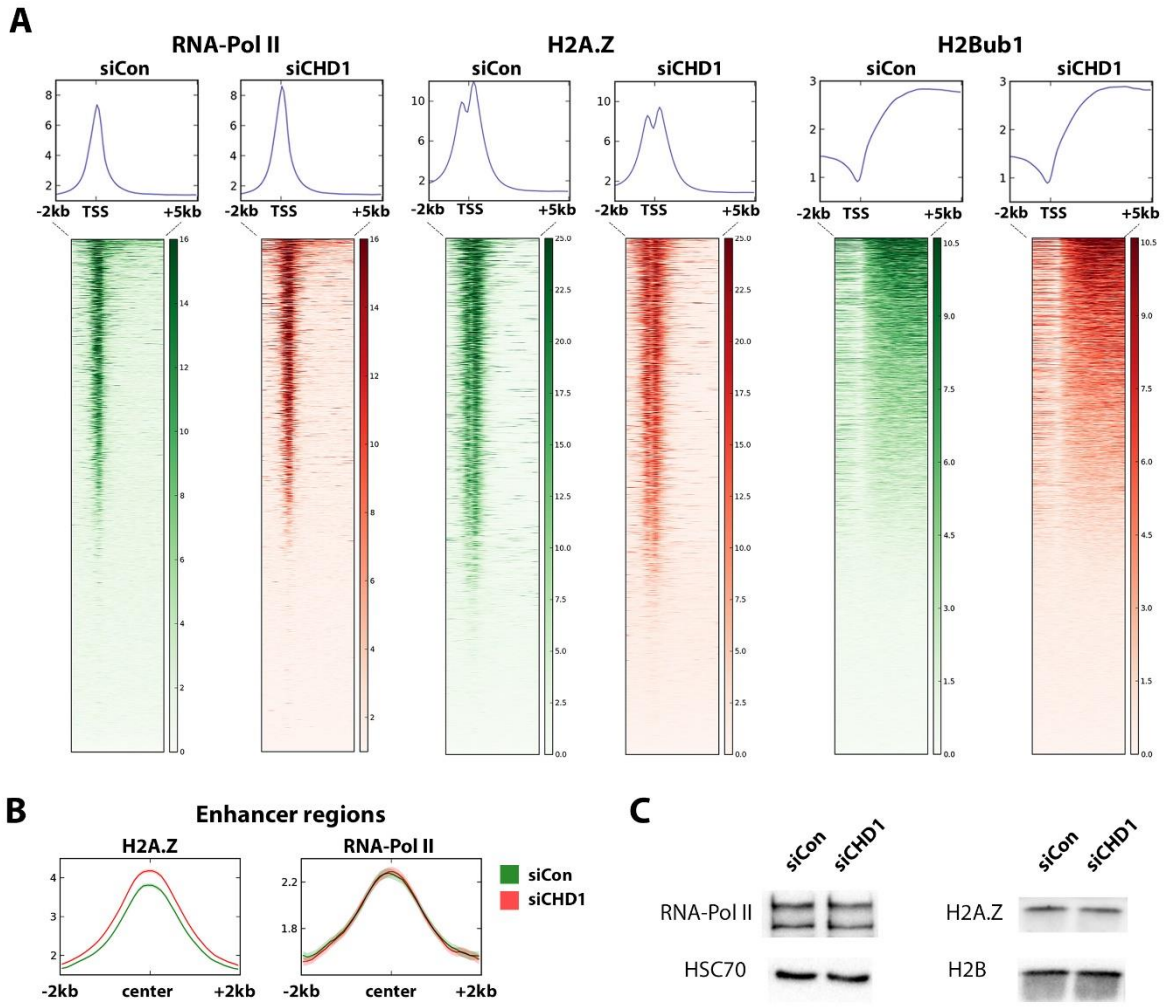

Figure 19: CHD1 depletion increases RNA-Pol II and decreases H2A.Z binding around TSS. **A** Heat maps represent binding of RNA-Pol II, H2A.Z and H2Bub1 of control (green heat maps) or CHD1-depleted (red heat maps) osteoblast differentiated FOB around TSS. Gene regions were sorted from high to low signal intensity. The average binding profiles above each heat map show the mean binding signal between 2 kb upstream to 5 kb downstream of the TSS (y-axis). The color keys are shown right to the respective heat map. **B** Average profile plots depict binding of H2A.Z and RNA-Pol II in control (green) or CHD1-depleted (red) condition 2 kb around active enhancers bound by BRD4. The signal intensities (y-axis) of mean values with standard deviations are plotted relative to the center of enhancer regions. **C** Immunodetection of RNA-Pol II, HSC70, H2A.Z or H2B with antibodies by Western blot analysis of whole cell protein lysates of differentiated and siCon or siCHD1 transfected FOB.

4.16 CHD1 dependent genes show unchanged RNA-Pol II levels around their TSS

As the global patterns of H2A.Z and RNA-Pol II binding around TSS were impaired after CHD1 depletion, but not all genes were differentially expressed, we sought to further investigate the binding patterns at the CHD1 regulated genes. Surprisingly, RNA-Pol II levels in CHD1-depleted cells were almost unchanged at the TSS-regions compared to control, although the gene expression was reduced after CHD1 depletion (Figure 20A). As expected, enhanced expressed genes showed increased enrichment of RNA-Pol II close to the TSS, but unregulated genes had counter intuitively increased RNA-Pol II signals, as well. However, concordant with reduced gene expression after CHD1 depletion a drop of H2Bub1, a mark for transcriptional elongation, was observed over the gene body (Figure 20A). Moreover, genes with increased transcription after CHD1 depletion indeed showed increased H2Bub1 marks, but, as expected, were transcriptionally unchanged genes not altered in H2Bub1 average levels. This revealed that CHD1-sensitive genes had low transcription levels and indeed reduced H2Bub1 binding over the gene body, but unexpectedly almost unchanged RNA-Pol II occupancy at the TSS. Further, CHD1 unregulated genes also had increased RNA-Pol II levels at the TSS-regions, but neither a change in H2Bub1 nor in gene expression. This together strongly indicates a stalling of RNA-Pol II when CHD1 protein concentration is reduced.
When comparing H2A.Z levels between the differentially expressed genes, no strong differences were observed in either control or siCHD1 condition, except that enhanced expressed genes had higher levels of H2A.Z in the biphasic peaks (Figure 20A). The almost equal levels of H2A.Z at the TSS in CHD1 reduced condition indicates that the lower H2A.Z occupancy correlated well with genome-wide increased RNA-Pol II at the TSS-regions, however it was not reflecting the change of gene expression caused by CHD1 depletion.

As genes repressed by CHD1 depletion showed lower levels of H2Bub1 and RNA-Pol II in control condition we were curious to investigate how these genes were expressed before and after differentiation. First, the gene regulation during differentiation of CHD1 regulated genes in FOB was analyzed. Genes which were attenuated in their expression upon reduction of CHD1 protein levels were strong induced during differentiation (Figure 20B). Moreover, genes unregulated or higher

expressed upon CHD1 depletion showed no or even reduced activation during differentiation, respectively. Interestingly, genes which were sensitive to CHD1 depletion also showed the lowest expression in undifferentiated condition, but were elevated to similar expression levels after differentiation. Most striking however was that the genes in differentiated CHD1-depleted condition were similar in their gene expression levels to undifferentiated status. This is in accordance with previous findings where CHD1 depletion reduced gene expression changes taking place in osteoblast differentiation. Together with the ChIP-seq data, these findings suggest that CHD1 is required for the induction of genes activated during differentiation. It also implicates that the regulation took place downstream of the TSS by affecting early RNA-Pol II-mediated transcription elongation.

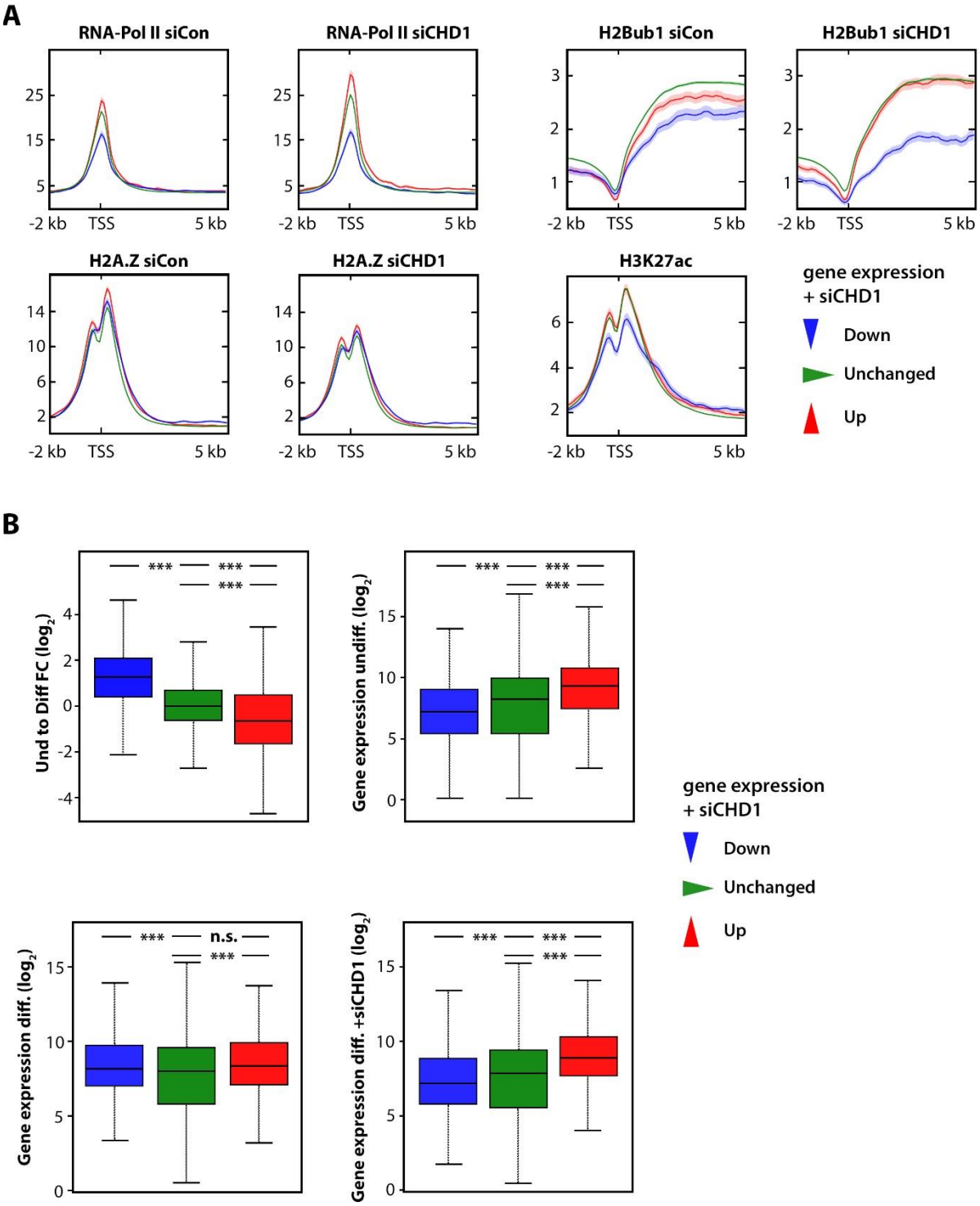

Figure 20: Unchanged RNA-Pol II occupancy around TSS of repressed genes after CHD1 depletion. A Average profile plots of RNA-Pol II, H2Bub1, H2A.Z binding of control or CHD1 depleted differentiated FOB were plotted relative to the TSS of lower (blue), unchanged (green) or higher (red) expressed genes after CHD1 depletion. Genes were subset by thresholds as described before (+ or - 0.5 log_2FC, p-adj. < 0.05, Figure 9A). Mean normalized read counts of respective ChIP-seq samples at 2 kb upstream and 5 kb downstream of TSS are shown with their standard deviation. **B** Box plots depict repressed (blue), unregulated (green) and activated genes (red) after CHD1 depletion for fold changes (FC) in i) gene expression during differentiation (top left box plots), ii) gene expression in undifferentiated FOB (top right box plots), iii) gene expression in differentiated FOB (bottom left box plots) and iv) gene expression in CHD1 depleted differentiated FOB (bottom right box plots). Values

are shown after log_2 transformation. Statistical analysis was performed by Wilcoxon-rank sum test (n.s. – non significant, * p-val. < 0.05, ** p-val. < 0.01, *** p-val. < 0.001).

4.17 ChIP-seq profiles reveal RNA-Pol II stalling also on single gene level

To confirm the observed genome-wide effects on single-gene scale ChIP-seq profiles in FOB of control and CHD1-depleted condition were compared for differently regulated genes. Three representative examples of differentially expressed genes in CHD1-reduced conditions were studied at their genomic region close to the TSS. This analysis of the single-gene profiles also clarified the order of peaks at the TSS-region of CHD1, RNA-Pol II and H2A.Z and their change after CHD1 depletion. First, the CHD1 peak was located downstream of the TSS and the stalled RNA-Pol II (Figure 21). Next, the RNA-Pol II signals were biphasically flanked by H2A.Z peaks, which was well observed for the repressed high mobility group AT-hook 2 (*HMGA2)*, unregulated guanine nucleotide-binding protein G(I) subunit alpha-1 (*GNAI1*) or higher expressed syndecan 1 (*SDC1*). Notably, also the H2A.Z profiles at the TSS were decreased when CHD1 was reduced, but peaks upstream of the TSS were less effected, particularly at the higher expressed paired-like homeodomain 1 (*PITX1*) or the repressed *KLF9* gene. This observation of TSS-region independent regulation was concordant with the similar levels of H2A.Z at FOB-specific enhancer (Figure 19B). Further, CHD1 depletion stronger decreased the H2A.Z peak downstream of the TSS, as it was observed at the *ELN* gene-region.

The *ELN* gene was of special interest as it is associated with enhanced ectopic bone formation (Larsen et al., 2010; Twine et al., 2014) and repressed by low levels of CHD1 protein (Figure 6C, Figure 7C). In this single-gene profile, increased RNA-Pol II levels were detected downstream of the TSS, but decreased levels at the gene body in CHD1-depleted condition. This represents an interesting example of a gene with strong CHD1-dependent regulation. Thus we asked if this pattern of high RNA-Pol II around the TSS but low-occupancy at the gene body was general for CHD1

sensitive genes.

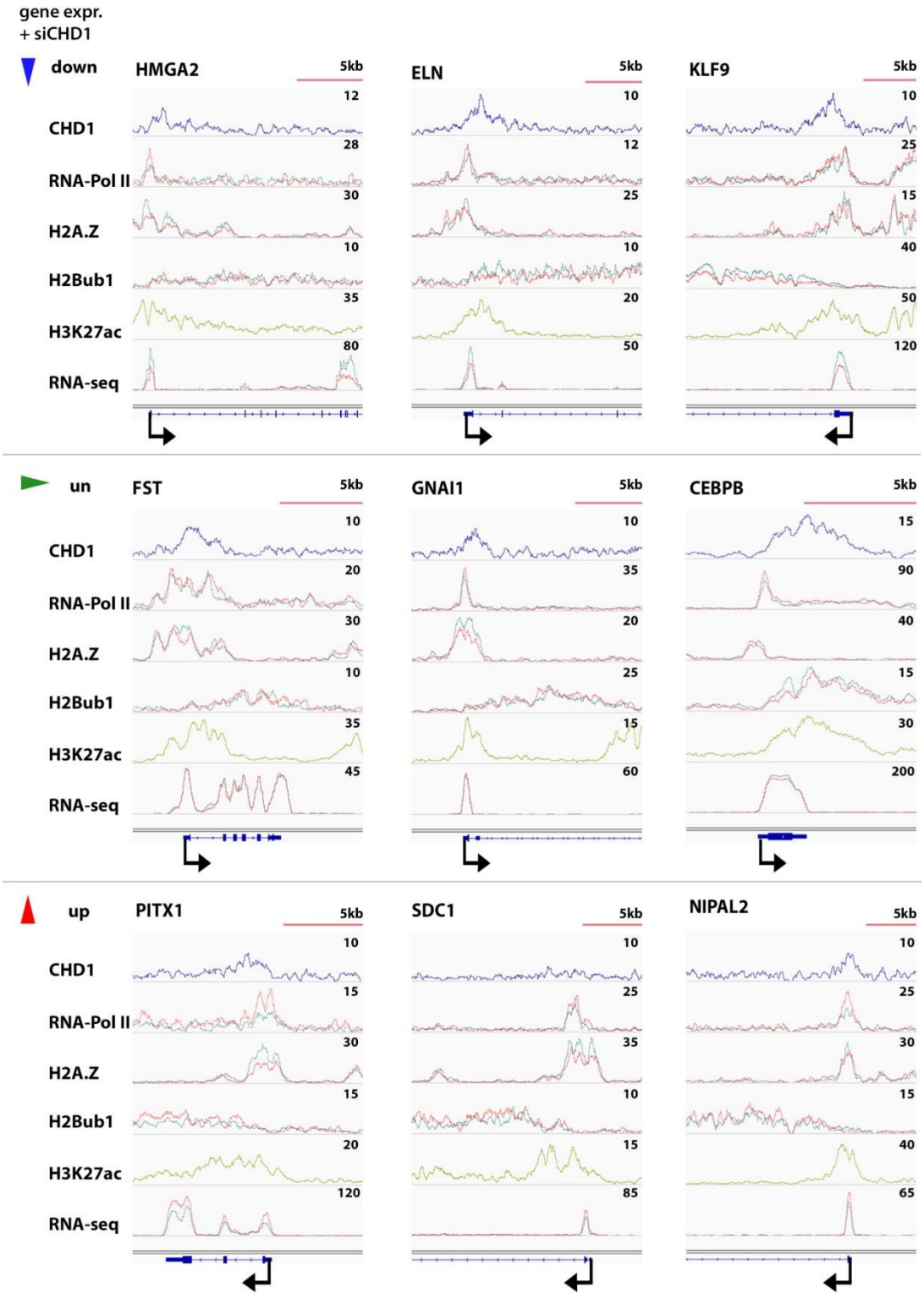

Figure 21: Single-gene profiles describe different pattern of RNA-Pol II profiles after CHD1 depletion. ChIP-seq profiles of CHD1, RNA-Pol II, H2A.Z and H2Bub1 of siCon (green) or siCHD1 (red) transfected FOB are shown along with H3K27ac ChIP-seq and RNA-seq signals. Genes significantly repressed (blue arrow), activated (red arrow) or unchanged (green arrow) after CHD1 depletion were selected as described previously (+ or - 0.5 log_2FC, p-adj. < 0.05, Figure 9A). Scale bars are shown top right in kilo base pairs (kb) units. Signal intensities are represented in normalized read counts shown top right. Black arrowheads indicate TSS and directionality of genes.

4.18 Highest RNA-Pol II stalling ratios at TSS-regions of CHD1 dependent genes

To further unravel the transcription regulation after CHD1 depletion the genome-wide RNA-Pol II binding was quantified around the TSS and on the gene body (GB) to analyze RNA-Pol II stalling ratios. Therefore, RNA-Pol II intensities were measured in a 300 bp region around the centered TSS and divided by values obtained from the GB (Figure 22A). A similar calculation was described previously by others (Lin et al., 2012). The values were measured for the different groups of genes regulated by CHD1 (+ or - 0.5 log_2FC, p-adj. < 0.05, Figure 20A).

First, the binding occupancy of RNA-Pol II around the TSS was compared between the different gene sets in control and CHD1 depleted condition. As observed previously RNA-Pol II values were increased at TSS of unregulated and enhanced transcribed genes, but a decreased median of RNA-Pol II binding at the TSS of repressed genes was measured (Figure 22B). Though, if comparing the mean values, no significant difference was detected (data not shown). Most interesting were the effects observed at the gene bodies. Genes less expressed after CHD1 depletion indeed had significantly less RNA-Pol II binding at the GB. As expected, no difference was observed at unregulated genes. Highly expressed genes had an increased median of RNA-Pol II at the GB, which was, however, not significant. Finally, when comparing the RNA-Pol II ratio between values measured at the TSS and GB, all gene groups showed an increased stalling ratio with low CHD1 protein levels. Intriguingly, we observed the highest difference for repressed genes. This indicates the highest retention of RNA-Pol II is present at genes which are repressed after CHD1 depletion. Although unregulated and highly expressed genes had also an increased stalling of RNA-Pol II around TSS, similar median levels of RNA-Pol II or increased levels of RNA-Pol II at GB were measured in non-regulated or highly expressed genes, respectively. This together indicates that RNA-Pol II is impaired in its early elongation release rate into the gene body in a genome-wide manner and gets stalled at the TSS in CHD1 depleted condition. The fact that still not all genes are reduced in their expression is likely by a compensation of increased RNA-Pol II occupancy at TSS-regions. Genes which are reduced in their mRNA-expression may not have sufficient increase of RNA-Pol II to adapt to the increased stalling ratio.

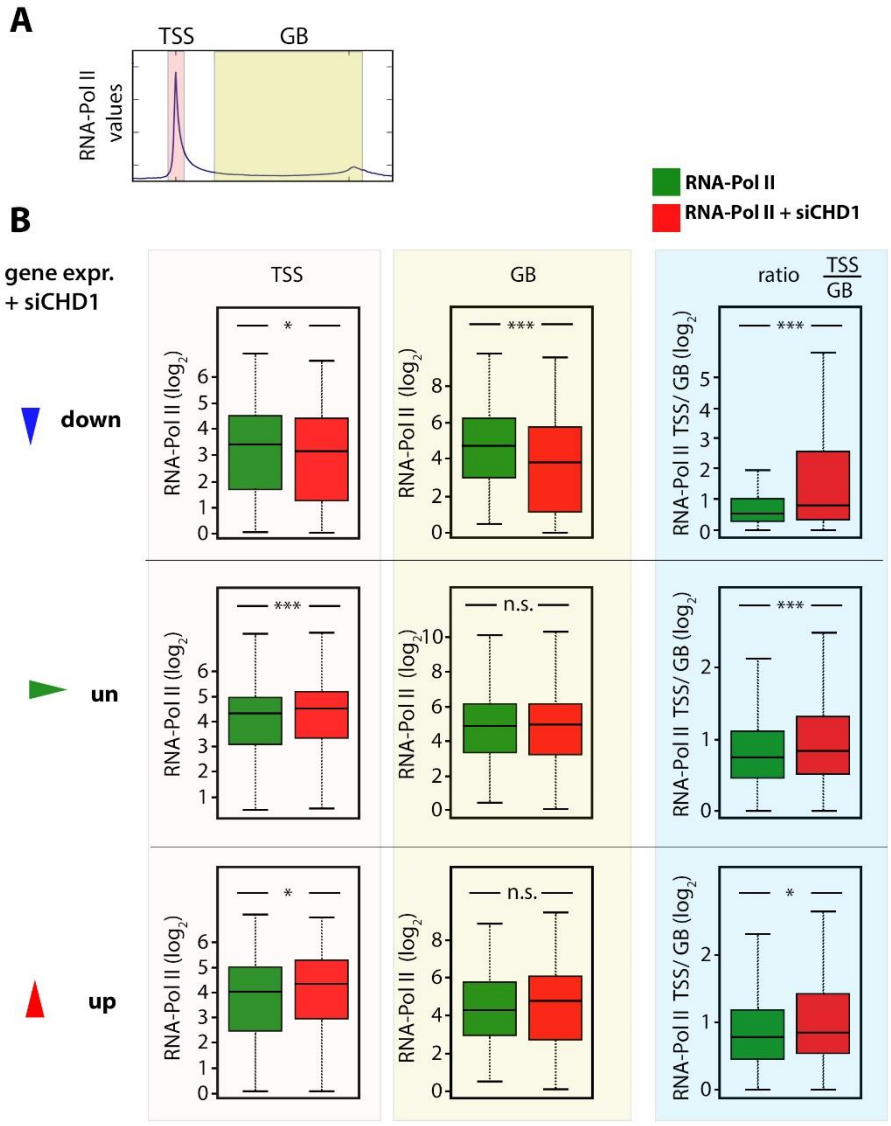

Figure 22: RNA-Pol II stalling ratios are highest in repressed genes after CHD1 depletion. **A** Schematic average profile plot of RNA-Pol II signals over a meta-gene with the transcriptional start site (TSS) region (red box), defined by 300 bp around the centered TSS and the gene body (GB) region defined as 30% of gene length downstream of the TSS to 3 kb downstream of the transcription termination site (TTS) (yellow box). These regions were used to calculate the RNA-Pol II occupancy by the DiffBind software (Lin et al., 2012). **B** Box plots show values of RNA-Pol II occupancy at the TSS-region, in the GB or the ratio of both values (TSS divided by GB) in control (green) or CHD1 depleted (red) FOB. Measurements of normalized ChIP-seq values were calculated for genes which were less (down), unchanged (un), or higher expressed (up) after CHD1 depletion in FOB (+ or - 0.5 log_2FC, p-adj. < 0.05, Figure 20). Statistical analysis was performed by Wilcoxon-rank sum test (n.s. – non significant, * p-val. < 0.05, ** p-val. < 0.01, *** p-val. < 0.001). Values depicted were log_2 transformed.

5 Discussion

Transcriptional regulation plays an essential role in determining the cell fate during differentiation. Importantly, epigenetic processes are pivotal in coordinating various signals within the cell and respond to the physiological stimuli. Besides histone modifications, the chromatin undergoes extensive remodeling at genes and gene regulatory regions. Though, these regulatory mechanisms are often co-regulatory. The ATP-dependent chromatin remodeler CHD1 is a well described transcriptional co-regulator. However, the mechanistic role of CHD1 during stem cell differentiation is poorly studied. Here, we could show that CHD1 is required for lineage-specific differentiation of MSC and FOB by regulating the expression of differentiation-specific genes. Genome-wide CHD1 occupancy analyses revealed its increased binding at TSS of differentiation-induced genes, thus promoting their transcription activation. Mechanistically we could show that CHD1 depletion caused increased stalling of RNA-Pol II at the TSS region, especially on induced genes during differentiation. Furthermore, global H2A.Z levels around TSS were decreased with CHD1 knockdown, which may cause a higher stability of the +1 nucleosome at the TSS and led to increased stalling. Finally, ectopic bone formation in mice was decreased with constitutive knockdown of CHD1 confirming its role in bone differentiation *in vivo*. This altogether showed that CHD1 can act as a regulator of stem cell differentiation partly by affecting the stalling of RNA-Pol II and H2A.Z occupancy which regulate differentiation-dependent gene expression.

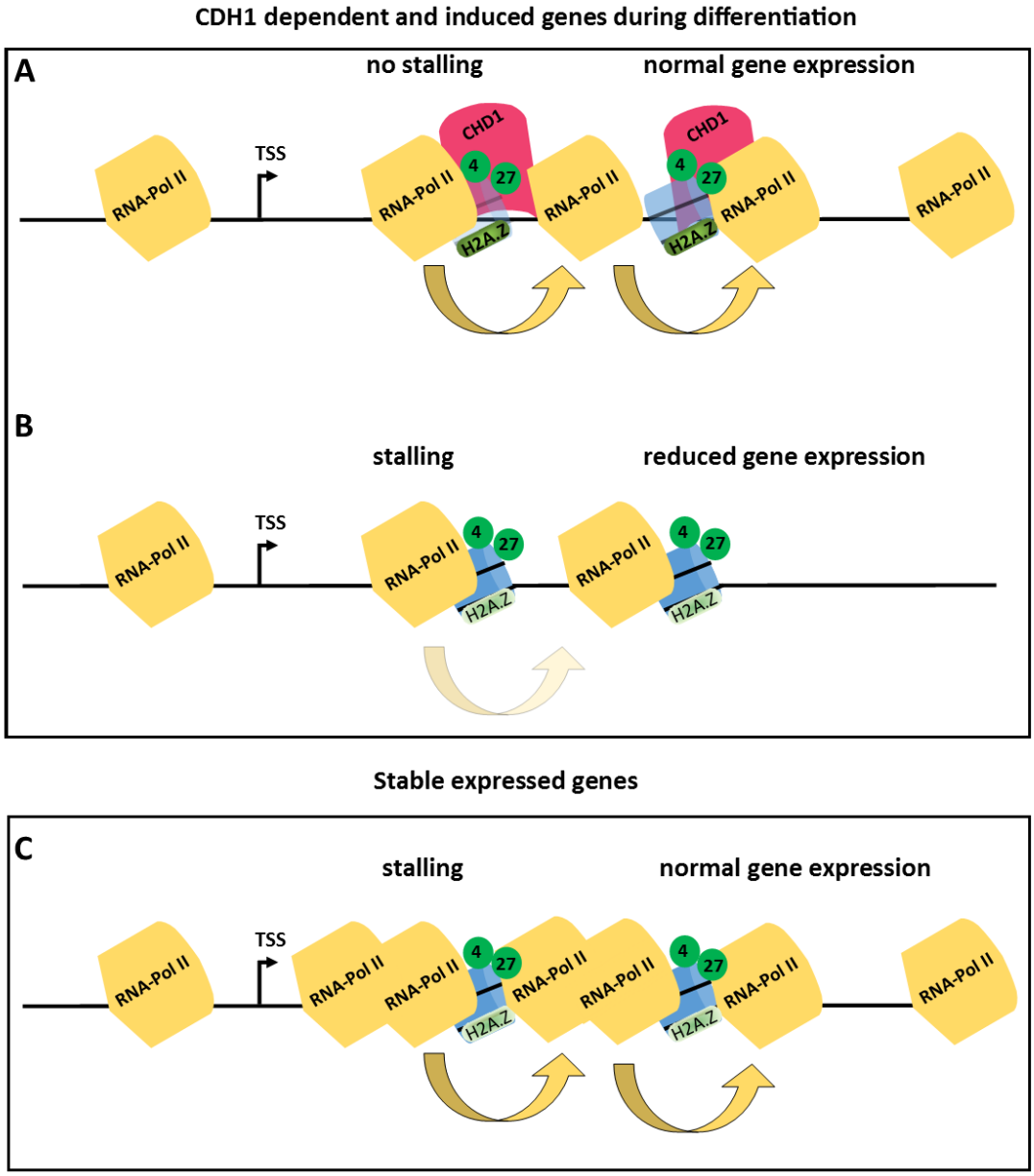

Figure 23 Model of CHD1-regulated gene expression during differentiation of induced and stably transcribed, non-induced genes. A The induced gene is transcriptionally activated and bound by CHD1 (red) which remodels the nucleosome barrier for efficient, early-elongation of the RNA-Polymerase II (RNA-Pol II). CHD1 binding downstream of the transcriptional start site (TSS), close to the nucleosome marked with H3K4me3 (green four) and H3K27ac (green 27), increases the nucleosome turnover and the incorporation of the histone variant H2A.Z. This incorporation further destabilizes the nucleosome for an efficient RNA-Pol II passage. The less intense color of H2A.Z indicates its reduced occupancy. **B** In the absence of CHD1 the RNA-Pol II is stalled during the early-elongation process downstream of the TSS. The overcoming of the nucleosome barrier is reduced which causes decreased gene expression for a low expressed and induced gene. Low levels of H2A.Z might further increase the nucleosome stability. **C** A stable expressed gene which is further induced by differentiation has stalled RNA-Pol II downstream of the TSS as well, when CHD1 is depleted. However increased RNA-Pol II levels around the TSS increase the likelihood of overcoming the nucleosome barrier which leads to unchanged gene expression, even though H2A.Z levels are low.

5.1 Genome-wide transcription effects of CHD1 by regulating RNA-Pol II stalling

CHD1 is described as a global co-activator of gene expression in mice and human (Koh et al., 2015; Sims et al., 2007). However, most of the studies in yeast or mouse observed only mild effects of CHD1 on global gene expression (Gaspar-Maia et al., 2009; Lee et al., 2012a). Nonetheless, only few studies performed genome-wide transcription analyses in a CHD1-impaired system after various stimuli for example by stress or differentiation (Koh et al., 2015; Park et al., 2014). In this study we observed that transcriptional activation was regulated and that CHD1 depletion had differential effects during differentiation. Thus, we hypothesize that CHD1 is required for a cell fate change. Indeed, effects on de-differentiation were observed earlier in mouse when Gaspar-Maia and colleges reprogrammed CHD1-depleted MEFs by introducing the Yamanaka factors, where a significant reduction of iPS colony formation was observed when CHD1 was depleted by RNAi (Gaspar-Maia et al., 2009). A recent *in vivo* study of the same group showed that CHD1 is necessary for the differentiation of endothelial progenitor cells to HSC by blocking differentiation-specific genes (Koh et al., 2015). However, if genes induced during differentiation or if already stable expressed genes were CHD1-sensitive stayed elusive. With our investigations we were able to show that CHD1 is required for the direct activation of induced genes during osteoblast differentiation. This indicated gene specific regulation. Though, another study reported that CHD1 is necessary for a global increase of transcriptional output in highly proliferating mouse epiblasts, but with decreased RNA-Pol II occupancy levels around TSS in CHD1 knockout embryonic stem cells (Guzman-Ayala et al., 2015). However consistent with our findings, a study in non-embryonic human system observed the RNA-Pol II stalling as the central regulatory mechanism for differential transcription regulation too (Skene et al., 2014).

5.1.1 How is CHD1 depletion affecting gene expression in particular?

To elucidate the molecular mechanism of CHD1-specific gene regulation, we studied the occupancy of RNA-Pol II, H2A.Z and H2Bub1 under CHD1-depleted conditions. In consistence with the association of RNA-Pol II with CHD1 in overcoming the +1 nucleosome barrier (Skene et al., 2014), we observed that CHD1 depletion affects global RNA-Pol II stalling. Here we extended the regulatory mechanism by showing that only particular genes were sensitive in differential gene expression to RNA-Pol II stalling after CHD1 depletion. Unaffected and higher expressed genes after CHD1

depletion gained RNA-Pol II, but repressed genes did not. This led us to hypothesize that the higher nucleosome barrier was overcome by increased RNA-Pol II at the TSS region. Indeed, different *in vitro* studies have shown that the levels of RNA-Pol II are important to overcome a transcriptional barrier (Epshtein and Nudler, 2003; Saeki and Svejstrup, 2009). Further, it was shown that an increased number of RNA-Pol II closely occupying a DNA region could “collide” and push each other which increased the energy of the first RNA-Pol II to overcome a pause site. Concordantly with this it was observed that a highly expressed DNA template, with more RNA-Pol II bound, were less susceptible for stalling at a pause site than a lower expressed template (Kulish and Struhl, 2001). This indicates why high expressed genes were less affected by CHD1 depletion than the low expressed genes. Summarized these studies show that the increased RNA-Pol II levels at the TSS regions observed by us were sufficient to maintain the normal transcriptional output when CHD1 was depleted. However, repressed genes had similar occupancy levels of RNA-Pol II and were less likely to overcome the nucleosome barrier with low CHD1 protein levels.

Interestingly another study showed in yeast that pausing of RNA-Pol II occurs also over the entire gene body (Churchman and Weissman, 2011). This might extend the role of CHD1 to support the overcome of the nucleosome barrier not only at the TSS, but also at the gene body, as we and others observed CHD1 binding at the entire gene.

Further we saw that particularly genes were highest stalled after CHD1 knockdown which got induced during differentiation. Other studies had observed that genes highly responsive to stimulation or activated during development were stalled before induction and that stalling was reduced after their activation (Muse et al., 2007; Zeitlinger et al., 2007). CHD1 might be important for the activation of these stalled genes. Thus it would be important to test if the genes affected by CHD1 depletion were stalling in undifferentiated condition.

In addition to positive elongation factors, RNA-Pol II release from TSS can be also stimulated by histone modifications like H3K27ac, H3K122Ac or H3K115Ac (Manohar et al., 2009; Stasevich et al., 2014). Surprisingly, in our study, we observed low levels of H3K27ac around TSS of CHD1-sensitive genes irrespective of their expression. Similarly, differentiation-regulated genes which were low in H3K27ac occupancy, but had normal gene expression like stably expressed genes, were described in

D. melanogaster (Pérez-Lluch et al., 2015). Furthermore, other studies observed the effect of low or no histone modifications in induced and activated genes (Chen et al., 2013; Hödl and Basler, 2012; Zhang et al., 2014). These suggest the dynamic nature of histone code in their regulation of gene expression and the association with CHD1.

5.1.2 Reduced H2A.Z levels upon CHD1 depletion may link to decreased nucleosome turnover

Besides higher RNA-Pol II stalling, we observed less occupancy of the histone variant H2A.Z around TSS upon CHD1 knockdown. Interestingly, it was described that H2A.Z incorporation into the +1 nucleosome decreases the nucleosome barrier and that depletion of H2A.Z cause higher RNA-Pol II stalling (Weber et al., 2014). This highly suggests that the lower H2A.Z levels observed after CHD1 depletion caused increased RNA-Pol II stalling. This effect however was not observed at active enhancers and argues for a TSS-specific effect. Yet, if the lower H2A.Z occupancy around the TSS is due a lower steady-state level of the +1 nucleosome or solely due to lower H2A.Z levels can here only be speculated.

What argues for a lower steady-state nucleosome occupancy was the observation that a CHD1 mutant which caused decreased nucleosome turnover at the TSS led to surprisingly lower steady-state levels of the +1 nucleosome (Skene et al., 2014). This would favor a model where the reassembly of the nucleosome after the passage of RNA-Pol II is disrupted by CHD1 depletion which cause a low occupancy of nucleosomes, as it was observed in yeast (Lee et al., 2012a).

Alternatively, CHD1 might aid the incorporation or removal of H2A.Z during the +1 nucleosome remodeling and thereby decrease H2A.Z levels specifically. It already had been shown that CHD1 was required for the incorporation of histone variants H3.3 and CENP-H into nucleosomes (Konev et al., 2007; Okada et al., 2009). Performing ChIP-seq of H3 or H2B is therefore necessary to rule-out the possibility of less nucleosome occupancy upon CHD1 depletion and can emphasize on the effect of H2A.Z occupancy. Interestingly the histone variant H3.3 commonly co-occupies H2A.Z nucleosomes which further destabilizes them (Jin et al., 2009). Thus, it could be hypothesized that CHD1 may be required for H3.3 specific incorporations into nucleosomes at TSS regions too. Therefore, performing H3.3 ChIP at TSS-specific regions upon CHD1 depletion would further improve our knowledge on the role of CHD1 as a chromatin remodeler in incorporating histone variants.

5.1.3 H2Bub1 and CHD1

Previous studies showed that CHD1 was required for the maintenance of global H2Bub1 levels (Lee et al., 2012a). H2Bub1 was shown to be necessary for MSC differentiation to osteoblast and adipocytes (Karpiuk et al., 2012). Thus, we hypothesized that the differentiation defects observed in our study after CHD1 depletion were due to reduced H2Bub1 levels. However, in our system, we did not see any regulation in H2Bub1 levels upon CHD1 depletion, neither in MSC nor in FOB which might be due to the usage of different cell lines. Lee et al. used yeast and human 293 cells for their studies, but not stem cells. Probably, high levels of H2Bub1 need to be established prior to observe CHD1-specific effects on H2Bub1. Karpiuk et al. showed that undifferentiated MSC possess very negligible amount of H2Bub1 and they gain H2Bub1 during differentiation (Karpiuk et al., 2012). Thus, it could be interesting to test if CHD1 affects H2Bub1 stronger in already differentiated cells than during differentiation. Moreover, CHD2, which is also an ATPase-dependent chromatin remodeler and structurally resembles CHD1, may have redundant functions as CHD1 in MSC and FOB, but were not expressed in human 293 cells (Siggens et al., 2015).

5.2 Genome-wide binding pattern of CHD1

Several studies and the ENCODE consortium performed ChIP-seq on CHD1 in yeast or human (ENCODE Project Consortium, 2012; Lee et al., 2012a; Siggens et al., 2015). However, comparison of dynamic binding patterns of CHD1 before and after stimulation is poorly understood. Here, we provide a comprehensive overview of CHD1 binding in undifferentiated MSC and after adipocyte and osteoblast differentiation. The observed CHD1 binding regions may possess the following possible regulatory mechanisms:

5.2.1 CHD1 regulation around TSS

CHD1 has a broad binding pattern over gene bodies and might act in several ways on transcriptional processes, however its main regulatory role in mammals was thought to be at TSS (Gaspar-Maia et al., 2009; Siggens et al., 2015; Skene et al., 2014). Indeed, in our study, we observed the highest CHD1 binding intensity closely downstream to TSS. Furthermore, we showed that CHD1 binding around TSS positively correlated with gene expression levels and active histone modifications H3K4me3 and H3K27ac. Previous studies revealed similar correlations between

actively transcribed genes and CHD1 binding at their TSS regions, but categorized the gene expression status quite broad by active, inactive or modestly transcribed sets (Siggens et al., 2015). Here we sought to extend this information and showed for each gene the respective CHD1 binding downstream of its TSS. Especially in osteoblast differentiated MSC, we observed that low and medium expressed genes had high CHD1 binding around their TSS. Furthermore, we could measure that genes induced during differentiation had higher binding of CHD1 which was required for their activation. Altogether, our study demonstrates a strong mechanistic insight connecting the occupancy of CHD1 around TSS and the activity of differentiation-induced genes.

5.2.2 How is CHD1 recruited to differentiation-induced genes?

Interaction of CHD1 with transcription-associated complexes like FACT, SAGA or mediator were described before and this could suggest different possibilities for recruitment of CHD1 to the chromatin (Lin et al., 2011; Pray-Grant et al., 2005; Simic et al., 2003). CHD1 may possess differential binding affinities to various complexes. Indeed, strong interaction between CHD1 and Mediator Complex Subunit-1 (MED1) was observed (Lin et al., 2011). Furthermore, another strong interaction was observed between CHD1 and the General Transcription Factor IIH (TFIIH) complex, which is opening up the DNA at the TSS (Guzmán and Lis, 1999). Interestingly, TFIIH is involved in nuclear receptor-associated binding and modulating its activity in gene expression (Compe and Egly, 2012). It was shown to be interacting with RAR, PPARG, AR or the vitamin D receptor (VDR) which also play fundamental roles in regulating differentiation-related gene expression (Jeong and Mangelsdorf, 2009). This altogether indicates that CHD1 may be recruited differentially to TSS by their interaction partners TFIIH or MED1 which can modulate its binding affinity to TSS (Esnault et al., 2008; Mizuta et al., 2014). Performing ChIP-seq on MED1, TFIIH subunits or the nuclear receptors during MSC differentiation can help in understanding the correlation in their binding with CHD1 and looking at CHD1 occupancy upon depletion of these factors would aid us in elucidating the mechanism of CHD1 recruitment to the chromatin.

5.2.3 When is CHD1 recruited to differentiation-induced genes?

A large part of primed and inactive genes in human ESC are however often marked with H3K4me3 (Guenther et al., 2007). These genes are related to differentiation

processes and get activated during differentiation. In our study, we observed that high levels of CHD1 are positively correlated with high levels of H3K4me3 at the TSS. In contrast, TSS highly marked with H3K4me3 are not necessarily correlated with CHD1 binding. One could speculate that these H3K4me3-enriched genes which are exclusive of CHD1 might be primed for differentiation-specific stimulation. Furthermore, these primed genes can be marked bivalent by H3K4me3 and H3K27me3 which had been described before to play a role in stem cell differentiation (Bernstein et al., 2006; Voigt et al., 2013). It could be possible that CHD1 gets recruited after primed genes lose H3K27me3 and are activated. The reasons could be: First, CHD1 and H3K27me3 does not co-occupy as observed in mESC (Gaspar-Maia et al., 2009). Second, occupancy of the strong interaction partner of CHD1, MED1 is reduced at bivalent genes which do not possess the binding of Really Interesting New Gene 1b (RING1B), a PRC1 complex member involved in maintenance of bivalency (Lehmann et al., 2012; Lin et al., 2011). Third, CHD1 is more correlated with active mark H3K27ac than H3K4me3, which does not necessarily mark active genes. Nonetheless is a detailed binding analysis between activating transcription factors, histone modifications and CHD1 occupancy necessary to further understand the dynamics in gene activation during differentiation and the part of CHD1 within it.

5.2.4 Regulatory roles of CHD1 at gene bodies

Many of the published binding regions of CHD1 in yeast and human are localized within the gene body (ENCODE Project Consortium, 2012; Lee et al., 2012a; Siggens et al., 2015). Here, we performed quantification of genome-wide CHD1-enriched binding regions and could show that the highest proportion were located within the gene and not at the TSS. Although, the signal intensity of CHD1 occupancy is lower compared to TSS, it could have affected the gene expression in various ways:

5.2.4.1 CHD1 role in regulation of Cryptic transcription

It is known that CHD1 interacts with the FACT complex in *S. cerevisiae*, *D. melanogaster* and human to order the nucleosomes after RNA-Pol II passage into a regularly spaced array which represses cryptic transcription (Hennig et al., 2012; Kelley et al., 1999; Lin et al., 2011; Simic et al., 2003; Smolle et al., 2012). However, this function was described only in yeast. Nonetheless we also observed CHD1 binding over the gene body which argues for a similar function. Supporting a

conserved role in repression of cryptic transcription, two studies in yeast and human showed that a mutation in the ATPase-domain of CHD1 caused a decreased nucleosome density over the gene body which is characteristic for cryptic transcription (Hennig and Fischer, 2013; Hennig et al., 2012; Skene et al., 2014). In our study, we sequenced poly-adenylated mRNA in a non-directional approach and thus could not capture cryptic transcripts, which are not poly-adenylated. To study cryptic transcription, one could use deep sequencing of nascent RNA transcripts of RNA-Pol II which would help to capture even very unstable cryptic transcripts (Churchman and Weissman, 2011). Even though cryptic transcription had only mild effects on global transcriptional changes in CHD1 depleted system, it might act in fine tuning gene expression (Colin et al., 2011). If CHD1 affects cryptic transcription in a lineage-specific manner would be interesting to test.

5.2.4.2 CHD1 and splicing

Besides repression of cryptic transcription, CHD1 is also linked with splicing of pre-mRNA (Sims et al., 2007). Sims et al. showed that CHD1 in human interacts with different components of the small nuclear Ribonucleoprotein 2 (snRNP2) riboprotein complex, a part of the huge spliceosome, and is required to associate the complex to the chromatin. Concordantly, a recent study in yeast reported that a CHD1-depleted strain decreased the nucleosome turnover at 3´ end of introns and CHD1 was thought to be necessary to release RNA-Pol II from 5´ intron-exon boundary which might affect splice site recognition (Jonkers and Lis, 2015; Park et al., 2014).In in our study, we also observed a high proportion of CHD1 binding regions within exons. These observations indicated that CHD1 may be involved in the release of RNA-Pol II of intron-exon boundaries and pre-mRNA splicing in MSC and FOB. Deep, strand-specific RNA-seq under CHD1-depleted conditions could help to further elucidate this question by detection of alternatively spliced transcripts (Mills et al., 2013).

Furthermore, one could speculate that less nucleosome occupancy over the gene body as observed in CHD1 mutant cells affect RNA-Pol II traveling speed over the gene which was described to regulate alternative splicing events (Naftelberg et al., 2015; Skene et al., 2014). Additionally to RNA-Pol II traveling speed also the nucleosome distribution at intron-exon boundaries regulate the recognition of splice sites which is also important for alternative spliced mRNA (Iannone et al., 2015; Schwartz et al., 2009; Tilgner et al., 2009). Interestingly, alternative splicing is

involved in osteoblast differentiation as osteoblast differentiation factors like FosB or Lef1 are alternatively spliced and cause differential regulation (Jensen et al., 2010). Moreover, alternatively spliced isoforms of RUNX2 regulate BGLAP expression in different ways, which could be one explanation for the observed differentially expression of BGLAP in MSC and FOB (Makita et al., 2008).

5.2.4.3 CHD1 around TTS

Additional to the prominent peak of CHD1 at the TSS, we observed a second smaller peak closely downstream at the transcriptional termination site (TTS). Even though no studies in metazoans are known in this regard, a study in *S. pombe* showed that the CHD1 homologue *hrp1* acts as a transcriptional termination factor (Alén et al., 2002). Interestingly, another recent study linked CHD1 to the H3 histone dynamics at the 3´-end of long genes in *S. cerevisiae* (Radman-Livaja et al., 2012). We also observed that long genes were significantly less expressed in CHD1-depleted conditions in MSC, but not in FOB (data not shown). Regulation of transcriptional termination by CHD1 is poorly understood. Nevertheless, CHD1 is involved in nucleosome positioning and might help to maintain a nucleosome free region at the TTS which could support the disassembly of RNA-Pol II from the DNA for mRNA cleavage (Core et al., 2008; Mavrich et al., 2008). Furthermore, CHD1 may also be involved in nucleosome turnover at TTS other than TSS (Materne et al.; Radman-Livaja et al., 2012).

5.2.4.4 CHD1 at enhancer

Recently, CHD1 binding was described at enhancer regions which were marked by different H3K4me1/2/3 methylation patterns (Siggens et al., 2015). Indeed, CHD1 also binds to H3K4me2, a mark which is present at active enhancers (Sims et al., 2005; Wang et al., 2014). Although we did not focus on enhancer regions in our study, we detected only a small portion of CHD1 binding at intergenic regions, in MSC as well as FOB. However, mapping of H2A.Z and RNA-Pol II on active enhancers in FOB showed no obvious changes upon CHD1 depletion, though occupancy of both proteins were affected by CHD1 depletion around TSS and play pivotal roles in the regulation of enhancer activity (Brunelle et al., 2015). This indicates that the effects of CHD1 may be negligible at enhancers in our system. Furthermore, we observed a small increase of intergenic bound regions in differentiated cells compared to undifferentiated conditions, which could reflect higher

binding on enhancers during differentiation. Moreover, mapping CHD1 binding to H3K4me1 and H3K27ac sites which are exclusive of H3K4me3 could improve its binding properties on active enhancer regions.

5.3 Biological implications on osteoblast differentiation upon CHD1 depletion

Transcription factors, histone modifying enzymes and chromatin remodeler are important for a rapid transcriptional response to intra- and extracellular signals. During the early and late osteogenesis showed differentiation associated genes a high dynamicity in transcription (Kulterer et al., 2007; Twine et al., 2014). For example, fluctuated the expression of RUNX2 or BGLAP during differentiation, however their dynamic regulation is so far only poorly understood. Nonetheless it is important that this coordinated interplay is maintained and that the factors are expressed at the right time, as one factor can enhance or block differentiation, depending on the differentiation status of a cell (Kahler and Westendorf, 2003; Kahler et al., 2006; Regard et al., 2012). CHD1 likely plays a role in stabilizing this coordinated process by supporting the transcription of fast activated genes as discussed above.

5.3.1 CHD1 regulation of bone development associated gene ontology terms

During osteoblast differentiation the extracellular matrix (ECM) is reorganized and organic substrates mainly collagen are deposit on the cell surface (Clarke, 2008). The modification of the ECM is not only a consequence of differentiation but can also affect osteoblast differentiation (Mathews et al., 2012; Xiao et al., 2002). In this study we observed that the highest enrichment of deregulated genes was associated with parts of the ECM. Further, the ECM proteins *BGLAP* and *ELN* were one of the strongest deregulated genes in CHD1 depleted conditions. Besides our also another study highlighted the importance of the ECM in transcriptome wide regulation during early osteoblast differentiation (Kulterer et al., 2007). Furthermore, also secreted factors are included in the extracellular region part which were dependent on CHD1 for a normal regulation. More recently, secreted factors were shown to support the coordination of osteoblast differentiation and interestingly were also connected to a systemic signaling (Mrak et al., 2007; Oury et al., 2013; Sabek et al., 2015; Zhong et al., 2012). This together shows that the genes regulated by CHD1 during differentiation might impair osteogenesis also over indirect pathways and not by renowned transcription factors.

Besides the ECM, deregulated genes were also significantly enriched for the biological processes such as vascularization and blood vessel development. Several studies had implicated a role of MSC signaling on HSC differentiation and development of the microvascular environment in the bone (Deckers et al., 2002; Eshkar-Oren et al., 2009; Furumatsu et al., 2003). These reports were supported by a recent finding of the MSC stem cell niche which resides together with HSC and is located perivascular in direct contact with the blood vessels (Méndez-Ferrer et al., 2010). In sum this implies that applications *in vivo* could consider the effects of CHD1 on vascularization in particular in cell therapeutic approaches (further discussed below).

5.3.2 Ectopic bone formation and effects *in vivo* based on CHD1

Osteoblastic differentiation consist in general of three phases: proliferation, extracellular matrix organization and subsequent mineralization of this extracellular scaffold (Lian and Stein, 1992). Phenotypically matrix reorganization begins around 5 days after differentiation and includes deposition of organic compounds mainly consisting of different types of collagen (Broek et al., 1985; Kulterer et al., 2007; Niyibizi and Eyre, 1989; Pihlajaniemi et al., 1990). In this study the ectopic bone formation experiment showed low deposition of extracellular matrix in CHD1 depleted conditions. This was concordant with the deregulated genes identified in our RNA-seq study which were enriched for terms in ECM organization. Further the observation supports the assumption of an osteoblast differentiation defect before day 5.

Recent studies described a group of genes predicting a strong ectopic bone formation in mice (Larsen et al., 2010; Twine et al., 2014). Surprisingly, the *bona fide* osteoblast marker genes *ALPL* and *BGLAP* were not specified within this group characteristic for enhanced ectopic bone formation (Larsen et al., 2010). Of particular interest for us was that ELN turned out to be one of the best predictors for ectopic bone formation, which was directly regulated by CHD1. The mechanism of how ELN is acting on bone formation is unknown, however it is expressed during craniofacial bone development in mice and can be induced by TGFβ, which plays an essential role in osteoblast differentiation (Diez-Roux et al., 2011; Sethi et al., 2011). In other tissues ELN was shown to serve as a scaffold protein for mineralization of the ECM which could be transferred to osteoblasts too (Seligman et al., 1975; Starcher and

Urry, 1973). Further studies will be necessary to unravel its importance in bone formation and if the strong regulatory effect of CHD1 on *ELN* expression also holds true in other systems.

5.3.3 Expression of *ALPL* and *BGLAP* in osteogenesis after CHD1 depletion

ALPL and BGLAP are well established marker for osteoblast differentiation. In this study *ALPL* was higher expressed in MSC but only slightly affected in FOB after CHD1 depletion. Though we observed that the TSS region of *ALPL* was lowly bound by CHD1 which indicates an indirect regulation by CHD1 depletion. Thus probably the cellular background of MSC and FOB could explain the observed differences in gene regulation. It could further be speculated that the cells are at a different stage of osteoblast differentiation which is supported by absent expression of BGLAP in FOBs.

Interestingly *ALPL* and *BGLAP* are both coordinative activated by the retinoblastoma protein 1 (pRB1) and E2F transcription factor 1 (E2F1) (Flowers et al., 2013). Our RNA-seq study revealed that *E2F1* is only lowly expressed in FOB osteoblast differentiated cells, but expressed at an average level in MSC (data not shown). Although MSC and FOB can be both differentiated to osteoblast the different cellular background shown by *BGLAP* or *E2F1* expression indicate that osteogenesis might be triggered in various ways.

5.4 Translation for clinical therapeutic approaches

Worldwide currently 320 open clinical studies exist which include mesenchymal stem cells (ClinicalTrial.gov). MSC had been used now for over a decade in cell therapies because of their regenerative and immunomodulatory properties as well as their good safety record in humans (Lepperdinger et al., 2008; Zaher et al., 2014). Besides therapeutic studies in non-skeletal tissues and treatment of immune diseases their regenerative properties were already successfully used for the regeneration of bone and cartilage in human (Gangji et al., 2005; Le Blanc et al., 2005; Quarto et al., 2001; Wakitani et al., 2007). However the repair of skeletal or cartilage depends on the ability of the injected cells to differentiate and form new tissue (Undale et al., 2009). This makes it essential to understand their regenerative and differentiation potential before injection. Though, the canonical osteoblast markers do not predict accurately the *in vivo* bone formation (Kuznetsov et al 1997, Larsen KH et al 2010). Here we

suggest with CHD1 another marker which could help to better predict the regenerative potential for bone tissue and maybe cartilage repair.

In cell therapy MSC are commonly expanded *ex vivo* before transplantation to obtain sufficient material for regenerative purposes (Undale et al., 2009). For example, 1 – 2 million cells per kilogram of body weight are required for a systemic cell therapeutic approach (Schallmoser et al., 2008). A challenge during this culturing *ex vivo* is to maintain the stem cell characteristics and probably their epigenetic profile (Ng et al., 2014). In this study we showed that CHD1 depletion decreased the differentiation potential and was required for broad introduction of transcriptional changes. These properties might be used to decrease the differentiation *ex vivo* during cell expansion. To my knowledge no small inhibitors of CHD1 exist, however transient siRNA mediated depletion of CHD1 could be applied during *ex vivo* culturing. Nonetheless deeper investigations especially on transcriptional effects in the undifferentiated state and on the epigenome by CHD1 will unravel its use for therapeutic approaches.

In summary this work reveals a novel regulatory function of CHD1 in gene activation during osteoblast differentiation and shows its necessity for ectopic bone formation. Markers for safe cell therapy are still poorly described, we suggest to consider CHD1 as one. Further we extend the mechanistic role of CHD1 on global RNA-Pol II stalling around TSS in humans and highlight its requirement for differentiation specific gene activation. Moreover, a new regulatory connection of CHD1 associated H2A.Z incorporation into the +1 nucleosome is hypothesized. Further insights will help to understand if inhibition of CHD1 or H2A.Z are potential targets in stem cell therapy to selectively block differentiation.

6 Reference List

Abbott, D.W., Ivanova, V.S., Wang, X., Bonner, W.M., and Ausió, J. (2001). Characterization of the Stability and Folding of H2A.Z Chromatin Particles Implications for transcriptional activation. J. Biol. Chem. *276*, 41945–41949.

Abdallah, B.M., and Kassem, M. (2012). New factors controlling the balance between osteoblastogenesis and adipogenesis. Bone *50*, 540–545.

Abdallah, B.M., Ditzel, N., and Kassem, M. (2008). Assessment of bone formation capacity using in vivo transplantation assays: procedure and tissue analysis. Methods Mol. Biol. Clifton NJ *455*, 89–100.

Ahmad, K., and Henikoff, S. (2002). The Histone Variant H3.3 Marks Active Chromatin by Replication-Independent Nucleosome Assembly. Mol. Cell *9*, 1191–1200.

Ahmadian, M., Suh, J.M., Hah, N., Liddle, C., Atkins, A.R., Downes, M., and Evans, R.M. (2013). PPARγ signaling and metabolism: the good, the bad and the future. Nat. Med. *99*, 557–566.

Albert, I., Mavrich, T.N., Tomsho, L.P., Qi, J., Zanton, S.J., Schuster, S.C., and Pugh, B.F. (2007). Translational and rotational settings of H2A.Z nucleosomes across the Saccharomyces cerevisiae genome. Nature *446*, 572–576.

Alberts B, Johnson A, Lewis J, et al. (2002). Chromosomal DNA and Its Packaging in the Chromatin Fiber. Mol. Biol. Cell N. Y. Garland Sci. *4th edition.*

Alén, C., Kent, N.A., Jones, H.S., O'Sullivan, J., Aranda, A., and Proudfoot, N.J. (2002). A Role for Chromatin Remodeling in Transcriptional Termination by RNA Polymerase II. Mol. Cell *10*, 1441–1452.

Allan, J., Mitchell, T., Harborne, N., Bohm, L., and Crane-Robinson, C. (1986). Roles of H1 domains in determining higher order chromatin structure and H1 location. J. Mol. Biol. *187*, 591–601.

Al-Nbaheen, M., Vishnubalaji, R., Ali, D., Bouslimi, A., Al-Jassir, F., Megges, M., Prigione, A., Adjaye, J., Kassem, M., and Aldahmash, A. (2012). Human Stromal (Mesenchymal) Stem Cells from Bone Marrow, Adipose Tissue and Skin Exhibit Differences in Molecular Phenotype and Differentiation Potential. Stem Cell Rev. Rep. *9*, 32–43.

Álvarez-Errico, D., Vento-Tormo, R., Sieweke, M., and Ballestar, E. (2015). Epigenetic control of myeloid cell differentiation, identity and function. Nat. Rev. Immunol. *15*, 7–17.

Amado, L.C., Saliaris, A.P., Schuleri, K.H., St John, M., Xie, J.-S., Cattaneo, S., Durand, D.J., Fitton, T., Kuang, J.Q., Stewart, G., et al. (2005). Cardiac repair with intramyocardial injection of allogeneic mesenchymal stem cells after myocardial infarction. Proc. Natl. Acad. Sci. U. S. A. *102*, 11474–11479.

Anders, S., and Huber, W. (2010). Differential expression analysis for sequence count data. Genome Biol. *11*, R106.

Antebi, B., Pelled, G., and Gazit, D. (2014). Stem cell therapy for osteoporosis. Curr. Osteoporos. Rep. *12*, 41–47.

Atoui, R., and Chiu, R.C.J. (2012). Concise Review: Immunomodulatory Properties of Mesenchymal Stem Cells in Cellular Transplantation: Update, Controversies, and Unknowns. Stem Cells Transl. Med. *1*, 200–205.

Badis, G., Chan, E.T., van Bakel, H., Pena-Castillo, L., Tillo, D., Tsui, K., Carlson, C.D., Gossett, A.J., Hasinoff, M.J., Warren, C.L., et al. (2008). A library of yeast transcription factor motifs reveals a widespread function for Rsc3 in targeting nucleosome exclusion at promoters. Mol. Cell *32*, 878–887.

Banaszynski, L.A., Wen, D., Dewell, S., Whitcomb, S.J., Lin, M., Diaz, N., Elsässer, S.J., Chapgier, A., Goldberg, A.D., Canaani, E., et al. (2013). Hira-dependent histone H3.3 deposition facilitates PRC2 recruitment at developmental loci in ES cells. Cell *155*, 107–120.

Bannister, A.J., and Kouzarides, T. (2011). Regulation of chromatin by histone modifications. Cell Res. *21*, 381–395.

Barth, T.K., and Imhof, A. (2010). Fast signals and slow marks: the dynamics of histone modifications. Trends Biochem. Sci. *35*, 618–626.

Bernstein, B.E., Mikkelsen, T.S., Xie, X., Kamal, M., Huebert, D.J., Cuff, J., Fry, B., Meissner, A., Wernig, M., Plath, K., et al. (2006). A bivalent chromatin structure marks key developmental genes in embryonic stem cells. Cell *125*, 315–326.

Bernstein, B.E., Stamatoyannopoulos, J.A., Costello, J.F., Ren, B., Milosavljevic, A., Meissner, A., Kellis, M., Marra, M.A., Beaudet, A.L., Ecker, J.R., et al. (2010). The NIH Roadmap Epigenomics Mapping Consortium. Nat. Biotechnol. *28*, 1045–1048.

Bianco, P., and Robey, P.G. (2015). Skeletal stem cells. Development *142*, 1023–1027.

Billon, P., and Côté, J. (2013). Precise deposition of histone H2A.Z in chromatin for genome expression and maintenance. Biochim. Biophys. Acta *1819*, 290–302.

de Boer, J., Siddappa, R., Gaspar, C., van Apeldoorn, A., Fodde, R., and van Blitterswijk, C. (2004). Wnt signaling inhibits osteogenic differentiation of human mesenchymal stem cells. Bone *34*, 818–826.

Boland, G.M., Perkins, G., Hall, D.J., and Tuan, R.S. (2004). Wnt 3a promotes proliferation and suppresses osteogenic differentiation of adult human mesenchymal stem cells. J. Cell. Biochem. *93*, 1210–1230.

Bönisch, C., and Hake, S.B. (2012). Histone H2A variants in nucleosomes and chromatin: more or less stable? Nucleic Acids Res. *40*, 10719–10741.

Broek, D.L., Madri, J., Eikenberry, E.F., and Brodsky, B. (1985). Characterization of the tissue form of type V collagen from chick bone. J. Biol. Chem. *260*, 555–562.

Brunelle, M., Nordell Markovits, A., Rodrigue, S., Lupien, M., Jacques, P.-É., and Gévry, N. (2015). The histone variant H2A.Z is an important regulator of enhancer activity. Nucleic Acids Res. *43*, 9742–9756.

Bugga, L., McDaniel, I.E., Engie, L., and Armstrong, J.A. (2013). The Drosophila melanogaster CHD1 Chromatin Remodeling Factor Modulates Global Chromosome Structure and Counteracts HP1a and H3K9me2. PLoS ONE *8*, e59496.

Burkhardt, L., Fuchs, S., Krohn, A., Masser, S., Mader, M., Kluth, M., Bachmann, F., Huland, H., Steuber, T., Graefen, M., et al. (2013). CHD1 Is a 5q21 Tumor Suppressor Required for ERG Rearrangement in Prostate Cancer. Cancer Res. *73*, 2795–2805.

Cairns, B.R. (2007). Chromatin remodeling: insights and intrigue from single-molecule studies. Nat. Struct. Mol. Biol. *14*, 989–996.

Carvalho, S., Raposo, A.C., Martins, F.B., Grosso, A.R., Sridhara, S.C., Rino, J., Carmo-Fonseca, M., and de Almeida, S.F. (2013). Histone methyltransferase SETD2 coordinates FACT recruitment with nucleosome dynamics during transcription. Nucleic Acids Res. *41*, 2881–2893.

Chadwick, B.P., and Willard, H.F. (2001). A Novel Chromatin Protein, Distantly Related to Histone H2a, Is Largely Excluded from the Inactive X Chromosome. J. Cell Biol. *152*, 375–384.

Chang, C.H., and Luse, D.S. (1997). The H3/H4 tetramer blocks transcript elongation by RNA polymerase II in vitro. J. Biol. Chem. *272*, 23427–23434.

Chapel, A., Bertho, J.M., Bensidhoum, M., Fouillard, L., Young, R.G., Frick, J., Demarquay, C., Cuvelier, F., Mathieu, E., Trompier, F., et al. (2003). Mesenchymal stem cells home to injured tissues when co-infused with hematopoietic cells to treat a radiation-induced multi-organ failure syndrome. J. Gene Med. *5*, 1028–1038.

Chen, G., Deng, C., and Li, Y.-P. (2012). TGF-β and BMP signaling in osteoblast differentiation and bone formation. Int. J. Biol. Sci. *8*, 272–288.

Chen, K., Johnston, J., Shao, W., Meier, S., Staber, C., and Zeitlinger, J. (2013). A global change in RNA polymerase II pausing during the Drosophila midblastula transition. eLife *2*, e00861.

Chen, M., Qiao, H., Su, Z., Li, H., Ping, Q., and Zong, L. (2014a). Emerging therapeutic targets for osteoporosis treatment. Expert Opin. Ther. Targets *18*, 817–831.

Chen, P., Wang, Y., and Li, G. (2014b). Dynamics of histone variant H3.3 and its coregulation with H2A.Z at enhancers and promoters. Nucleus *5*, 21–27.

Chen, L. and Ditzel, N. (2015). In vivo Heterotopic Bone Formation Assay Using Isolated Mouse and Human Mesenchymal Stem Cells. Bio-Protoc.

Chi, T.H., Wan, M., Lee, P.P., Akashi, K., Metzger, D., Chambon, P., Wilson, C.B., and Crabtree, G.R. (2003). Sequential roles of Brg, the ATPase subunit of BAF chromatin remodeling complexes, in thymocyte development. Immunity *19*, 169–182.

Cho, I., Tsai, P.-F., Lake, R.J., Basheer, A., and Fan, H.-Y. (2013). ATP-Dependent Chromatin Remodeling by Cockayne Syndrome Protein B and NAP1-Like Histone Chaperones Is Required for Efficient Transcription-Coupled DNA Repair. PLoS Genet *9*, e1003407.

Churchman, L.S., and Weissman, J.S. (2011). Nascent transcript sequencing visualizes transcription at nucleotide resolution. Nature *469*.

Clapier, C.R., and Cairns, B.R. (2009). The biology of chromatin remodeling complexes. Annu. Rev. Biochem. *78*, 273–304.

Clarke, B. (2008). Normal Bone Anatomy and Physiology. Clin. J. Am. Soc. Nephrol. CJASN *3*, S131–S139.

Colin, J., Libri, D., and Porrua, O. (2011). Cryptic Transcription and Early Termination in the Control of Gene Expression. Genet. Res. Int. *2011*.

Compe, E., and Egly, J.-M. (2012). TFIIH: when transcription met DNA repair. Nat. Rev. Mol. Cell Biol. *13*, 343–354.

Cooper, G.M. (2000). Regulation of Transcription in Eukaryotes.

Core, L.J., Waterfall, J.J., and Lis, J.T. (2008). Nascent RNA sequencing reveals widespread pausing and divergent initiation at human promoters. Science *322*, 1845–1848.

Costanzi, C., and Pehrson, J.R. (1998). Histone macroH2A1 is concentrated in the inactive X chromosome of female mammals. Nature *393*, 599–601.

Damsky, C.H. (1999). Extracellular matrix–integrin interactions in osteoblast function and tissue remodeling. Bone *25*, 95–96.

Das, C., and Tyler, J.K. (2013). Histone exchange and histone modifications during transcription and aging. Biochim. Biophys. Acta *1819*, 332–342.

Das, A.V., James, J., Bhattacharya, S., Imbalzano, A.N., Antony, M.L., Hegde, G., Zhao, X., Mallya, K., Ahmad, F., Knudsen, E., et al. (2007). SWI/SNF chromatin remodeling ATPase Brm regulates the differentiation of early retinal stem cells/progenitors by influencing Brn3b expression and Notch signaling. J. Biol. Chem. *282*, 35187–35201.

Day, T.F., Guo, X., Garrett-Beal, L., and Yang, Y. (2005). Wnt/beta-catenin signaling in mesenchymal progenitors controls osteoblast and chondrocyte differentiation during vertebrate skeletogenesis. Dev. Cell *8*, 739–750.

Deckers, M.M.L., van Bezooijen, R.L., van der Horst, G., Hoogendam, J., van Der Bent, C., Papapoulos, S.E., and Löwik, C.W.G.M. (2002). Bone morphogenetic proteins stimulate angiogenesis through osteoblast-derived vascular endothelial growth factor A. Endocrinology *143*, 1545–1553.

Diez-Roux, G., Banfi, S., Sultan, M., Geffers, L., Anand, S., Rozado, D., Magen, A., Canidio, E., Pagani, M., Peluso, I., et al. (2011). A high-resolution anatomical atlas of the transcriptome in the mouse embryo. PLoS Biol. *9*, e1000582.

Dutta, D., Ray, S., Home, P., Saha, B., Wang, S., Sheibani, N., Tawfik, O., Cheng, N., and Paul, S. (2010). Regulation of Angiogenesis by Histone Chaperone HIRA-mediated Incorporation of Lysine 56-acetylated Histone H3.3 at Chromatin Domains of Endothelial Genes. J. Biol. Chem. *285*, 41567–41577.

Eckfeldt, C.E., Mendenhall, E.M., and Verfaillie, C.M. (2005). The molecular repertoire of the “almighty” stem cell. Nat. Rev. Mol. Cell Biol. *6*, 726–737.

Eijken, M., Meijer, I.M.J., Westbroek, I., Koedam, M., Chiba, H., Uitterlinden, A.G., Pols, H. a. P., and van Leeuwen, J.P.T.M. (2008). Wnt signaling acts and is regulated in a human osteoblast differentiation dependent manner. J. Cell. Biochem. *104*, 568–579.

ENCODE Project Consortium (2012). An integrated encyclopedia of DNA elements in the human genome. Nature *489*, 57–74.

Epshtein, V., and Nudler, E. (2003). Cooperation Between RNA Polymerase Molecules in Transcription Elongation. Science *300*, 801–805.

Eshkar-Oren, I., Viukov, S.V., Salameh, S., Krief, S., Oh, C., Akiyama, H., Gerber, H.-P., Ferrara, N., and Zelzer, E. (2009). The forming limb skeleton serves as a signaling center for limb vasculature patterning via regulation of Vegf. Dev. Camb. Engl. *136*, 1263–1272.

Esnault, C., Ghavi-Helm, Y., Brun, S., Soutourina, J., Van Berkum, N., Boschiero, C., Holstege, F., and Werner, M. (2008). Mediator-dependent recruitment of TFIIH modules in preinitiation complex. Mol. Cell *31*, 337–346.

Fletcher, T.M., and Hansen, J.C. (1996). The nucleosomal array: structure/function relationships. Crit. Rev. Eukaryot. Gene Expr. *6*, 149–188.

Flowers, S., Xu, F., and Moran, E. (2013). Cooperative Activation of Tissue-Specific Genes by pRB and E2F1. Cancer Res. *73*, 2150–2158.

Fritah, A., Saucier, C., Mester, J., Redeuilh, G., and Sabbah, M. (2005). p21WAF1/CIP1 Selectively Controls the Transcriptional Activity of Estrogen Receptor α. Mol. Cell. Biol. *25*, 2419–2430.

Fuchs, G., Hollander, D., Voichek, Y., Ast, G., and Oren, M. (2014). Cotranscriptional histone H2B monoubiquitylation is tightly coupled with RNA polymerase II elongation rate. Genome Res. *24*, 1572–1583.

Furumatsu, T., Shen, Z.N., Kawai, A., Nishida, K., Manabe, H., Oohashi, T., Inoue, H., and Ninomiya, Y. (2003). Vascular endothelial growth factor principally acts as the main angiogenic factor in the early stage of human osteoblastogenesis. J. Biochem. (Tokyo) *133*, 633–639.

Gaffney, D.J., McVicker, G., Pai, A.A., Fondufe-Mittendorf, Y.N., Lewellen, N., Michelini, K., Widom, J., Gilad, Y., and Pritchard, J.K. (2012). Controls of Nucleosome Positioning in the Human Genome. PLoS Genet *8*, e1003036.

Gama, A., Navet, B., Vargas, J.W., Castaneda, B., and Lézot, F. (2015). Bone resorption: an actor of dental and periodontal development? Craniofacial Biol. 319.

Gangji, V., Toungouz, M., and Hauzeur, J.-P. (2005). Stem cell therapy for osteonecrosis of the femoral head. Expert Opin. Biol. Ther. *5*, 437–442.

Gao, H., Lukin, K., Ramírez, J., Fields, S., Lopez, D., and Hagman, J. (2009). Opposing effects of SWI/SNF and Mi-2/NuRD chromatin remodeling complexes on epigenetic reprogramming by EBF and Pax5. Proc. Natl. Acad. Sci. U. S. A. *106*, 11258–11263.

Gaspar-Maia, A., Alajem, A., Polesso, F., Sridharan, R., Mason, M.J., Heidersbach, A., Ramalho-Santos, J., McManus, M.T., Plath, K., Meshorer, E., et al. (2009). Chd1 regulates open chromatin and pluripotency of embryonic stem cells. Nature *460*, 863–868.

Gelman, L., Zhou, G., Fajas, L., Raspé, E., Fruchart, J.C., and Auwerx, J. (1999). p300 interacts with the N- and C-terminal part of PPARgamma2 in a ligand-independent and -dependent manner, respectively. J. Biol. Chem. *274*, 7681–7688.

Gkikopoulos, T., Schofield, P., Singh, V., Pinskaya, M., Mellor, J., Smolle, M., Workman, J.L., Barton, G.J., and Owen-Hughes, T. (2011). A role for Snf2-related nucleosome-spacing enzymes in genome-wide nucleosome organization. Science *333*, 1758–1760.

Gomes, N.P., Bjerke, G., Llorente, B., Szostek, S.A., Emerson, B.M., and Espinosa, J.M. (2006). Gene-specific requirement for P-TEFb activity and RNA polymerase II phosphorylation within the p53 transcriptional program. Genes Dev. *20*, 601–612.

Gómez-Barrena, E., Rosset, P., Lozano, D., Stanovici, J., Ermthaller, C., and Gerbhard, F. (2015). Bone fracture healing: Cell therapy in delayed unions and nonunions. Bone *70*, 93–101.

Grandy, R.A., Whitfield, T.W., Wu, H., Fitzgerald, M.P., VanOudenhove, J.J., Zaidi, S.K., Montecino, M.A., Lian, J.B., vanWijnen, A.J., Stein, J.L., et al. (2015). Genome-wide Studies Reveal that H3K4me3 Modification in Bivalent Genes is Dynamically Regulated During the Pluripotent Cell Cycle and Stabilized Upon Differentiation. Mol. Cell. Biol.

Grasso, C.S., Wu, Y.-M., Robinson, D.R., Cao, X., Dhanasekaran, S.M., Khan, A.P., Quist, M.J., Jing, X., Lonigro, R.J., Brenner, J.C., et al. (2012). The mutational landscape of lethal castration-resistant prostate cancer. Nature *487*, 239–243.

Green, C.M., and Almouzni, G. (2002). When repair meets chromatin. First in series on chromatin dynamics. EMBO Rep. *3*, 28–33.

Grewal, S.I.S., and Jia, S. (2007). Heterochromatin revisited. Nat. Rev. Genet. *8*, 35–46.

Guenther, M.G., Levine, S.S., Boyer, L.A., Jaenisch, R., and Young, R.A. (2007). A Chromatin Landmark and Transcription Initiation at Most Promoters in Human Cells. Cell *130*, 77–88.

Guillemette, B., Bataille, A.R., Gévry, N., Adam, M., Blanchette, M., Robert, F., and Gaudreau, L. (2005). Variant Histone H2A.Z Is Globally Localized to the Promoters of Inactive Yeast Genes and Regulates Nucleosome Positioning. PLoS Biol *3*, e384.

Gurard-Levin, Z.A., Quivy, J.-P., and Almouzni, G. (2014). Histone Chaperones: Assisting Histone Traffic and Nucleosome Dynamics. Annu. Rev. Biochem. *83*, 487–517.

Guzmán, E., and Lis, J.T. (1999). Transcription factor TFIIH is required for promoter melting in vivo. Mol. Cell. Biol. *19*, 5652–5658.

Guzman-Ayala, M., Sachs, M., Koh, F.M., Onodera, C., Bulut-Karslioglu, A., Lin, C.-J., Wong, P., Nitta, R., Song, J.S., and Ramalho-Santos, M. (2015). Chd1 is essential for the high transcriptional output and rapid growth of the mouse epiblast. Development *142*, 118–127.

Hansen, J.C. (2002). Conformational Dynamics of the Chromatin Fiber in Solution: Determinants, Mechanisms, and Functions. Annu. Rev. Biophys. Biomol. Struct. *31*, 361–392.

Harris, S.A., Enger, R.J., Riggs, L.B., and Spelsberg, T.C. (1995). Development and characterization of a conditionally immortalized human fetal osteoblastic cell line. J. Bone Miner. Res. *10*, 178–186.

Hauk, G., McKnight, J.N., Nodelman, I.M., and Bowman, G.D. (2010). The Chromodomains of the Chd1 Chromatin Remodeler Regulate DNA Access to the ATPase Motor. Mol. Cell *39*, 711–723.

Heard, E., and Disteche, C.M. (2006). Dosage compensation in mammals: fine-tuning the expression of the X chromosome. Genes Dev. *20*, 1848–1867.

Heintzman, N.D., Hon, G.C., Hawkins, R.D., Kheradpour, P., Stark, A., Harp, L.F., Ye, Z., Lee, L.K., Stuart, R.K., Ching, C.W., et al. (2009). Histone Modifications at Human Enhancers Reflect Global Cell Type-Specific Gene Expression. Nature *459*, 108–112.

Heinz, S., Romanoski, C.E., Benner, C., and Glass, C.K. (2015). The selection and function of cell type-specific enhancers. Nat. Rev. Mol. Cell Biol. *16*, 144–154.

Henikoff, S., Henikoff, J.G., Sakai, A., Loeb, G.B., and Ahmad, K. (2009). Genome-wide profiling of salt fractions maps physical properties of chromatin. Genome Res. *19*, 460–469.

Hennig, B.P., and Fischer, T. (2013). The great repression. Transcription *4*, 97–101.

Hennig, B.P., Bendrin, K., Zhou, Y., and Fischer, T. (2012). Chd1 chromatin remodelers maintain nucleosome organization and repress cryptic transcription. EMBO Rep. *13*, 997–1003.

Hill, T.P., Später, D., Taketo, M.M., Birchmeier, W., and Hartmann, C. (2005). Canonical Wnt/β-Catenin Signaling Prevents Osteoblasts from Differentiating into Chondrocytes. Dev. Cell *8*, 727–738.

Hoch, A.I., and Leach, J.K. (2014). Concise Review: Optimizing Expansion of Bone Marrow Mesenchymal Stem/Stromal Cells for Clinical Applications. Stem Cells Transl. Med. *3*, 643–652.

Hödl, M., and Basler, K. (2012). Transcription in the absence of histone H3.2 and H3K4 methylation. Curr. Biol. CB *22*, 2253–2257.

Hsieh, F.-K., Kulaeva, O.I., Patel, S.S., Dyer, P.N., Luger, K., Reinberg, D., and Studitsky, V.M. (2013). Histone chaperone FACT action during transcription through chromatin by RNA polymerase II. Proc. Natl. Acad. Sci. U. S. A. *110*, 7654–7659.

Hu, H., Hilton, M.J., Tu, X., Yu, K., Ornitz, D.M., and Long, F. (2005). Sequential roles of Hedgehog and Wnt signaling in osteoblast development. Dev. Camb. Engl. *132*, 49–60.

Huang, D.W., Sherman, B.T., and Lempicki, R.A. (2009). Bioinformatics enrichment tools: paths toward the comprehensive functional analysis of large gene lists. Nucleic Acids Res. *37*, 1–13.

Huang, S., Gulzar, Z.G., Salari, K., Lapointe, J., Brooks, J.D., and Pollack, J.R. (2012). Recurrent deletion of CHD1 in prostate cancer with relevance to cell invasiveness. Oncogene *31*, 4164–4170.

Iannone, C., Pohl, A., Papasaikas, P., Soronellas, D., Vicent, G.P., Beato, M., and ValcáRcel, J. (2015). Relationship between nucleosome positioning and progesterone-induced alternative splicing in breast cancer cells. RNA N. Y. N *21*, 360–374.

Iouzalen, N., Moreau, J., and Méchali, M. (1996). H2A.Zl, a New Variant Histone Expressed during Xenopus Early Development Exhibits Several Distinct Features from the Core Histone H2A. Nucleic Acids Res. *24*, 3947–3952.

Jaenisch, R., and Bird, A. (2003). Epigenetic regulation of gene expression: how the genome integrates intrinsic and environmental signals. Nat. Genet. *33*, 245–254.

Jensen, E.D., Gopalakrishnan, R., and Westendorf, J.J. (2010). Regulation of Gene Expression in Osteoblasts. BioFactors Oxf. Engl. *36*, 25–32.

Jeong, Y., and Mangelsdorf, D.J. (2009). Nuclear receptor regulation of stemness and stem cell differentiation. Exp. Mol. Med. *41*, 525–537.

Jimeno-González, S., Gómez-Herreros, F., Alepuz, P.M., and Chávez, S. (2006). A Gene-Specific Requirement for FACT during Transcription Is Related to the Chromatin Organization of the Transcribed Region. Mol. Cell. Biol. *26*, 8710–8721.

Jin, C., and Felsenfeld, G. (2007). Nucleosome stability mediated by histone variants H3.3 and H2A.Z. Genes Dev. *21*, 1519–1529.

Jin, C., Zang, C., Wei, G., Cui, K., Peng, W., Zhao, K., and Felsenfeld, G. (2009). H3.3/H2A.Z double variant–containing nucleosomes mark “nucleosome-free regions” of active promoters and other regulatory regions. Nat. Genet. *41*, 941–945.

Jonkers, I., and Lis, J.T. (2015). Getting up to speed with transcription elongation by RNA polymerase II. Nat. Rev. Mol. Cell Biol. *16*, 167–177.

Kahler, R.A., and Westendorf, J.J. (2003). Lymphoid enhancer factor-1 and beta-catenin inhibit Runx2-dependent transcriptional activation of the osteocalcin promoter. J. Biol. Chem. *278*, 11937–11944.

Kahler, R.A., Galindo, M., Lian, J., Stein, G.S., van Wijnen, A.J., and Westendorf, J.J. (2006). Lymphocyte enhancer-binding factor 1 (Lef1) inhibits terminal differentiation of osteoblasts. J. Cell. Biochem. *97*, 969–983.

Kahler, R.A., Yingst, S.M.C., Hoeppner, L.H., Jensen, E.D., Krawczak, D., Oxford, J.T., and Westendorf, J.J. (2008). Collagen 11a1 is indirectly activated by lymphocyte enhancer-binding factor 1 (Lef1) and negatively regulates osteoblast maturation. Matrix Biol. J. Int. Soc. Matrix Biol. *27*, 330–338.

Kamakaka, R.T., and Biggins, S. (2005). Histone variants: deviants? Genes Dev. *19*, 295–316.

Kamakaka, R.T., and Thomas, J.O. (1990). Chromatin structure of transcriptionally competent and repressed genes. EMBO J. *9*, 3997–4006.

Kanatani, N., Fujita, T., Fukuyama, R., Liu, W., Yoshida, C.A., Moriishi, T., Yamana, K., Miyazaki, T., Toyosawa, S., and Komori, T. (2006). Cbf beta regulates Runx2 function isoform-dependently in postnatal bone development. Dev. Biol. *296*, 48–61.

Karlić, R., Chung, H.-R., Lasserre, J., Vlahoviček, K., and Vingron, M. (2010). Histone modification levels are predictive for gene expression. Proc. Natl. Acad. Sci. U. S. A. *107*, 2926–2931.

Karpiuk, O., Najafova, Z., Kramer, F., Hennion, M., Galonska, C., König, A., Snaidero, N., Vogel, T., Shchebet, A., Begus-Nahrmann, Y., et al. (2012a). The Histone H2B Monoubiquitination Regulatory Pathway Is Required for Differentiation of Multipotent Stem Cells. Mol. Cell *46*, 705–713.

Kassem, M., and Bianco, P. (2015). Skeletal Stem Cells in Space and Time. Cell *160*, 17–19.

Kato, S., Inoue, K., and Youn, M.-Y. (2010). Emergence of the osteo-epigenome in bone biology. IBMS BoneKEy *7*, 314–324.

Kelley, D.E., Stokes, D.G., and Perry, R.P. (1999). CHD1 interacts with SSRP1 and depends on both its chromodomain and its ATPase/helicase-like domain for proper association with chromatin. Chromosoma *108*, 10–25.

Kim, J.-M., Lee, S.-T., Chu, K., Jung, K.-H., Song, E.-C., Kim, S.-J., Sinn, D.-I., Kim, J.-H., Park, D.-K., Kang, K.-M., et al. (2007). Systemic transplantation of human adipose stem cells attenuated cerebral inflammation and degeneration in a hemorrhagic stroke model. Brain Res. *1183*, 43–50.

Kireeva, M.L., Walter, W., Tchernajenko, V., Bondarenko, V., Kashlev, M., and Studitsky, V.M. (2002). Nucleosome Remodeling Induced by RNA Polymerase II: Loss of the H2A/H2B Dimer during Transcription. Mol. Cell *9*, 541–552.

Koch, C.M., Andrews, R.M., Flicek, P., Dillon, S.C., Karaöz, U., Clelland, G.K., Wilcox, S., Beare, D.M., Fowler, J.C., Couttet, P., et al. (2007). The landscape of histone modifications across 1% of the human genome in five human cell lines. Genome Res. *17*, 691–707.

Koh, F.M., Lizama, C.O., Wong, P., Hawkins, J.S., Zovein, A.C., and Ramalho-Santos, M. (2015). Emergence of hematopoietic stem and progenitor cells involves a Chd1-dependent increase in total nascent transcription. Proc. Natl. Acad. Sci. *112*, E1734–E1743.

Komori, T. (2009). Regulation of Osteoblast Differentiation by Runx2. In Osteoimmunology, Y. Choi, ed. (Springer US), pp. 43–49.

Konev, A.Y., Tribus, M., Park, S.Y., Podhraski, V., Lim, C.Y., Emelyanov, A.V., Vershilova, E., Pirrotta, V., Kadonaga, J.T., Lusser, A., et al. (2007). CHD1 motor protein is required for deposition of histone variant H3.3 into chromatin in vivo. Science *317*, 1087–1090.

Kornberg, R.D. (1974). Chromatin structure: a repeating unit of histones and DNA. Science *184*, 868–871.

Krogan, N.J., Kim, M., Ahn, S.H., Zhong, G., Kobor, M.S., Cagney, G., Emili, A., Shilatifard, A., Buratowski, S., and Greenblatt, J.F. (2002). RNA Polymerase II Elongation Factors of Saccharomyces cerevisiae: a Targeted Proteomics Approach. Mol. Cell. Biol. *22*, 6979–6992.

Ku, M., Jaffe, J.D., Koche, R.P., Rheinbay, E., Endoh, M., Koseki, H., Carr, S.A., and Bernstein, B.E. (2012). H2A.Z landscapes and dual modifications in pluripotent and multipotent stem cells underlie complex genome regulatory functions. Genome Biol. *13*, R85.

Kulish, D., and Struhl, K. (2001). TFIIS Enhances Transcriptional Elongation through an Artificial Arrest Site In Vivo. Mol. Cell. Biol. *21*, 4162–4168.

Kulterer, B., Friedl, G., Jandrositz, A., Sanchez-Cabo, F., Prokesch, A., Paar, C., Scheideler, M., Windhager, R., Preisegger, K.-H., and Trajanoski, Z. (2007). Gene expression profiling of human mesenchymal stem cells derived from bone marrow during expansion and osteoblast differentiation. BMC Genomics *8*, 70.

Kwon, H., Imbalzano, A.N., Khavari, P.A., Kingston, R.E., and Green, M.R. (1994). Nucleosome disruption and enhancement of activator binding by a human SW1/SNF complex. Nature *370*, 477–481.

Lam, M.T., Li, W., Rosenfeld, M.G., and Glass, C.K. (2014). Enhancer RNAs and regulated transcriptional programs. Trends Biochem. Sci. *39*, 170–182.

Langmead, B., and Salzberg, S.L. (2012). Fast gapped-read alignment with Bowtie 2. Nat. Methods *9*, 357–359.

Langmead, B., Trapnell, C., Pop, M., and Salzberg, S.L. (2009). Ultrafast and memory-efficient alignment of short DNA sequences to the human genome. Genome Biol. *10*, R25.

Larsen, K.H., Frederiksen, C.M., Burns, J.S., Abdallah, B.M., and Kassem, M. (2010). Identifying a molecular phenotype for bone marrow stromal cells with in vivo bone-forming capacity. J. Bone Miner. Res. *25*, 796–808.

Le Blanc, K., Götherström, C., Ringdén, O., Hassan, M., McMahon, R., Horwitz, E., Anneren, G., Axelsson, O., Nunn, J., Ewald, U., et al. (2005). Fetal mesenchymal stem-cell engraftment in bone after in utero transplantation in a patient with severe osteogenesis imperfecta. Transplantation *79*, 1607–1614.

Ledoux, S., Queguiner, I., Msika, S., Calderari, S., Rufat, P., Gasc, J.-M., Corvol, P., and Larger, E. (2008). Angiogenesis Associated With Visceral and Subcutaneous Adipose Tissue in Severe Human Obesity. Diabetes *57*, 3247–3257.

Lee, J.-S., Garrett, A.S., Yen, K., Takahashi, Y.-H., Hu, D., Jackson, J., Seidel, C., Pugh, B.F., and Shilatifard, A. (2012a). Codependency of H2B monoubiquitination and nucleosome reassembly on Chd1. Genes Dev. *26*, 914–919.

Lee, J.W., Fang, X., Gupta, N., Serikov, V., and Matthay, M.A. (2009). Allogeneic human mesenchymal stem cells for treatment of E. coli endotoxin-induced acute lung injury in the ex vivo perfused human lung. Proc. Natl. Acad. Sci. U. S. A. *106*, 16357–16362.

Lee, K.S., Kim, H.J., Li, Q.L., Chi, X.Z., Ueta, C., Komori, T., Wozney, J.M., Kim, E.G., Choi, J.Y., Ryoo, H.M., et al. (2000). Runx2 is a common target of transforming growth factor beta1 and bone morphogenetic protein 2, and cooperation between Runx2 and Smad5 induces osteoblast-specific gene expression in the pluripotent mesenchymal precursor cell line C2C12. Mol. Cell. Biol. *20*, 8783–8792.

Lee, M.-H., Kim, Y.-J., Kim, H.-J., Park, H.-D., Kang, A.-R., Kyung, H.-M., Sung, J.-H., Wozney, J.M., Kim, H.-J., and Ryoo, H.-M. (2003). BMP-2-induced Runx2 Expression Is Mediated by Dlx5, and TGF-β1 Opposes the BMP-2-induced Osteoblast Differentiation by Suppression of Dlx5 Expression. J. Biol. Chem. *278*, 34387–34394.

Lehmann, L., Ferrari, R., Vashisht, A.A., Wohlschlegel, J.A., Kurdistani, S.K., and Carey, M. (2012). Polycomb Repressive Complex 1 (PRC1) Disassembles RNA Polymerase II Preinitiation Complexes♦. J. Biol. Chem. *287*, 35784–35794.

Lepperdinger, G., Brunauer, R., Jamnig, A., Laschober, G., and Kassem, M. (2008). Controversial issue: is it safe to employ mesenchymal stem cells in cell-based therapies? Exp. Gerontol. *43*, 1018–1023.

Li, G., and Reinberg, D. (2011). Chromatin higher-order structures and gene regulation. Curr. Opin. Genet. Dev. *21*, 175–186.

Li, J., and Gilmour, D.S. (2013). Distinct mechanisms of transcriptional pausing orchestrated by GAGA factor and M1BP, a novel transcription factor. EMBO J. *32*, 1829–1841.

Li, B., Carey, M., and Workman, J.L. (2007). The Role of Chromatin during Transcription. Cell *128*, 707–719.

Li, G., Margueron, R., Hu, G., Stokes, D., Wang, Y.-H., and Reinberg, D. (2010). Highly Compacted Chromatin Formed In Vitro Reflects the Dynamics of Transcription Activation In Vivo. Mol. Cell *38*, 41–53.

Li, H., Handsaker, B., Wysoker, A., Fennell, T., Ruan, J., Homer, N., Marth, G., Abecasis, G., and Durbin, R. (2009). The Sequence Alignment/Map format and SAMtools. Bioinformatics *25*, 2078–2079.

Lian, J.B., and Stein, G.S. (1992). Concepts of Osteoblast Growth and Differentiation: Basis for Modulation of Bone Cell Development and Tissue Formation. Crit. Rev. Oral Biol. Med. *3*, 269–305.

Lin, C.Y., Lovén, J., Rahl, P.B., Paranal, R.M., Burge, C.B., Bradner, J.E., Lee, T.I., and Young, R.A. (2012). Transcriptional amplification in tumor cells with elevated c-Myc. Cell *151*, 56–67.

Lin, J.J., Lehmann, L.W., Bonora, G., Sridharan, R., Vashisht, A.A., Tran, N., Plath, K., Wohlschlegel, J.A., and Carey, M. (2011). Mediator coordinates PIC assembly with recruitment of CHD1. Genes Dev. *25*, 2198–2209.

Long, F. (2012). Building strong bones: molecular regulation of the osteoblast lineage. Nat. Rev. Mol. Cell Biol. *13*, 27–38.

Lorch, Y., LaPointe, J.W., and Kornberg, R.D. (1987). Nucleosomes inhibit the initiation of transcription but allow chain elongation with the displacement of histones. Cell *49*, 203–210.

Luger, K., Mäder, A.W., Richmond, R.K., Sargent, D.F., and Richmond, T.J. (1997). Crystal structure of the nucleosome core particle at 2.8 Å resolution. Nature *389*, 251–260.

Lusser, A., Urwin, D.L., and Kadonaga, J.T. (2005). Distinct activities of CHD1 and ACF in ATP-dependent chromatin assembly. Nat. Struct. Mol. Biol. *12*, 160–166.

Makita, N., Suzuki, M., Asami, S., Takahata, R., Kohzaki, D., Kobayashi, S., Hakamazuka, T., and Hozumi, N. (2008). Two of four alternatively spliced isoforms of RUNX2 control osteocalcin gene expression in human osteoblast cells. Gene *413*, 8–17.

Manohar, M., Mooney, A.M., North, J.A., Nakkula, R.J., Picking, J.W., Edon, A., Fishel, R., Poirier, M.G., and Ottesen, J.J. (2009). Acetylation of Histone H3 at the Nucleosome Dyad Alters DNA-Histone Binding. J. Biol. Chem. *284*, 23312–23321.

Marfella, C.G.A., and Imbalzano, A.N. (2007). The Chd Family of Chromatin Remodelers. Mutat. Res. *618*, 30–40.

Mariman, E.C.M., and Wang, P. (2010). Adipocyte extracellular matrix composition, dynamics and role in obesity. Cell. Mol. Life Sci. *67*, 1277–1292.

Marques, M., Laflamme, L., Gervais, A.L., and Gaudreau, L. (2010). Reconciling the positive and negative roles of histone H2A.Z in gene transcription. Epigenetics *5*, 267–272.

Materne, P., Anandhakumar, J., Migeot, V., Soriano, I., Yague-Sanz, C., Hidalgo, E., Mignion, C., Quintales, L., Antequera, F., and Hermand, D. Promoter nucleosome dynamics regulated by signalling through the CTD code. eLife *4*.

Mathews, S., Bhonde, R., Gupta, P.K., and Totey, S. (2012). Extracellular matrix protein mediated regulation of the osteoblast differentiation of bone marrow derived human mesenchymal stem cells. Differ. Res. Biol. Divers. *84*, 185–192.

Mavrich, T.N., Ioshikhes, I.P., Venters, B.J., Jiang, C., Tomsho, L.P., Qi, J., Schuster, S.C., Albert, I., and Pugh, B.F. (2008). A barrier nucleosome model for statistical positioning of nucleosomes throughout the yeast genome. Genome Res. *18*, 1073–1083.

McDaniel, I.E., Lee, J.M., Berger, M.S., Hanagami, C.K., and Armstrong, J.A. (2008). Investigations of CHD1 Function in Transcription and Development of Drosophila melanogaster. Genetics *178*, 583–587.

McKnight, J.N., Jenkins, K.R., Nodelman, I.M., Escobar, T., and Bowman, G.D. (2011). Extranucleosomal DNA Binding Directs Nucleosome Sliding by Chd1. Mol. Cell. Biol. *31*, 4746–4759.

Méndez-Ferrer, S., Michurina, T.V., Ferraro, F., Mazloom, A.R., MacArthur, B.D., Lira, S.A., Scadden, D.T., Ma'ayan, A., Enikolopov, G.N., and Frenette, P.S. (2010). Mesenchymal and haematopoietic stem cells form a unique bone marrow niche. Nature *466*, 829–834.

Meneghini, M.D., Wu, M., and Madhani, H.D. (2003). Conserved histone variant H2A.Z protects euchromatin from the ectopic spread of silent heterochromatin. Cell *112*, 725–736.

Mills, J.D., Kawahara, Y., and Janitz, M. (2013). Strand-Specific RNA-Seq Provides Greater Resolution of Transcriptome Profiling. Curr. Genomics *14*, 173–181.

Min, I.M., Waterfall, J.J., Core, L.J., Munroe, R.J., Schimenti, J., and Lis, J.T. (2011). Regulating RNA polymerase pausing and transcription elongation in embryonic stem cells. Genes Dev. *25*, 742–754.

Mito, Y., Henikoff, J.G., and Henikoff, S. (2005). Genome-scale profiling of histone H3.3 replacement patterns. Nat. Genet. *37*, 1090–1097.

Mizuta, S., Minami, T., Fujita, H., Kaminaga, C., Matsui, K., Ishino, R., Fujita, A., Oda, K., Kawai, A., Hasegawa, N., et al. (2014). CCAR1/CoCoA pair-mediated recruitment of the Mediator defines a novel pathway for GATA1 function. Genes Cells Devoted Mol. Cell. Mech. *19*, 28–51.

Morettini, S., Tribus, M., Zeilner, A., Sebald, J., Campo-Fernandez, B., Scheran, G., Wörle, H., Podhraski, V., Fyodorov, D.V., and Lusser, A. (2011). The chromodomains of CHD1 are critical for enzymatic activity but less important for chromatin localization. Nucleic Acids Res. *39*, 3103–3115.

Mori, T., Sakaue, H., Iguchi, H., Gomi, H., Okada, Y., Takashima, Y., Nakamura, K., Nakamura, T., Yamauchi, T., Kubota, N., et al. (2005). Role of Krüppel-like factor 15 (KLF15) in transcriptional regulation of adipogenesis. J. Biol. Chem. *280*, 12867–12875.

Mrak, E., Villa, I., Lanzi, R., Losa, M., Guidobono, F., and Rubinacci, A. (2007). Growth hormone stimulates osteoprotegerin expression and secretion in human osteoblast-like cells. J. Endocrinol. *192*, 639–645.

Mueller-Planitz, F., Klinker, H., and Becker, P.B. (2013). Nucleosome sliding mechanisms: new twists in a looped history. Nat. Struct. Mol. Biol. *20*, 1026–1032.

Mukherjee, R., Jow, L., Croston, G.E., and Paterniti, J.R. (1997). Identification, characterization, and tissue distribution of human peroxisome proliferator-activated receptor (PPAR) isoforms PPARgamma2 versus PPARgamma1 and activation with retinoid X receptor agonists and antagonists. J. Biol. Chem. *272*, 8071–8076.

Muse, G.W., Gilchrist, D.A., Nechaev, S., Shah, R., Parker, J.S., Grissom, S.F., Zeitlinger, J., and Adelman, K. (2007). RNA polymerase is poised for activation across the genome. Nat. Genet. *39*, 1507–1511.

Naftelberg, S., Schor, I.E., Ast, G., and Kornblihtt, A.R. (2015). Regulation of Alternative Splicing Through Coupling with Transcription and Chromatin Structure. Annu. Rev. Biochem. *84*, 165–198.

Nagarajan, S., Benito, E., Fischer, A., and Johnsen, S.A. (2015). H4K12ac is regulated by estrogen receptor-alpha and is associated with BRD4 function and inducible transcription. Oncotarget *6*, 7305–7317.

Nelson, J.D., Denisenko, O., and Bomsztyk, K. (2006). Protocol for the fast chromatin immunoprecipitation (ChIP) method. Nat. Protoc. *1*, 179–185.

Ng, C.P., Mohamed Sharif, A.R., Heath, D.E., Chow, J.W., Zhang, C.B., Chan-Park, M.B., Hammond, P.T., Chan, J.K., and Griffith, L.G. (2014). Enhanced ex vivo expansion of adult mesenchymal stem cells by fetal mesenchymal stem cell ECM. Biomaterials *35*, 4046–4057.

Niyibizi, C., and Eyre, D.R. (1989). Identification of the cartilage alpha 1(XI) chain in type V collagen from bovine bone. FEBS Lett. *242*, 314–318.

Oishi, Y., Manabe, I., Tobe, K., Tsushima, K., Shindo, T., Fujiu, K., Nishimura, G., Maemura, K., Yamauchi, T., Kubota, N., et al. (2005). Krüppel-like transcription factor KLF5 is a key regulator of adipocyte differentiation. Cell Metab. *1*, 27–39.

Okada, M., Okawa, K., Isobe, T., and Fukagawa, T. (2009). CENP-H–containing Complex Facilitates Centromere Deposition of CENP-A in Cooperation with FACT and CHD1. Mol. Biol. Cell *20*, 3986–3995.

Oury, F., Ferron, M., Huizhen, W., Confavreux, C., Xu, L., Lacombe, J., Srinivas, P., Chamouni, A., Lugani, F., Lejeune, H., et al. (2013). Osteocalcin regulates murine and human fertility through a pancreas-bone-testis axis. J. Clin. Invest. *123*, 2421–2433.

Owen, M., and Friedenstein, A.J. (1988). Stromal stem cells: marrow-derived osteogenic precursors. Ciba Found. Symp. *136*, 42–60.

Parekkadan, B., van Poll, D., Suganuma, K., Carter, E.A., Berthiaume, F., Tilles, A.W., and Yarmush, M.L. (2007). Mesenchymal stem cell-derived molecules reverse fulminant hepatic failure. PloS One *2*, e941.

Park, D., Shivram, H., and Iyer, V.R. (2014). Chd1 co-localizes with early transcription elongation factors independently of H3K36 methylation and releases stalled RNA polymerase II at introns. Epigenetics Chromatin *7*, 32.

Patel, A., Chakravarthy, S., Morrone, S., Nodelman, I.M., McKnight, J.N., and Bowman, G.D. (2013). Decoupling nucleosome recognition from DNA binding dramatically alters the properties of the Chd1 chromatin remodeler. Nucleic Acids Res. *41*, 1637–1648.

Pavri, R., Zhu, B., Li, G., Trojer, P., Mandal, S., Shilatifard, A., and Reinberg, D. (2006). Histone H2B monoubiquitination functions cooperatively with FACT to regulate elongation by RNA polymerase II. Cell *125*, 703–717.

Pérez-Lluch, S., Blanco, E., Tilgner, H., Curado, J., Ruiz-Romero, M., Corominas, M., and Guigó, R. (2015). Absence of canonical marks of active chromatin in developmentally regulated genes. Nat. Genet. *47*, 1158–1167.

Persson, J., and Ekwall, K. (2010). Chd1 remodelers maintain open chromatin and regulate the epigenetics of differentiation. Exp. Cell Res. *316*, 1316–1323.

Petesch, S.J., and Lis, J.T. (2012). Overcoming the Nucleosome Barrier During Transcript Elongation. Trends Genet. TIG *28*, 285–294.

Pihlajaniemi, T., Tamminen, M., Sandberg, M., Hirvonen, H., and Vuorio, E. (1990). The α1 Chain of Type XIII Collagen. Ann. N. Y. Acad. Sci. *580*, 440–443.

Pointner, J., Persson, J., Prasad, P., Norman-Axelsson, U., Strålfors, A., Khorosjutina, O., Krietenstein, N., Svensson, J.P., Ekwall, K., and Korber, P. (2012). CHD1 remodelers regulate nucleosome spacing in vitro and align nucleosomal arrays over gene coding regions in S. pombe. EMBO J. *31*, 4388–4403.

Polo, J.M., Liu, S., Figueroa, M.E., Kulalert, W., Eminli, S., Tan, K.Y., Apostolou, E., Stadtfeld, M., Li, Y., Shioda, T., et al. (2010). Cell type of origin influences the molecular and functional properties of mouse induced pluripotent stem cells. Nat. Biotechnol. *28*, 848–855.

Post, S., Abdallah, B.M., Bentzon, J.F., and Kassem, M. (2008). Demonstration of the presence of independent pre-osteoblastic and pre-adipocytic cell populations in bone marrow-derived mesenchymal stem cells. Bone *43*, 32–39.

Pray-Grant, M.G., Daniel, J.A., Schieltz, D., Yates, J.R., and Grant, P.A. (2005). Chd1 chromodomain links histone H3 methylation with SAGA- and SLIK-dependent acetylation. Nature *433*, 434–438.

Quarto, R., Mastrogiacomo, M., Cancedda, R., Kutepov, S.M., Mukhachev, V., Lavroukov, A., Kon, E., and Marcacci, M. (2001). Repair of large bone defects with the use of autologous bone marrow stromal cells. N. Engl. J. Med. *344*, 385–386.

Rachner, T.D., Khosla, S., and Hofbauer, L.C. (2011). Osteoporosis: now and the future. Lancet Lond. Engl. *377*, 1276–1287.

Radman-Livaja, M., Quan, T.K., Valenzuela, L., Armstrong, J.A., van Welsem, T., Kim, T., Lee, L.J., Buratowski, S., van Leeuwen, F., Rando, O.J., et al. (2012). A Key Role for Chd1 in Histone H3 Dynamics at the 3′ Ends of Long Genes in Yeast. PLoS Genet *8*, e1002811.

Ramírez, F., Dündar, F., Diehl, S., Grüning, B.A., and Manke, T. (2014). deepTools: a flexible platform for exploring deep-sequencing data. Nucleic Acids Res. gku365.

Ravens, S., Yu, C., Ye, T., Stierle, M., and Tora, L. (2015). Tip60 complex binds to active Pol II promoters and a subset of enhancers and co-regulates the c-Myc network in mouse embryonic stem cells. Epigenetics Chromatin *8*, 45.

Ray-Gallet, D., Quivy, J.-P., Scamps, C., Martini, E.M.-D., Lipinski, M., and Almouzni, G. (2002). HIRA Is Critical for a Nucleosome Assembly Pathway Independent of DNA Synthesis. Mol. Cell *9*, 1091–1100.

R Development Core Team (2008). R: A Language and Environment for Statistical Computing.

Regard, J.B., Zhong, Z., Williams, B.O., and Yang, Y. (2012). Wnt Signaling in Bone Development and Disease: Making Stronger Bone with Wnts. Cold Spring Harb. Perspect. Biol. *4*, a007997.

Reynolds, N., Latos, P., Hynes-Allen, A., Loos, R., Leaford, D., O'Shaughnessy, A., Mosaku, O., Signolet, J., Brennecke, P., Kalkan, T., et al. (2012). NuRD suppresses pluripotency gene expression to promote transcriptional heterogeneity and lineage commitment. Cell Stem Cell *10*, 583–594.

Rickard, D.J., Kassem, M., Hefferan, T.E., Sarkar, G., Spelsberg, T.C., and Riggs, B.L. (1996). Isolation and characterization of osteoblast precursor cells from human bone marrow. J. Bone Miner. Res. *11*, 312–324.

Robinson, J.T., Thorvaldsdóttir, H., Winckler, W., Guttman, M., Lander, E.S., Getz, G., and Mesirov, J.P. (2011). Integrative Genomics Viewer. Nat. Biotechnol. *29*, 24–26.

Rodda, S.J., and McMahon, A.P. (2006). Distinct roles for Hedgehog and canonical Wnt signaling in specification, differentiation and maintenance of osteoblast progenitors. Dev. Camb. Engl. *133*, 3231–3244.

Rodrigues, L.U., Rider, L., Nieto, C., Romero, L., Karimpour-Fard, A., Loda, M., Lucia, M.S., Wu, M., Shi, L., Cimic, A., et al. (2015). Coordinate loss of MAP3K7 and CHD1 promotes aggressive prostate cancer. Cancer Res. *75*, 1021–1034.

Rosen, C.J., and Bouxsein, M.L. (2006). Mechanisms of Disease: is osteoporosis the obesity of bone? Nat. Clin. Pract. Rheumatol. *2*, 35–43.

Rosen, E.D., and MacDougald, O.A. (2006). Adipocyte differentiation from the inside out. Nat. Rev. Mol. Cell Biol. *7*, 885–896.

Rosset, P., Deschaseaux, F., and Layrolle, P. (2014). Cell therapy for bone repair. Orthop. Traumatol. Surg. Res. OTSR *100*, S107–S112.

Ross-Innes, C.S., Stark, R., Teschendorff, A.E., Holmes, K.A., Ali, H.R., Dunning, M.J., Brown, G.D., Gojis, O., Ellis, I.O., Green, A.R., et al. (2012). Differential oestrogen receptor binding is associated with clinical outcome in breast cancer. Nature *481*, 389–393.

Roth, D.B., and Roth, S.Y. (2000). Unequal access: regulating V(D)J recombination through chromatin remodeling. Cell *103*, 699–702.

Russell, K.C., Phinney, D.G., Lacey, M.R., Barrilleaux, B.L., Meyertholen, K.E., and O'Connor, K.C. (2010). In Vitro High-Capacity Assay to Quantify the Clonal Heterogeneity in Trilineage Potential of Mesenchymal Stem Cells Reveals a Complex Hierarchy of Lineage Commitment. STEM CELLS *28*, 788–798.

Ryan, D.P., Sundaramoorthy, R., Martin, D., Singh, V., and Owen-Hughes, T. (2011). The DNA-binding domain of the Chd1 chromatin-remodelling enzyme contains SANT and SLIDE domains. EMBO J. *30*, 2596–2609.

Sabek, O.M., Nishimoto, S.K., Fraga, D., Tejpal, N., Ricordi, C., and Gaber, A.O. (2015). Osteocalcin Effect on Human β-Cells Mass and Function. Endocrinology *156*, 3137–3146.

Saeki, H., and Svejstrup, J.Q. (2009). Stability, Flexibility, and Dynamic Interactions of Colliding RNA Polymerase II Elongation Complexes. Mol. Cell *35*, 191–205.

Sainsbury, S., Bernecky, C., and Cramer, P. (2015). Structural basis of transcription initiation by RNA polymerase II. Nat. Rev. Mol. Cell Biol. *16*, 129–143.

Salma, N., Xiao, H., Mueller, E., and Imbalzano, A.N. (2004). Temporal Recruitment of Transcription Factors and SWI/SNF Chromatin-Remodeling Enzymes during Adipogenic Induction of the Peroxisome Proliferator-Activated Receptor γ Nuclear Hormone Receptor. Mol. Cell. Biol. *24*, 4651–4663.

Sarai, N., Nimura, K., Tamura, T., Kanno, T., Patel, M.C., Heightman, T.D., Ura, K., and Ozato, K. (2013). WHSC1 links transcription elongation to HIRA-mediated histone H3.3 deposition. EMBO J. *32*, 2392–2406.

Schallmoser, K., Rohde, E., Reinisch, A., Bartmann, C., Thaler, D., Drexler, C., Obenauf, A.C., Lanzer, G., Linkesch, W., and Strunk, D. (2008). Rapid large-scale expansion of functional mesenchymal stem cells from unmanipulated bone marrow without animal serum. Tissue Eng. Part C Methods *14*, 185–196.

Schenk, R., Jenke, A., Zilbauer, M., Wirth, S., and Postberg, J. (2011). H3.5 is a novel hominid-specific histone H3 variant that is specifically expressed in the seminiferous tubules of human testes. Chromosoma *120*, 275–285.

Schwartz, S., Meshorer, E., and Ast, G. (2009). Chromatin organization marks exon-intron structure. Nat. Struct. Mol. Biol. *16*, 990–995.

Schwartzentruber, J., Korshunov, A., Liu, X.-Y., Jones, D.T.W., Pfaff, E., Jacob, K., Sturm, D., Fontebasso, A.M., Quang, D.-A.K., Tönjes, M., et al. (2012). Driver mutations in histone H3.3 and chromatin remodelling genes in paediatric glioblastoma. Nature *482*, 226–231.

Seligman, M., Eilberg, D.R.G., and Fishman, L. (1975). Mineralization of elastin extracted from human aortic tissues. Calcif. Tissue Res. *17*, 229–234.

de la Serna, I.L., Ohkawa, Y., and Imbalzano, A.N. (2006). Chromatin remodelling in mammalian differentiation: lessons from ATP-dependent remodellers. Nat. Rev. Genet. *7*, 461–473.

Sethi, A., Jain, A., Zode, G.S., Wordinger, R.J., and Clark, A.F. (2011). Role of TGFβ/Smad Signaling in Gremlin Induction of Human Trabecular Meshwork Extracellular Matrix Proteins. Invest. Ophthalmol. Vis. Sci. *52*, 5251–5259.

Shim, Y.S., Choi, Y., Kang, K., Cho, K., Oh, S., Lee, J., Grewal, S.I.S., and Lee, D. (2012). Hrp3 controls nucleosome positioning to suppress non-coding transcription in eu- and heterochromatin. EMBO J. *31*, 4375–4387.

Shin, H., Liu, T., Manrai, A.K., and Liu, X.S. (2009). CEAS: cis-regulatory element annotation system. Bioinforma. Oxf. Engl. *25*, 2605–2606.

Siggens, L., Cordeddu, L., Rönnerblad, M., Lennartsson, A., and Ekwall, K. (2015a). Transcription-coupled recruitment of human CHD1 and CHD2 influences chromatin accessibility and histone H3 and H3.3 occupancy at active chromatin regions. Epigenetics Chromatin *8*.

Simic, R., Lindstrom, D.L., Tran, H.G., Roinick, K.L., Costa, P.J., Johnson, A.D., Hartzog, G.A., and Arndt, K.M. (2003). Chromatin remodeling protein Chd1 interacts with transcription elongation factors and localizes to transcribed genes. EMBO J. *22*, 1846–1856.

Simonsen, J.L., Rosada, C., Serakinci, N., Justesen, J., Stenderup, K., Rattan, S.I.S., Jensen, T.G., and Kassem, M. (2002a). Telomerase expression extends the proliferative life-span and maintains the osteogenic potential of human bone marrow stromal cells. Nat. Biotechnol. *20*, 592–596.

Sims, R.J., Chen, C.-F., Santos-Rosa, H., Kouzarides, T., Patel, S.S., and Reinberg*, D. (2005). HUMAN BUT NOT YEAST CHD1 BINDS DIRECTLY AND SELECTIVELY TO HISTONE H3 METHYLATED AT LYSINE 4 VIA ITS TANDEM CHROMODOMAINS. J. Biol. Chem. *280*, 41789–41792.

Sims, R.J., Millhouse, S., Chen, C.-F., Lewis, B.A., Erdjument-Bromage, H., Tempst, P., Manley, J.L., and Reinberg, D. (2007). Recognition of trimethylated histone H3 lysine 4 facilitates the recruitment of transcription postinitiation factors and pre-mRNA splicing. Mol. Cell *28*, 665–676.

Skene, P.J., Hernandez, A.E., Groudine, M., and Henikoff, S. (2014). The nucleosomal barrier to promoter escape by RNA polymerase II is overcome by the chromatin remodeler Chd1. eLife *3*, e02042.

Smolle, M., Venkatesh, S., Gogol, M.M., Li, H., Zhang, Y., Florens, L., Washburn, M.P., and Workman, J.L. (2012). Chromatin remodelers Isw1 and Chd1 maintain chromatin structure during transcription by preventing histone exchange. Nat. Struct. Mol. Biol. *19*, 884–892.

Starcher, B.C., and Urry, D.W. (1973). Elastin coacervate as a matrix for calcification. Biochem. Biophys. Res. Commun. *53*, 210–216.

Stasevich, T.J., Hayashi-Takanaka, Y., Sato, Y., Maehara, K., Ohkawa, Y., Sakata-Sogawa, K., Tokunaga, M., Nagase, T., Nozaki, N., McNally, J.G., et al. (2014). Regulation of RNA polymerase II activation by histone acetylation in single living cells. Nature *516*, 272–275.

Strahl, B.D., and Allis, C.D. (2000). The language of covalent histone modifications. Nature *403*, 41–45.

Struhl, K., and Segal, E. (2013). Determinants of nucleosome positioning. Nat. Struct. Mol. Biol. *20*, 267–273.

Subramaniam, M., Jalal, S.M., Rickard, D.J., Harris, S.A., Bolander, M.E., and Spelsberg, T.C. (2002). Further characterization of human fetal osteoblastic hFOB 1.19 and hFOB/ER alpha cells: bone formation in vivo and karyotype analysis using multicolor fluorescent in situ hybridization. J. Cell. Biochem. *87*, 9–15.

Suto, R.K., Clarkson, M.J., Tremethick, D.J., and Luger, K. (2000). Crystal structure of a nucleosome core particle containing the variant histone H2A.Z. Nat. Struct. Biol. *7*, 1121–1124.

Svensson, J.P., Shukla, M., Menendez-Benito, V., Norman-Axelsson, U., Audergon, P., Sinha, I., Tanny, J.C., Allshire, R.C., and Ekwall, K. (2015). A nucleosome turnover map reveals that the stability of histone H4 Lys20 methylation depends on histone recycling in transcribed chromatin. Genome Res. gr.188870.114.

Szenker, E., Lacoste, N., and Almouzni, G. (2012). A developmental requirement for HIRA-dependent H3.3 deposition revealed at gastrulation in Xenopus. Cell Rep. *1*, 730–740.

Taipaleenmäki, H., Abdallah, B.M., AlDahmash, A., Säämänen, A.-M., and Kassem, M. (2011). Wnt signalling mediates the cross-talk between bone marrow derived pre-adipocytic and pre-osteoblastic cell populations. Exp. Cell Res. *317*, 745–756.

Takahashi, K., and Yamanaka, S. (2006). Induction of pluripotent stem cells from mouse embryonic and adult fibroblast cultures by defined factors. Cell *126*, 663–676.

Tang, Q.-Q., Otto, T.C., and Lane, M.D. (2003). CCAAT/enhancer-binding protein beta is required for mitotic clonal expansion during adipogenesis. Proc. Natl. Acad. Sci. U. S. A. *100*, 850–855.

Thakar, A., Gupta, P., Ishibashi, T., Finn, R., Silva-Moreno, B., Uchiyama, S., Fukui, K., Tomschik, M., Ausio, J., and Zlatanova, J. (2009). H2A.Z and H3.3 histone variants affect nucleosome structure: biochemical and biophysical studies. Biochemistry (Mosc.) *48*, 10852–10857.

Tilgner, H., Nikolaou, C., Althammer, S., Sammeth, M., Beato, M., Valcárcel, J., and Guigó, R. (2009). Nucleosome positioning as a determinant of exon recognition. Nat. Struct. Mol. Biol. *16*, 996–1001.

Tonna, S., El-Osta, A., Cooper, M.E., and Tikellis, C. (2010). Metabolic memory and diabetic nephropathy: potential role for epigenetic mechanisms. Nat. Rev. Nephrol. *6*, 332–341.

Tremethick, D.J. (2007). Higher-Order Structures of Chromatin: The Elusive 30 nm Fiber. Cell *128*, 651–654.

Tropberger, P., Pott, S., Keller, C., Kamieniarz-Gdula, K., Caron, M., Richter, F., Li, G., Mittler, G., Liu, E.T., Bühler, M., et al. (2013). Regulation of transcription through acetylation of H3K122 on the lateral surface of the histone octamer. Cell *152*, 859–872.

Tsukiyama, T., Palmer, J., Landel, C.C., Shiloach, J., and Wu, C. (1999). Characterization of the imitation switch subfamily of ATP-dependent chromatin-remodeling factors in Saccharomyces cerevisiae. Genes Dev. *13*, 686–697.

Twine, N.A., Chen, L., Pang, C.N., Wilkins, M.R., and Kassem, M. (2014a). Identification of differentiation-stage specific markers that define the ex vivo osteoblastic phenotype. Bone *67*, 23–32.

Tzaribachev, N., Vaegler, M., Schaefer, J., Reize, P., Rudert, M., Handgretinger, R., and Müller, I. (2008). Mesenchymal stromal cells: a novel treatment option for steroid-induced avascular osteonecrosis. Isr. Med. Assoc. J. IMAJ *10*, 232–234.

Undale, A.H., Westendorf, J.J., Yaszemski, M.J., and Khosla, S. (2009). Mesenchymal Stem Cells for Bone Repair and Metabolic Bone Diseases. Mayo Clin. Proc. *84*, 893–902.

Van Holde, K.E., Allen, J.R., Tatchell, K., Weischet, W.O., and Lohr, D. (1980). DNA-histone interactions in nucleosomes. Biophys. J. *32*, 271–282.

Venkatesh, S., and Workman, J.L. (2015). Histone exchange, chromatin structure and the regulation of transcription. Nat. Rev. Mol. Cell Biol. *16*, 178–189.

Voigt, P., Tee, W.-W., and Reinberg, D. (2013). A double take on bivalent promoters. Genes Dev. *27*, 1318–1338.

Voss, T.C., and Hager, G.L. (2014). Dynamic regulation of transcriptional states by chromatin and transcription factors. Nat. Rev. Genet. *15*, 69–81.

Waddington, C.H. (1957). The strategy of the genes; a discussion of some aspects of theoretical biology (New York: Macmillan).

Wakitani, S., Nawata, M., Tensho, K., Okabe, T., Machida, H., and Ohgushi, H. (2007). Repair of articular cartilage defects in the patello-femoral joint with autologous bone marrow mesenchymal cell transplantation: three case reports involving nine defects in five knees. J. Tissue Eng. Regen. Med. *1*, 74–79.

Wang, Y., Li, X., and Hu, H. (2014). H3K4me2 reliably defines transcription factor binding regions in different cells. Genomics *103*, 222–228.

Weber, C.M., Henikoff, J.G., and Henikoff, S. (2010). H2A.Z nucleosomes enriched over active genes are homotypic. Nat. Struct. Mol. Biol. *17*, 1500–1507.

Weber, C.M., Ramachandran, S., and Henikoff, S. (2014). Nucleosomes Are Context-Specific, H2A.Z-Modulated Barriers to RNA Polymerase. Mol. Cell *53*, 819–830.

Wei, X., Yang, X., Han, Z., Qu, F., Shao, L., and Shi, Y. (2013). Mesenchymal stem cells: a new trend for cell therapy. Acta Pharmacol. Sin. *34*, 747–754.

Whitehouse, I., and Tsukiyama, T. (2006). Antagonistic forces that position nucleosomes in vivo. Nat. Struct. Mol. Biol. *13*, 633–640.

Wirbelauer, C., Bell, O., and Schübeler, D. (2005). Variant histone H3.3 is deposited at sites of nucleosomal displacement throughout transcribed genes while active histone modifications show a promoter-proximal bias. Genes Dev. *19*, 1761–1766.

Xiao, G., Gopalakrishnan, R., Jiang, D., Reith, E., Benson, M.D., and Franceschi, R.T. (2002). Bone morphogenetic proteins, extracellular matrix, and mitogen-activated protein kinase signaling pathways are required for osteoblast-specific gene expression and differentiation in MC3T3-E1 cells. J. Bone Miner. Res. Off. J. Am. Soc. Bone Miner. Res. *17*, 101–110.

Xue, Y., Wong, J., Moreno, G.T., Young, M.K., Côté, J., and Wang, W. (1998). NURD, a novel complex with both ATP-dependent chromatin-remodeling and histone deacetylase activities. Mol. Cell *2*, 851–861.

Zaher, W., Harkness, L., Jafari, A., and Kassem, M. (2014). An update of human mesenchymal stem cell biology and their clinical uses. Arch. Toxicol. *88*, 1069–1082.

Zeitlinger, J., Stark, A., Kellis, M., Hong, J.-W., Nechaev, S., Adelman, K., Levine, M., and Young, R.A. (2007). RNA polymerase stalling at developmental control genes in the Drosophila melanogaster embryo. Nat. Genet. *39*, 1512–1516.

Zhang, H., Roberts, D.N., and Cairns, B.R. (2005). Genome-Wide Dynamics of Htz1, a Histone H2A Variant that Poises Repressed/Basal Promoters for Activation through Histone Loss. Cell *123*, 219–231.

Zhang, H., Gao, L., Anandhakumar, J., and Gross, D.S. (2014). Uncoupling Transcription from Covalent Histone Modification. PLoS Genet *10*, e1004202.

Zhang, Y., Liu, T., Meyer, C.A., Eeckhoute, J., Johnson, D.S., Bernstein, B.E., Nusbaum, C., Myers, R.M., Brown, M., Li, W., et al. (2008). Model-based Analysis of ChIP-Seq (MACS). Genome Biol. *9*, R137.

Zhong, Z., Zylstra-Diegel, C.R., Schumacher, C.A., Baker, J.J., Carpenter, A.C., Rao, S., Yao, W., Guan, M., Helms, J.A., Lane, N.E., et al. (2012). Wntless functions in mature osteoblasts to regulate bone mass. Proc. Natl. Acad. Sci. U. S. A. *109*, E2197–E2204.

Zhou, B.O., Yue, R., Murphy, M.M., Peyer, J.G., and Morrison, S.J. (2014). Leptin-Receptor-Expressing Mesenchymal Stromal Cells Represent the Main Source of Bone Formed by Adult Bone Marrow. Cell Stem Cell *15*, 154–168.

Zhu, Q., and Wani, A.A. (2010). Histone Modifications: Crucial Elements for Damage Response and Chromatin Restoration. J. Cell. Physiol. *223*, 283–288.

Zlatanova, J., and Thakar, A. (2008). H2A.Z: View from the Top. Structure *16*, 166–179.

7 Acknowledgements

I deeply thank my scientific mentor and supervisor Prof. Dr. Steven A. Johnsen. You always motivated me, were supportive and available at all times. I know that you gave honest and encouraging advices. Besides that, I think you are pivotal for the friendly and relaxed working atmosphere in our lab. You have a contagious and inspiring devotion for science which helps to grow in a professional and personal way.

I also thank my thesis committee members Prof. Dr. Heidi Hahn and Prof. Dr. Jürgen Wienands for the great discussions and friendly and helpful advices. Thanks to you I knew who to contact when necessary or in need. In particular, I thank you, Prof. Dr. Heidi Hahn, for your time and for providing the second review of my thesis.

I want to show my gratitude to the department directors Prof. Dr. Matthias Dobbelstein and Prof. Dr. Klaus Pantel by thanking them for the warm welcome to Göttingen and Hamburg, respectively. I am very glad and grateful to have met and worked with Prof. Dr. Hans Will who was so supportive and helpful before and during my thesis. A huge thank you goes to all colleagues from the lab for the open, friendly and funny atmosphere. In particular, I would like to thank Zeynab Najafova, Tareq Hossan, Wanhua Xie and the former members Dr. Upasana Bedi and Dr. Sankari Nagarajan, who offered great advice during the writing of my thesis. I really enjoyed having plenty of interesting discussions, coffee breaks and dinner outings with you and the whole great team.

I am sending big thanks to our collaborators in Denmark, Prof. Dr. Moustapha Kassem and Nicholas Ditzel, who performed the ectopic bone formation experiment.

Finally, I thank those important people in my life that are very special to me. My parents, Christine and Rüdiger Baumgart as well as my brother Markus Baumgart who have given the greatest support, trust and love independent of any circumstances. You are the strongest backing I could ever have wished for.

Insa, last but never least, I especially thank you for being my best friend and soul mate. Your patience, support and innovative concepts move my life into a better direction.